Dissertation zur Erlangung des Grades eines Doktors der Naturwissenschaften (doctor rerum naturalium)

GLACIAL AND FLUVIAL EVOLUTION OF LANDFORMS IN HELLAS PLANITIA, MARS

(Entwicklung von fluvialen und glazialen Erosions- und Sedimentationsformen in Hellas Planitia, Mars)

vorgelegt von

Martin Voelker, M.Sc.

im Fachbereich Geowissenschaften
der Freien Universität Berlin

Berlin, 2018

Erstgutachter: Prof. Dr. Ralf Jaumann

Freie Universität Berlin
Institut für Geologische Wissenschaften
Fachrichtung Planetologie und Fernerkundung

Deutsches Zentrum für Luft- und Raumfahrt
Institut für Planetenforschung, Planetengeologie

Zweitgutachterin: Prof. Dr. Anne Bernhardt

Freie Universität Berlin
Institut für Geologische Wissenschaften
Tektonik und Sedimentäre Systeme

Tag der Disputation: 12. Juli 2018

Standing on a new world and look beyond it to the next one.
Mission to Mars, 2000

Eidesstattliche Erklärung

Hiermit versichere ich, die vorliegende Arbeit selbstständig angefertigt, und keine anderen als der angeführten Quellen und Hilfsmittel benutzt zu haben.

Martin Voelker

Berlin, den 23. April 2018

Abstract

The focus of this thesis is the geospatial analysis of both fluvial and glacial landforms in Hellas Planitia Mars. The ancient impact structure contains the deepest point on the surface, and hence, the highest air pressure. Its interior is among the places with the highest likelihood for the transient existence of liquid water and the highest protection against solar radiation (both with implications for potential past or present habitability). The investigation of landforms with respect to their geographical distribution, evolution, and mutual relation, is essential for any attempt to link form to process, i.e. to reconstruct climatic conditions through the study of surface morphology.

In order to quantify the distribution of 24 pre-selected landforms in Hellas Planitia, the so-called grid-mapping method has been applied; i. a. for glacier-like flows, gullies, sheet deposits, and latitude-dependent ice-dust deposits. The results provided evidence about possible clockwise-rotating wind circulation systems within Hellas Planitia. Moreover, a lack of glacial features and gullies in the lowest parts of the basin has been detected; despite the high air pressure potentially allowing water to be liquid. The systematic search at high-resolution scale did also not reveal clear evidence for extensive shoreline morphologies as suggested by several authors; hence a hypothesized lake within Hellas Planitia could not be confirmed.

Among others, grid-mapping revealed widespread lobate sheet deposits at the lower reaches of Dao Vallis in eastern Hellas Planitia (being one of the big outflow channels draining into the basin). Similar features have already been interpreted in several regions of the planet as either volcanic or fluvial origin. Assessing both scenarios, a water-related formation is more likely, as most surface features can be better explained by fluvial rather than volcanic processes. The result is consistent with other stratigraphic findings and formation scenarios of the related Dao Vallis system.

This work revealed that Hellas Planitia has always been a matter of environmental change. While there is many evidence for fluvial activities during all Martian epochs (e. g., light-toned deposits, channels, gullies), there are also several indications of glacial activities (glacier-like flows or viscos-flow features). However, the results of this work do not support the existence of a lake within that vast depression.

This thesis has demonstrated that grid mapping is a very helpful and effective method for quantifying the distribution of landforms over huge areas, revealing information and relations about climate and landscape evolution, which are only visible from a much wider perspective; from ancient Noachian to very recent Amazonian landforms. For future research this approach can also be applied to other terrestrial bodies and space missions.

Kurzfassung

Im Zentrum der folgenden Arbeit steht die räumliche Analyse fluvialer und glazialer Oberflächenformen im Hellas Becken, Mars. Die sehr alte Impaktstruktur beinhaltet die tiefsten Punkte der planetaren Oberflächen, und Folge dessen auch den höchsten Luftdruck. Daher gilt das Innere des Beckens als einer der wahrscheinlichsten Orte, an dem flüssiges Wasser temporär an der Oberfläche existieren kann. Des Weiteren bietet die hohe Luftsäule auch einen erhöhten Schutz gegen lebensgefährdende solare Strahlung. Diese beiden Aspekte machen das Hellas-Becken zu einem besonderen Ort auf der Suche nach heutigem und historischem Leben außerhalb der Erde. Die Untersuchung von Oberflächenformen bezogen auf ihre geographische Verteilung, Evolution und gegenseitige Wechselwirkungen, ist daher ein wesentlicher Bestandteil die Prozesse zu verstehen, die jene Morphologien entstehen ließen. Dadurch ist es möglich, klimatische Bedingungen zu rekonstruieren, die zur Entwicklung bedeutsamer Geländeformen geführt haben.

Um die geographische Verteilung von 24 vordefinierten Oberflächenformen im Hellas-Becken zu quantifizieren, wird im Folgenden die sogenannte Grid-Mapping Methode angewandt. Unter anderem für gletscher-ähnliche Formen, Erosionsrinnen, Schichtablagerungen, und breitengradabhängige Eis/Staub Ablagerungen. Die Ergebnisse geben Hinweise auf einen im Uhrzeigersinn wehenden Windfluss innerhalb des Beckens. Darüber hinaus wurde trotz des hohen Luftdrucks (welcher flüssiges Wasser ermöglicht) ein weitgehendes Fehlen glazialer Formen und Erosionsrinnen in den tiefsten Bereichen des Impaktbeckens festgestellt. Das systematische Sichten auf Basis hochauflösender Bilddaten konnte ebenfalls keine klaren Indizien für die Existenz alter Küstenlinien auffinden, wie von einigen Wissenschaftlern vermutet. Dadurch kann die Theorie eines ehemaligen Meeres in Hellas Planitia nicht unterstützt werden.

Des Weiteren enthüllte die Grid-Mapping Methode die Existenz sogenannter Schichtablagerungen am Unterlauf des Dao Vallis im östlichen Hellas-Becken; einer der großen Talsysteme die sich einst in Hellas ergossen. Ähnliche Ablagerungen wurden bereits in anderen Regionen des Mars als vulkanischen oder fluvialen Ursprungs interpretiert. Werden beide Szenarien gegenübergestellt, so erscheint eine hydrogene Entstehung plausibler, da die hier vorgestellten Ergebnisse stratigraphisch und genetisch zur hydrogenen Entstehung des anliegenden Dao Vallis passen.

Die vorliegende Arbeit belegt, dass Hellas Planitia seit jeher Änderungen unterlegen war. Nebst vielen Hinweisen auf fluvialen Aktivitäten (helle, geschichtete Ablagerungen, ausgetrocknete Fließgewässer und Runsen), gibt es auch Hinweise auf glaziale Prozesse (gletscherförmige Zungen und viskose Fließformen). Aber die bedeutende Frage, ob es jemals einen großen See in

dieser großen Niederung gab, kann basierend auf den Ergebnisse dieser Arbeit nicht unterstützt werden.

Die vorliegende Arbeit hat belegt, dass Grid-Mapping eine sehr hilfreiche und effektive Methode bei der räumlichen Quantifizierung von Oberflächenformen über große Gebiete ist. Sie ist in der Lage Informationen und Beziehungen über Klima und Landschaftsentwicklung zu enthüllen, welche nur aus einem größeren Blickwinkel festgestellt werden können; angefangen bei alten den Noachischen Formen bis hin zu den sehr jungen Amazonischen Morphologien. Für künftige geowissenschaftliche Untersuchungen anderer terrestrischer Himmelskörper kann dieser Ansatz daher auch von großem Nutzen sein.

Contents

Abstract 5
Kurzfassung 6
List of Figures 10
List of Tables 11
List of Abbreviations 12
Preface 13
Introduction 14
Motivation 14
Structure of Thesis 15
1. Background 17
1.1 Hellas Planitia 17
1.2 Grid-Mapping 20
1.3 Sheet Deposits 21
1.3.1 Volcanic Deposits 23
1.3.2 Fluvial Deposits 23
1.3.3 Glacial Deposits 25
2. Methods 27
2.1 Data 27
2.2 Grid-mapping 28
2.3 Mapping of Sheet Deposits 32
3. Results 35
3.1 Grid-mapping 35
3.1.1 Topography 35
3.1.2 Ice-related Landforms 35
3.1.3 Water-related Landforms 52
3.1.4 Other Landforms 58
3.2 Sheet Deposits 59
3.2.1 Geography and Physical Properties 61
3.2.2 Stratigraphy and Age Determinations 64
3.2.3 Thickness and Volume of Sheet Deposits 67
3.2.4 Comparison with Volcanic Sheet Flows on Mars 68
3.2.5 Hydrologic Assessment 69
3.2.6 Terrestrial Analogues 71
4. Discussion 74

4.1 Geography of Hellas Planitia 74
4.1.1 Ice-related Landforms 74
4.1.2 Water-related Landforms 79
4.2 Sheet Deposits in eastern Hellas 84
4.2.1 Geomorphology 84
4.2.2 Evolution 88
4.3 Synthesis 94
5. Conclusions 99
Summary 102
Acknowledgements 104
References 105
Curriculum Vitae 123
List of Publications and Conference Contributions 124

List of Figures

Fig. 1. Topographic map of Hellas basin with major geographic names approved by IAU. 18
Fig. 2. Wind circulation systems in and around Hellas Planitia (grey circle). 19
Fig. 3. Slope map based on MOLA data. 20
Fig. 4. Sheet deposits in eastern Hellas Planitia cover the banks of Dao Vallis. 22
Fig. 5. Topography of the study area (for location see Fig. 1). 24
Fig. 6. THEMIS-nighttime imagery (8-bit) for Hellas (USGS), centered at $\lambda = 69°$, $\varphi = 49°$. 27
Fig. 7. Multilayer coverage of an exemplary grid cell. 28
Fig. 8. Weighting factors used for the interpolation of the grids. 29
Fig. 9. Hypsometric curve for Hellas based on MOLA and the 20×20 km grid. 35
Fig. 10. Gridmap showing selected ice-related landforms in Hellas Planitia. 37
Fig. 11. Various morphologic expressions of LDM in Hellas. 38
Fig. 12. Muted and dissected LDM terrain north of Dao Vallis. 38
Fig. 13. Deflected scalloped terrain at the southern rim of Hellas Planitia. 39
Fig. 14. Box-Whisker plot showing the distribution of landforms regarding their absolute elevation. 41
Fig. 15. Box-Whisker plot showing the relative distribution of landforms regarding their elevation. 42
Fig. 16. Box-Whisker plots showing the distribution of landforms regarding their absolute slope. 43
Fig. 17. Box-Whisker plot showing the relative distribution of landforms regarding their slope. 44
Fig. 18. Boxplot presenting the absolute Thermal Inertia values of selected landforms. 45
Fig. 19. Boxplot presenting the relative Thermal Inertia values of selected landforms. 46
Fig. 20. Boxplot presenting the absolute dust cover index values (DCI) of selected landforms. ... 47
Fig. 21. Box-Whisker plot showing the relative distribution of landforms regarding their DCI. ... 48
Fig. 22. Banded terrain in the Alpheus Colles region. 49
Fig. 23. Crater filled with layered-remnant deposits (LRD). 50
Fig. 24. Normalized line graph contrasting the aspect behavior of scalloped terrain, VFF, and gullies. 51
Fig. 25. Gridmap showing the geography of potential water-related landforms. 53
Fig. 26. Extensive sheet deposits covering the banks of the lower Dao Vallis region. 54
Fig. 27. Relative elevation distribution of channels and light-toned deposits. 54
Fig. 28. Light-toned deposits in a nameless crater on the western Hellas floor. 56
Fig. 29. Geological and geomorphological map provides information about the geospatial behavior of sheet deposits in the study area in eastern Hellas Planitia. 60
Fig. 30. Conically shaped lineations on top of a sheet deposit. 61
Fig. 31. Left: Dendritic channel system on top of sheet deposit unit Asd4. 62
Fig. 32. Polygonal structures are only visible in high-resolution HiRISE images. 63
Fig. 33. Crater size-frequency distribution and modelled formation age of each sheet deposit unit. 65
Fig. 34. Correlation of units in the study area. 66
Fig. 35. Plot presenting the averaged profile of two parallel MOLA single shot datasets of a flow front of unit Asd5. 66
Fig. 36. HiRISE imagery of volcanic flows and the examined sheet deposits in Hellas. 70
Fig. 37. Image of the Mjezzem salt pan 35 km northeast of Ghadames, Libya. 72

Fig. 38. Small-scale mud flow on Svalbard at Kongsfjorden in summer 2016. 73
Fig. 39. Sketch illustrating the erosion of LDM by wind 76
Fig. 40. Juxtaposition of gully morphologies of similar sized craters in eastern Hellas. 85
Fig. 41. Lineations on a dry landslide in Valles Marineris (Coprates Chasma). 86
Fig. 42. Oblique view of Hadriacus Mons (HM), as well as the source regions of Dao Vallis (DV) and Niger Vallis (NV). 91
Fig. 43. Fluvial evolution of sheet deposits in eastern Hellas. 92
Fig. 44. Relative distribution of channels, light-toned deposits, and sheet deposits regarding their elevation. 95
Fig. 45. Stratigraphy and correlation of ice-related, water-related, and other landforms based on grid-mapping results. 98

List of Tables

Table 1. Rheologic, geomorphic, and sedimentary characteristics of fluvial sediment flows on Earth. 26
Table 2. Gathered features and parameters for the study area. 30
Table 3. Categories used in grid-mapping. 30
Table 4. Classification for each parameter for linear graphs. 31
Table 5. Morphometric properties of each sheet deposit unit of the study area and selected volcanic flows. 67
Table 6. Water volumes implied from sediment volumes for different transport types. 71

List of Abbreviations

CRISM	Compact Reconnaissance Imaging Spectrometer for Mars
CSFD	Crater-Size Frequency Distribution
CTX	Context Camera
DCI	Dust Cover Index
DEM	Digital Elevation Model
DLR	Deutsches Zentrum für Luft- und Raumfahrt
GIS	Geographic Information System
HHT	Hellas-Hesperia-Trough
HiRISE	High Resolution Imaging Science Experiment
HRSC	High-Resolution Stereo Camera
IAU	International Astronomical Union
LDM	Latitude-Dependent Mantle
LRD	Layered Remnant Deposit
LTD	Light-Toned Deposit
MOLA	Mars Orbiter Laser Altimeter
OMEGA	Observatoire pour la Minéralogie, l'Eau, les glaces et l'Activité
TES	Thermal Emission Spectrometer
THEMIS	Thermal Emission Imaging System
TI	Thermal Inertia
USGS	United States Geological Survey.
VBF	Vastitas Borealis Formation
VFF	Viscous-Flow Feature

Preface

In summer of 2003, the planet of Mars made its closest approach to Earth since over 60,000 years, being merely 55.8 million kilometers away from mankind. In that summer, I stared up into the skies of southern Germany and pointed my telescope towards the sparkling Red Planet. Although my telescope was relatively small, I was able to see a far world over yonder; surrounded by a deep darkness. But this little planet was not empty. I noticed a small white dot at its limb that turned out to be the remnant of the south polar cap. In the center of the disk there was a darker spot, called Syrtis Major (the Great Bay); a huge volcanic province dissected by troughs and ridges. And between these two features an even bigger structure caught my eye. It seemed to be very large and circular, but very pale in color. After I have consulted the old, still airbrushed, Martian maps on the endpaper of my book about Mars, I found that this dot has been named Hellas Planitia (Plain of Greece). Furthermore, the book told me that the feature is one of the largest and deepest known impact basins of the Solar System. The impact was so severe that it even weakened the planetary crust causing the evolution of huge volcanoes along its massive crater rim. Another unique character of Hellas Planitia is its huge depth, and hence, dense and active atmosphere. Thus, the impact basin is a major dustbowl of the planet, generating extensive dust storms. I noticed that this part of Mars is one of the most prominent features planetwide, and I became very curious how the landscape in that basin must look alike. I imagined a desolate and far plain beyond all measure. But I did not imagine that I would ever take a closer and professional look at this landmark. More than ten years later I got the unexpected chance to gain my doctoral degree by researching Hellas Planitia at the German Aerospace Center. So I was able to see what really existed in the depths of this huge basin: It was not desolate and plain at all! I found mountains, cliffs, channels, and deep chasms. Moreover, I noticed that my PhD supervisor was one of the three authors of the book about Mars I read these early days. So I finally worked on –that- Hellas Planitia; the structure I have seen with my own telescope many years before; the structure that seemed to be so far out of reach. But sometimes things come true you never believed to be possible. Considering this, I felt very welcome in space science and Hellas Planitia.

Introduction

Motivation

Located in the southern mid-latitudes of Mars, Hellas Planitia is the second-largest confirmed impact basin on the planet, with a diameter of 2,300 km. The basin also contains the topographically lowest parts of Mars, and hence, the highest atmospheric pressure on the planet of up to 11 millibar (Carr, 2006). Air and surface temperatures vary by season from ~150 to 275 K and 307° K, respectively (Millour et al., 2015 and Forget et al., 1999). Thus, this vast depression is one of the atmospherically most active regions of Mars as shown by the seasonal dust storm activity (e. g., Cantor et al., 2001; Cantor, 2007), and one of the few areas were liquid water might occur on the surface until today (Haberle et al., 2001). These conditions make Hellas a vital region on Mars to understand the distribution of landforms caused by water and ice, which, in turn, are of special astrobiological interest.

As a counterpart to the northern lowlands (Vastitas Borealis Formation, VBF) Hellas Planitia is also located at a mid-latitudinal positon, ranging from ~30° to 55°S. Both lowlands are located well below the Martian mean radius. While the average elevation of VBF is approx. 5,000 m (absolute minimum -7,000 m in Lyot crater, 50°N, 29°E), most of Hellas Planitia is located around -6,500 m (absolute minimum is -8,500 m in Badwater crater). Despite their geographical similarities their geomorphology varies. While most of VBF is relatively smooth and even, the floor of Hellas provides diverse facies. The northern lowlands have been studied in detail within the last decades; in contrast, research on Hellas Planitia was limited due to insufficient data coverage. Caused by its thick and dusty atmosphere, the interior of the basin is often filled with a dense haze, hindering the view down to its surface. However, this lack of high-resolution datasets was mostly overcome during the last few years when modern cameras monitored Hellas at a high spatio-temporal and visual resolution.

Orbital images show a high diversity of (peri-)glacial, fluvial and possibly lacustrine landforms on the basin floor; some of which are unique to the basin, like the banded terrain (Diot et al., 2014 and 2016) or the honeycomb terrain (Bernhardt et al., 2016). Similar to the northern plains, Hellas has big outflow channels too, draining into the basin. This observation led several authors to the assumption that a big lake once existed in Hellas (e. g., Moore and Wilhelms, 2001; Ansan et al., 2011).

The following thesis presents a methodic and scientific approach to combine the geography and geology of Hellas Planitia, and how to link each geomorphological process response system to another. The main questions are what system imbalances have led to the development of glaci-

ers and rivers, and possibly lakes, and what imbalances have (currently?) ceased their further genesis? And maybe the results found in Hellas can be transferred to the higher elevated parts of the planet. As Hellas has an air pressure of up to 11 mbar it might represent an historic environment that once was abundant everywhere on Mars when air pressure exceeded 10 mbar globally.

In order to derive even more information, the methods were not just focused on geologic and geomorphologic studies; a third compound, large-scale distribution of landforms, was also studied by applying the so-called grid-mapping method. In contrast to classic geologic maps (polyline) this method is based on a tick box approach (polygon) in order to gather spatial information of landforms quantitatively (Ramsdale et al., 2017). Each of these boxes has a size of 20×20 km and was examined at comparatively high resolution of 1:20,000; however, due to the large extend of the study area only every second grid has been mapped (~10,500 grids). The bypassed grids were interpolated after mapping has completed. By using this method, it was possible to analyze processes that are only visible from a wider perspective. However, this quantitative approach cannot stand alone in order to understand the evolution of such a huge impact basin. Besides this large-scale method this work contains a qualitative small-scale approach too. This is important as small landforms can act as little keys, being able to reveal large processes. In eastern Hellas such a key was identified in form lobate and multi-layered sheet deposits. For these deposits, the main motivation was to test if they are of volcanic, glacial, or fluvial origin. Hence, a classic geologic map of a small study area in eastern Hellas has been prepared. This was necessary to visualize and understand the geographic behavior and stratigraphy of sheet deposits. Moreover, volumetric measurements were made to analyze thickness and volumes of these deposits. By analyzing these sediments, it is possible to reconstruct the age, transport mechanism (volcanic, fluvial, or glacial), and potential water content (if of fluvial origin) that is required to deposit these sediments.

Combining these results on both large-scale and small-scale mapping (distribution, stratigraphy, and physical properties of landforms) it is possible to understand the evolution of Hellas Planitia, as the most important southern lowland, once and today.

Structure of Thesis

The text of the presented work is organized in a classic monographic manner combining elements taken over from two published papers. Additionally, the results of these papers are synthesized into one big picture, testing how well they can complete each other.

Voelker, M., Hauber, E., Schulzeck, F., Jaumann, R., 2017. Grid-mapping Hellas Planitia, Mars – Insights into distribution, evolution and geomorphology of (Peri)-glacial, fluvial and lacustrine landforms in Mars' deepest basin (Planet. Space Sci. 145, p. 49–70, doi:10.1016/j.pss.2017.07.012) has been published in Planetary Space Science. Application of the methods, interpretation of the results, creation of figures, and writing has been done by the main author. The idea, and grammatical improvement, as well as the design of some graphs (*Fig. 14* to *Fig. 21*) were provided by the co-authors. Some minor improvements were made by one anonymous reviewer.

The paper *Voelker, M., Hauber, E., Stephan, K., Jaumann, R., 2018. Volcanic flows versus water- and ice-related outburst deposits in eastern Hellas: A comparison (Icarus 307, p. 1–16, doi:10.1016/j.icarus.2018.02.023)* was published in Icarus. The main work; idea, application of the methods, maps and imagery, scientific interpretation, and writing has been carried out by the main author. The paragraphs describing methods and results of spectral data, contributed by K. Stephan are from line 727 to 754 and line 1,189 to 1,199. Further support of the co-authors and two anonymous reviewers was provided in form of scientific discussions and grammatical improvements.

The focus of this manuscript is an overall discussion of landforms found in Hellas Planitia. The structure of this work is separated into five main parts Background, Methods, Results, Discussion, and Synthesis, plus an Introduction and Summary.

The first part is introducing the study area, Hellas Planitia, presenting its environment and geology, based on state-of-the-art research. The chapter also contains an introduction into previous work about the newly developed grid-mapping method in planetary sciences as well as information about sheet deposits as possible proxies for landscape evolution.

The second chapter describes the applied methods (grid-mapping, photogeologic mapping, hydrologic calculations, and spectroscopy) and the datasets used.

The results of both the grid-mapping and the analysis of sheet deposits in eastern Hellas are provided in chapter three. The results of grid-mapping comprise its general topography as well as the distribution of landforms like ice- and water-related features. In order to provide a wide range of information, the results of landforms deemed less important for this work is presented too. The chapter also contains the results gained for the sheet deposits (geography, physical properties, stratigraphy, and age determinations). Furthermore, volumetric measurements of these sediments are presented. For comparing different transport mechanisms the properties of volcanic sheet flows and possible terrestrial analogues are presented too.

Possible interpretations of the results are discussed in chapter four. First, possible formation scenarios on a large-scale for both ice-and water-related surface features are presented; mainly based on their geography. Afterwards, the discussion narrows to a smaller scale; the evolution of sheet flows and their morphologies.

Finally, in chapter five the results and formation hypotheses of all landforms in Hellas Planitia are synthesized into one big picture; the large-scale results of grid-mapping are combined with those of the sheet deposits in eastern Hellas. Moreover, it is discussed how well the results fit into existing theories.

1. Background

1.1 Hellas Planitia

With a diameter of 1,500×1,900 km and a depth of up to 8,500 m below the Martian datum, Hellas Planitia is the biggest and deepest obviously visible impact basin on Mars (*Fig. 1* and *Fig. 3*). Formed 3.99±0.01 Ga ago (Werner, 2008) by an impactor measuring approximately 550 km (Arkani-Hamed, 2005), it is the most distinct physiogeographic feature on the southern highlands. Its highly elliptical form either suggests that Hellas Planitia might be a double-impact basin (Arkani-Hamed, 2010) or an oblique impact event (Leonard and Tanaka, 2001). Despite of its size, no inner impact rings can be distinguished. The rim of the basin is severely dissected. Only its northwestern half is more or less intact. To the east, the rim is breached by the so-called Hellas-Hesperia trough (HHT), and to the south by Malea Planum. Especially the latter is important for the climatic conditions of the Hellas basin as it induces the influx of cold air draining down from south polar highlands.

The landforms within Hellas are very diverse. Its discontinuous rim rises up to 5,000 m above the interior plains. Two breaches in the rim, measuring 600 to 900 km, occur in the east and southwest. Both gaps are apparently caused by volcanic processes, and show significant outflow channels, e. g., Dao Vallis, Harmakhis Vallis and Axius Valles (Tanaka and Leonard, 1995; Leonard and Tanaka, 2001; Williams et al., 2010). The bottom of Hellas Planitia can be separated into three major regions; Peneus Palus in the northwest is the lowest plain in Hellas and is mainly a flat and level lowland. However, it also contains some landforms, i.e. the honeycomb and reticulate terrain (Diot et al., 2014), that seem to be unique in Hellas. Moreover, there are several solitary peaks, located in circular depressions (Zuschneid and van Gasselt, 2015). At its easternmost point, Hellas Chasma, an up to 1,000 m-deep trough measuring 160 km in length and around 22 km in width. The second major region is characterized by the hilly terrain of Alpheus Colles, which covers the central plains of Hellas and shows a rugged surface consisting of myri-

ads of rounded knobs. The most enigmatic landform is the so-called banded terrain (Diot et al., 2014, 2016), which seems to be linked to the adjacent honeycomb and reticulate terrain in Peneus Palus. The third major region is an unnamed plain in eastern Hellas. It consists of an extensive set of wrinkle ridges, and is cut by Dao and Harmakhis Valles, which are crossing through this plain. Several chaotic terrains are located at the border between this area and Alpheus Colles. At its northwestern end this region transitions into Coronae Planum, a relatively small plain with a very smooth surface. This observation led several authors to the assumption that a big lake once existed in Hellas (e. g., Moore and Wilhelms, 2001; Ansan et al., 2011).

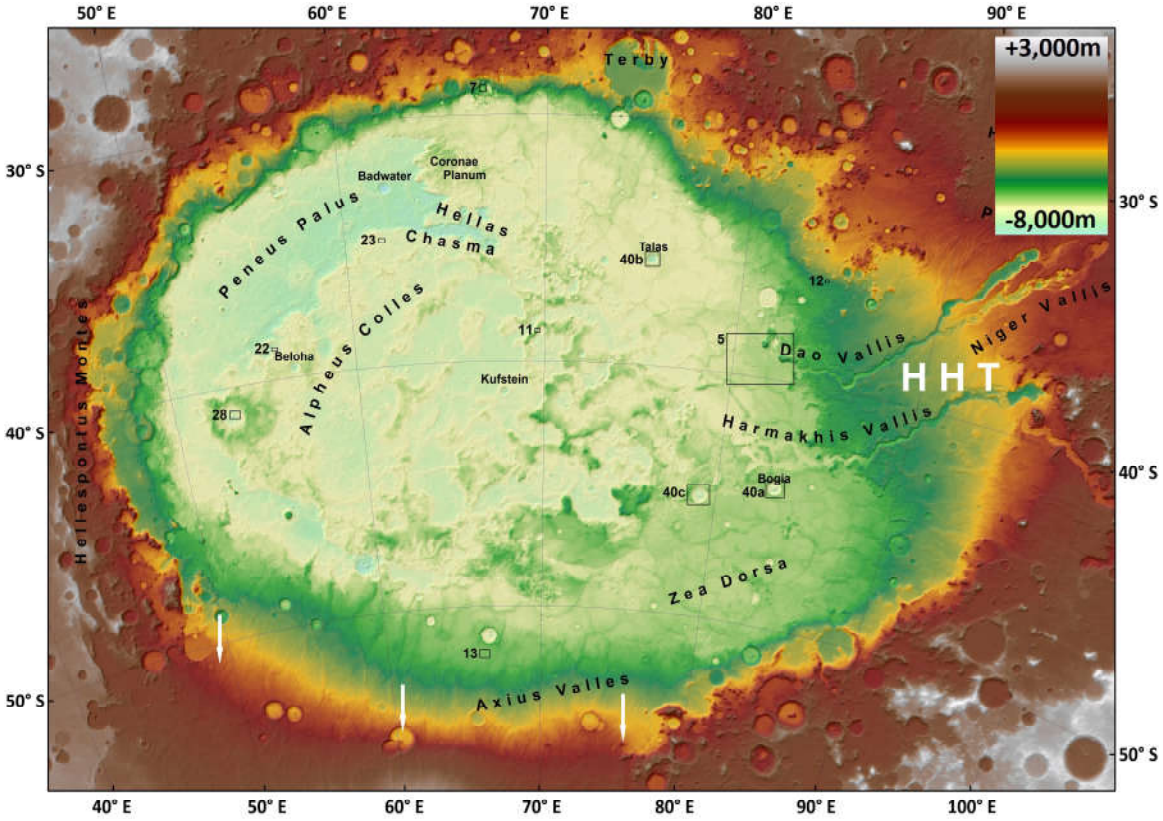

Fig. 1. *Topographic map of Hellas basin with major geographic names approved by IAU. The white arrows indicate the Malea Planum breach; HHT = Hellas-Hesperia trough; numbered boxes indicate locations of the corresponding figures; location of images used for studies about sheet deposit (red box) are shown in Fig. 5. Basemap: MOLA*

The geology of Hellas Planitia has already been mapped by several authors (e. g., Leonard and Tanaka, 2001; Bernhardt et al., 2016). Both suggest intensive Noachian and Hesperian magmatic activity and fluvial erosion on the basin's floor and rim, linked to the adjacent volcanic provinces to the east and south. Since the late Hesperian, intensive aeolian erosion affected the research area. Geophysically, the Martian crust shows in Hellas Planitia its lowest thickness values of just 5 to 15 km (Neumann et al., 2004).

Climatically, Hellas Planitia is of global importance. Its high air pressure is unique on the planet. Together with surface temperature highs of up to 307°K (Millour et al., 2015 and Forget et al., 1999), its environment can exceed the triple point of water easily. Moreover, it is one of the major topographical depressions on the planet having a high air pressure, and hence, being able to lift dust particles and produce dust storms (Cantor et al., 2001; Cantor, 2007). They are mainly caused by strong wind currents within the basin, which, in turn, are a result of Hellas Plantia's location and morphological arrangement (e. g., Ogohara and Satomura, 2008). Wind currents rotate clockwise in Hellas (Ogohara and Satomura, 2008; Howard et al., 2012), caused by two factors; (1) the breached rim at Malea Planum in SW Hellas supports katabatic winds, draining down northwards from cold south polar highlands (Howard et al., 2012), and (2) global westerlies in southern mid-latitudes force the air in northern Hellas to move east (Kahre et al., 2014). Several authors suggest these strict wind directions are the reason for the today's morphology of the basin floor. For example, Howard et al. (2012) and Bernhardt et al. (2016) hypothesize the evolution of the Peneus Palus depression might be caused by aeolian erosion. Another climatic phenomenon is the extension of the south polar cap up to 50°S, affecting the southernmost part of Hellas (Hansen et al., 2010).

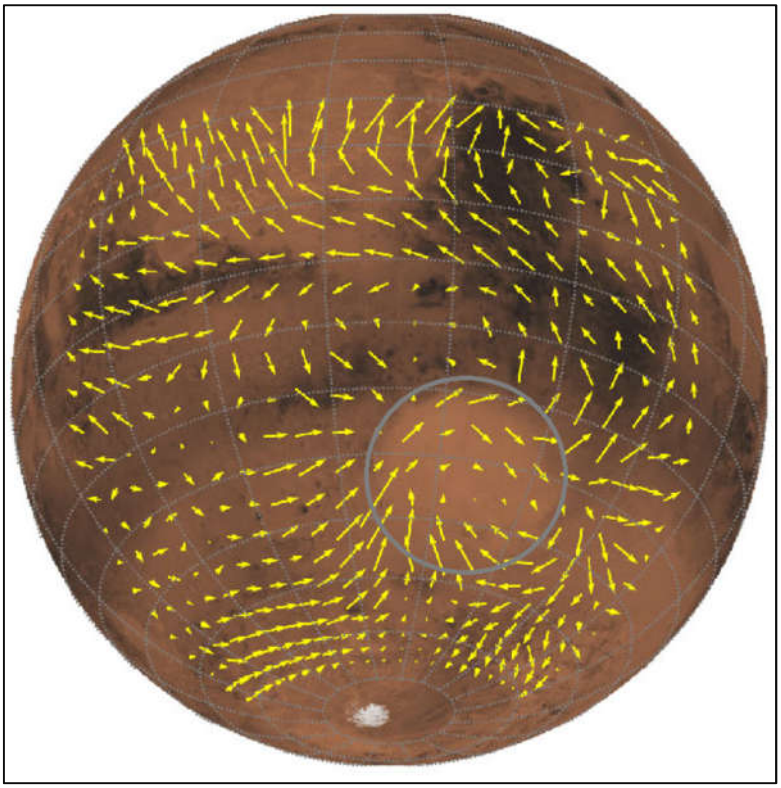

Fig. 2. *Wind circulation systems in and around Hellas Planitia (grey circle) based on the results of Howard et al. (2012). The longer the arrows the stronger the winds. The bright dot at the bottom is the southern polar cap. Please note the clockwise rotating winds within Hellas, and the main influx at its southwestern rim (long arrows). Imagery: Howard et al. (2012)*

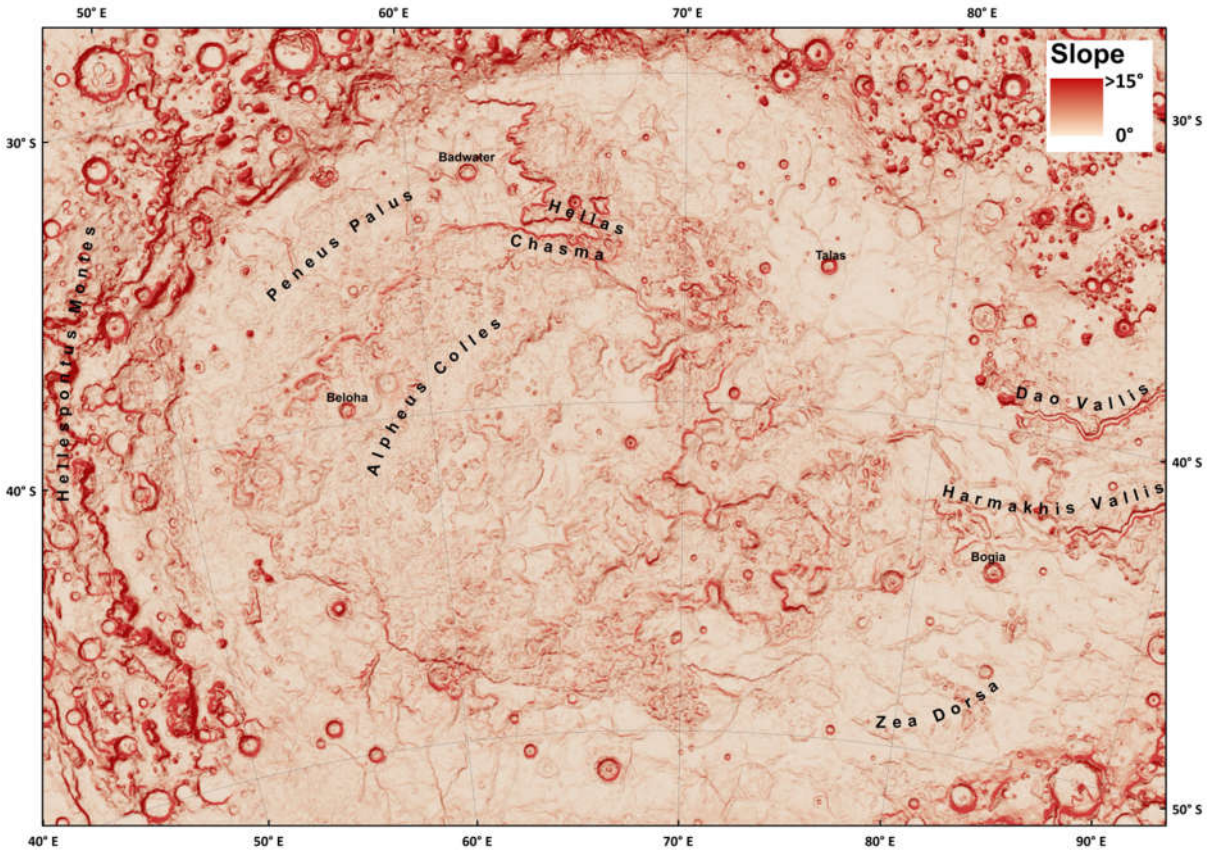

Fig. 3. *Slope map based on MOLA data. Stereographic projections centered at λ = 69°, φ = 49°. Please note that in wide parts of the basin there is a rough topography.*

1.2 Grid-Mapping

Because of its vast size and its high geographical diversity, the newly developed grid-mapping method has been applied (Ramsdale et al., 2017) in an ArcGIS-environment to contextualize the inventory of landforms and the landscape characteristics such as elevation, slope, and aspect (see chapter 2.2 for detailed description). This enabled quantifying the presence of selected landforms with respect to their geographic distribution. Grid mapping has already been applied successfully in the northern Martian lowlands (Brooker et al., 2015; Orgel et al.,2015; Ramsdale et al., 2017; Séjourné et al., 2015; Hauber et al., 2015). In contrast, Hellas Planitia, located on the opposite hemisphere, complements the work of mid-latitudinal and low-elevated landforms on Mars. By applying the grid-mapping method it was possible to examine Hellas for the first time in a high-resolution scale of 1:30,000. Thus, the evolution of the most recent glacial landforms in Hellas could be examined; e. g., its hydrological history, or if there are possible ancient shorelines. This technique enables to visualize and investigate the regional distribution patterns in a statistical and cartographic way. As a result, information about the evolution and interaction of several landforms like the latitude-dependent mantle (LDM) and the scalloped terrain could be derived.

1.3 Sheet Deposits

The intention of this work is not only the study of large-scale distribution of landforms, but the small-scale analyses of landforms too. Landforms, that are able to act as records for the morphologic evolution of Hellas Planitia. Sheet deposits, the remains of former sheet flows, were identified as such a proxy. Their stratigraphy and morphology allow both age determination and the identification of transport mechanisms. Hence, they help to approach the answer of vital questions. When did the outflow channels in eastern Hellas evolve? What kind of liquids formed them? Were the outflow channels able to fill the basin with water, making Hellas a vast sea?

Sheet deposits on Mars are extensive blankets of either sedimentary and/or volcanic material, which are often characterized by relatively high thermal inertia values (Kreslavsky and Head, 2002a; Burr and Parker, 2006; Keszthelyi et al., 2007; Voelker et al., 2013; Marra et al., 2015) presented in *Fig. 4*. The aim of this study is to provide a detailed discussion about the origin and evolution of sheet deposits in eastern Hellas. As very similar deposits are found in many different locations on Mars, their understanding can shed light on the sedimentary and volcanic evolution of the planet. Comparable flow deposits have previously been interpreted as the products of either volcanic (e. g., Fuller and Head, 2002; Hoffman and Tanaka, 2002; Leverington, 2011) or fluvial processes (Hoffman and Tanaka, 2002). Many of these deposits are observed close to volcanic regions (e. g., Tharsis and Elysium), suggesting a volcanic origin (e. g., lava flows or pyroclastic deposits). However, it appears likely that some of the sheet deposits might be of so-called (cryo-)fluvial origin, as they are apparently related to fluvially formed channels, e. g., Grjotá Valles (Burr and Parker, 2006) or Havel Vallis (Voelker et al., 2013) whose released flows were partially frozen under subaerial Martian conditions, resulting in a mixture of slurry ice and sediments. For the circum-Chryse outflow channels Kreslavsky and Head (2002a) suggested that suspensive sediment-laden currents might have debouched into the northern lowlands and filled them. Below, a geomorphological study of sheet deposits at the lower reaches of Dao Vallis (*Fig. 1* and *Fig. 5*), an outflow channel which is linked to a Hesperian/Noachian aged shield volcano, Hadriacus Mons (Leonard and Tanaka, 2001; Tanaka et al., 2014) is presented. By analyzing both geomorphology and the geographic context of these deposits, it is possible to juxtapose a fluvial and volcanic scenario of these deposits in order to understand their evolution. If sheet deposits were formed by cryo-(fluvial) processes they might provide insights into the earliest stages of the evolution and deposition of outflow channels, and might be hence, a complementary new agent in the hydrologic balance of the planet.

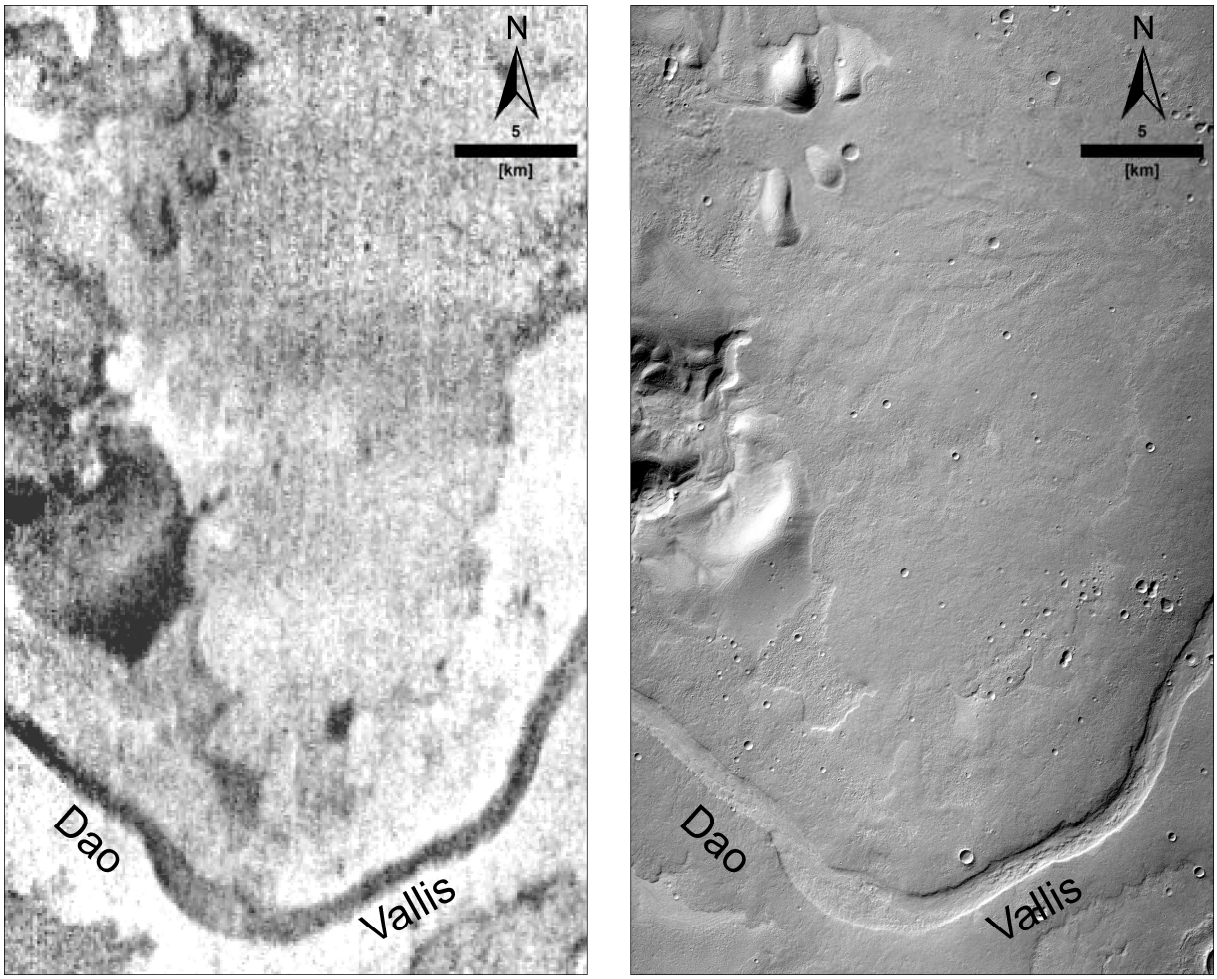

Fig. 4. *Sheet deposits in eastern Hellas Planitia cover the banks of Dao Vallis. Left: In THEMIS datasets these deposits are often characterized by high thermal inertia values presented in white color. Right: Note the lobate flow fronts and multiple layers. For location see Fig. 5.*

On Mars, several locations exhibit landforms which can be described as sheet deposits, e. g., Cerberus Fossae (Plescia, 2003), Arsia Mons (Mouginis-Mark and Christensen, 2005), Grjotá Valles (Burr and Parker, 2006), and Havel Vallis (Voelker et al., 2013). However, there is no common definition about the morphology of sheet deposits yet. They are characterized by laterally widespread, lobate flow fronts, and are mostly linked to adjacent channels and/or volcanic edifices. They are commonly arranged in multiple layers covering each other (e. g., Plescia, 2003; Voelker et al., 2013). In the published literature, they are commonly described as lava flows/flood lavas (e. g., Keszthelyi et al., 2004), or flood sediments (Burr and Parker, 2006), among others; dependent on the formation process each author preferred. Hereafter, the non-interpretative term sheet deposits is used.

1.3.1 Volcanic Deposits

On Mars, there are three major volcanic provinces of Hesperian to Amazonian age (Tanaka et al., 2014); Hesperia, Tharsis and Elysium; the two latter sites also show extensive sheet flows with distinctive flow fronts. As all regions show deposits of unambiguously volcanic origin, they are used as a reference of volcanic sheet deposits.

As on Earth, volcanic deposits on Mars are mostly composed of basaltic lavas, however, their ages and possibly rheology may vary (Carr, 2006). As a result, their morphological characteristics can be highly diverse. Assuming the same conditions for their development (e. g., effusion rates), the thickness of volcanic flows is supposed to be higher than terrestrial analogues, caused by lower gravity; however, their properties in viscosity and shear strength may be the same as on Earth (Wilson and Head, 1994). These conditions also allow flow lengths being up to six times longer than terrestrial lava flows (Wilson and Head, 1994).

1.3.2 Fluvial Deposits

On Earth there is a high diversity of fluvial mass wasting processes, resulting in a variety of classifications (e. g., Costa, 1988; Hutchinson, 1988; Varnes, 1978; Hungr et al., 2001). Hereafter, the concise and numeric nomenclature of Costa (1988) is applied. Based on texture, composition, and sorting, Costa (1988) described three main categories of terrestrial flood types: water flows, hyperconcentrated flows, and debris flows (*Table 1*).

Water floods are liquid mass movements with low sediment content. Their shear strength is extremely low. Water and clastic particles are two distinct phases. The main transport mechanisms of the sediments are rolling, saltation, and suspension (Costa, 1988).

Hyperconcentrated flows contain higher amounts of sediments (20 – 47%) than water floods. Thus, they show small to medium shear strengths. Water and sediments are still separated in two phases. Their rheological behavior is strongly influenced by the amount of fine-grained particles like clays or silts (Costa, 1988).

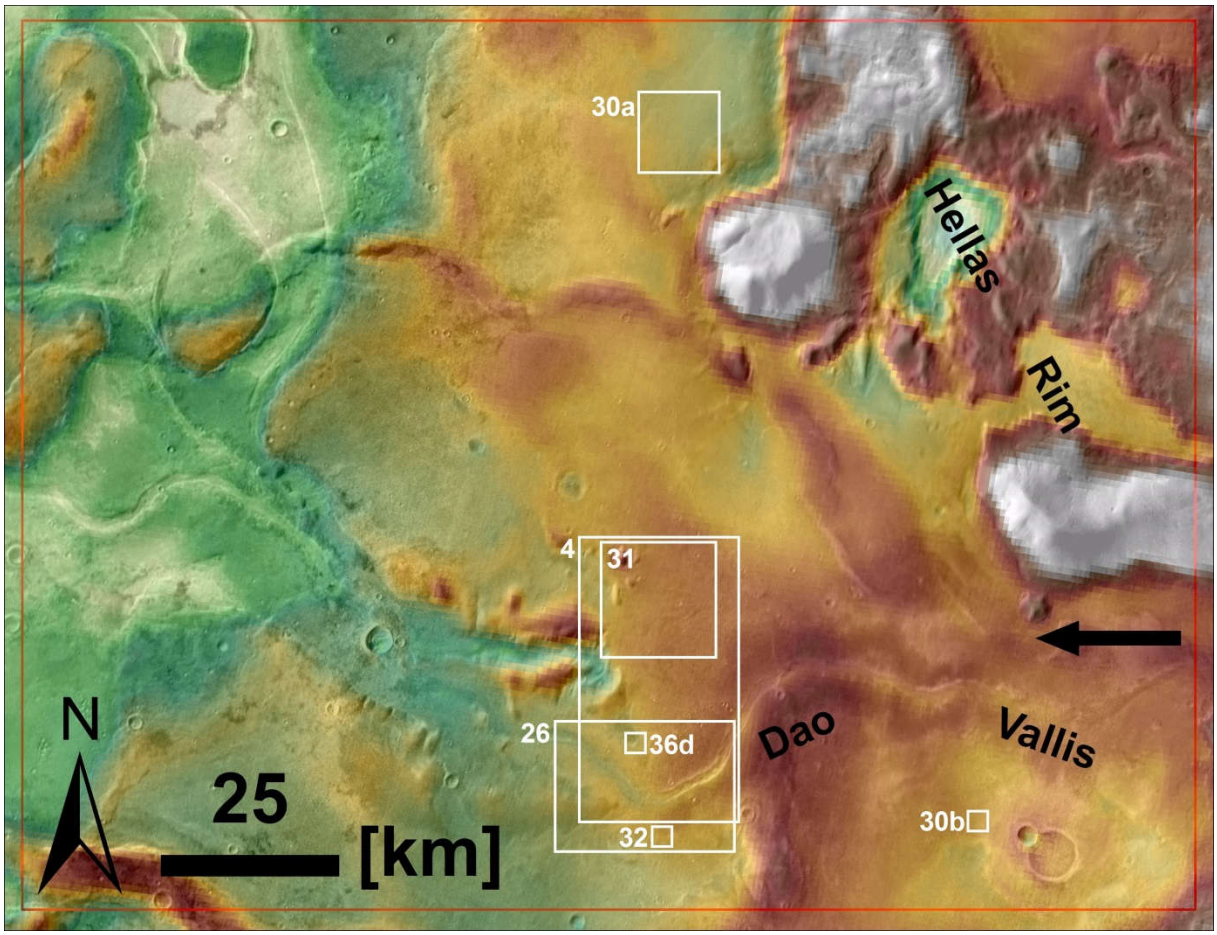

Fig. 5. *Topography of the study area (for location see Fig. 1). White boxes indicate the locations of the figures presented hereafter. The black arrow refers to the flow direction of Dao Vallis (Basemap MOLA and THEMIS).*

In debris flows both phases (water and sediments) move together, and thus, behave like one viscoplastic body (Costa, 1988). Hence, both the liquid and the solid phase move with the same velocity. Only extremely large and heavy particles may be deposited in the upper reaches of the flow while it is still running (Rodine and Johnson, 1976). Shear is confined to a thin horizontal boundary zone at the margins and the base of the flow. As for hyperconcentrated flows, the rheological behavior of debris flows depends on the amount of clays and silts (Costa, 1988). However, high amounts of small grain-sizes can also cause the debris flow to turn from a Newtonian fluid to a Bingham fluid (Parsons et al., 2001). This rheologic behavior can even cause an inverse sorting of the clasts transported; larger clasts are found near the surface of the flow, while smaller ones are concentrated at its base (Costa, 1984). A further important process indicative for debris flows is kinetic sieving along their flow fronts, causing an accumulation of large-sized particles. This concentration of, e. g., boulders, can cause an increase of friction within the flow front, and hence, a halt of the debris flow (Parsons et al., 2001).

For flows mainly composed of debris, Hungr et al. (2001) separated debris avalanches from debris flows. Their main morphological indicator for a debris avalanche is the absence of a distinctive channel, but the composition and rheology is the same or very similar to a debris flow. The deposits of debris avalanches are often arranged in widespread unconfined colluvial aprons, and do not usually use the same paths (Hungr et al., 2001). Moreover, they often occur in multiple surges.

1.3.3 Glacial Deposits

Lobate fan shaped deposits have also been described in glacial environments on Mars; e. g., along the northwestern flanks of the Tharsis volcanoes (e. g., Neukum et al., 2004a; Milkovich et al., 2006; Fastook et al., 2008). Their diverse morphologies comprise chaotic facies (interpreted as sublimation till), arcuate-ridged terrain (interpreted as the result of deposited supraglacial till deformed by the flow of underlying ice), and marginal ridges (interpreted as terminal moraines) (Milkovich et al., 2006). Due to their lack of fluvial features they have been described as cold-based piedmont glaciers (Milkovich et al., 2006). The origin of the ice material is likely caused by atmospheric precipitation (snow accumulation), deposited during episodes of high obliquity in Late Amazonian (Milkovich et al., 2006; Fastook et al., 2008).

Flood type	**Water flood**	**Hyperconcentrated flow**	**Debris flow**
Sediment concentration [by volume]	0.4 – 20%	20 – 47%	47 – 77%
Bulk density [g/cm³]	1.01 – 1.33	1.33 – 1.80	1.80 – 2.30
Fluid type	Newtonian	Non-newtonian (?)	Viscoplastic (?)
Viscosity [poise]	0.01 – 20	20 – ≥200	>>200
Fall velocity [% of clear water]	100 – 33	33 – 0	0
Predominant flow type	Turbulent	Turbulent to laminar	Laminar
Shear strength	Extremely low	Small to medium	Small shear at the base of the flow
Landforms and deposits	Bars, fans, sheets, splays, channel have large width-to-depth ratio	Similar to water floods	Marginal levees, terminal lobes, trapezoidal to u-shaped channel
Sediment characteristics	Rounded clasts, wide range of particle sizes	Poor sorted, predominantly coarse sand	Very poor to extremely poor sorted, extreme range of particles sizes, may contain megaclasts

2. Methods

2.1 Data

A Digital Elevation Model (DEM) derived from the Mars Orbiter Laser Altimeter (MOLA) (Smith et al., 1999; 2001) was used to prepare a base map for definition of the study area and especially the design of grid mapping. This dataset has also been used for thickness analyses of the sheet deposits.

The main database used for both grid- and geologic mapping is the imagery of the Context Camera (CTX, Malin et al., 2007). Besides, complementary datasets of the High Resolution Stereo Camera (HRSC, Neukum et al., 2004; Jaumann et al., 2007) and the High Resolution Imaging Science Experiment (HiRISE, McEwen et al., 2007) have been used.

Other datasets used in this study are THEMIS imagery (Christensen et al., 2004; Fergason et al., 2006; see *Fig. 6* and *Fig. 7*), the dust cover index (DCI; Ruff and Christensen, 2002), and the Observatoire pour la Minéralogie, l'Eau, les glaces et l'Activité experiment (OMEGA, Bibring et al., 2007) in order to determine spectral characteristics of sheet deposits.

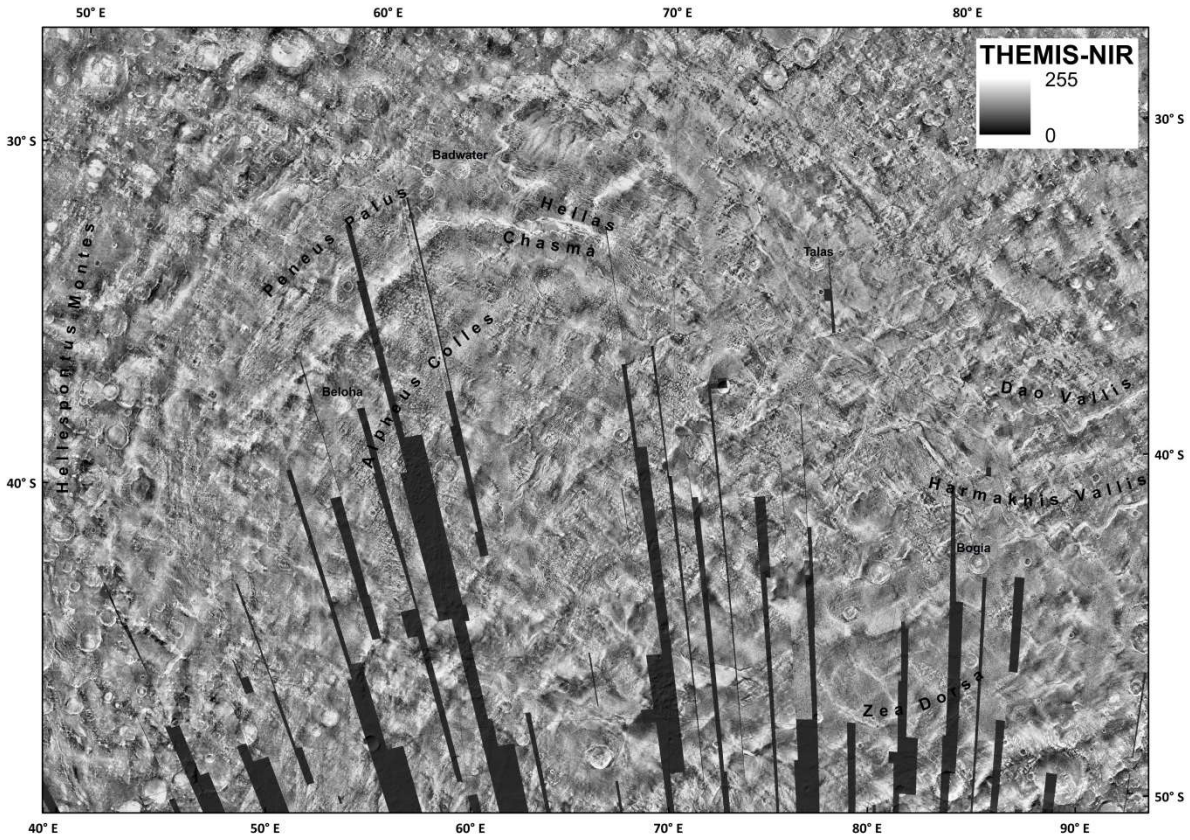

Fig. 6. *THEMIS-nighttime imagery (8-bit) for Hellas (USGS), centered at λ = 69°, φ = 49°.*

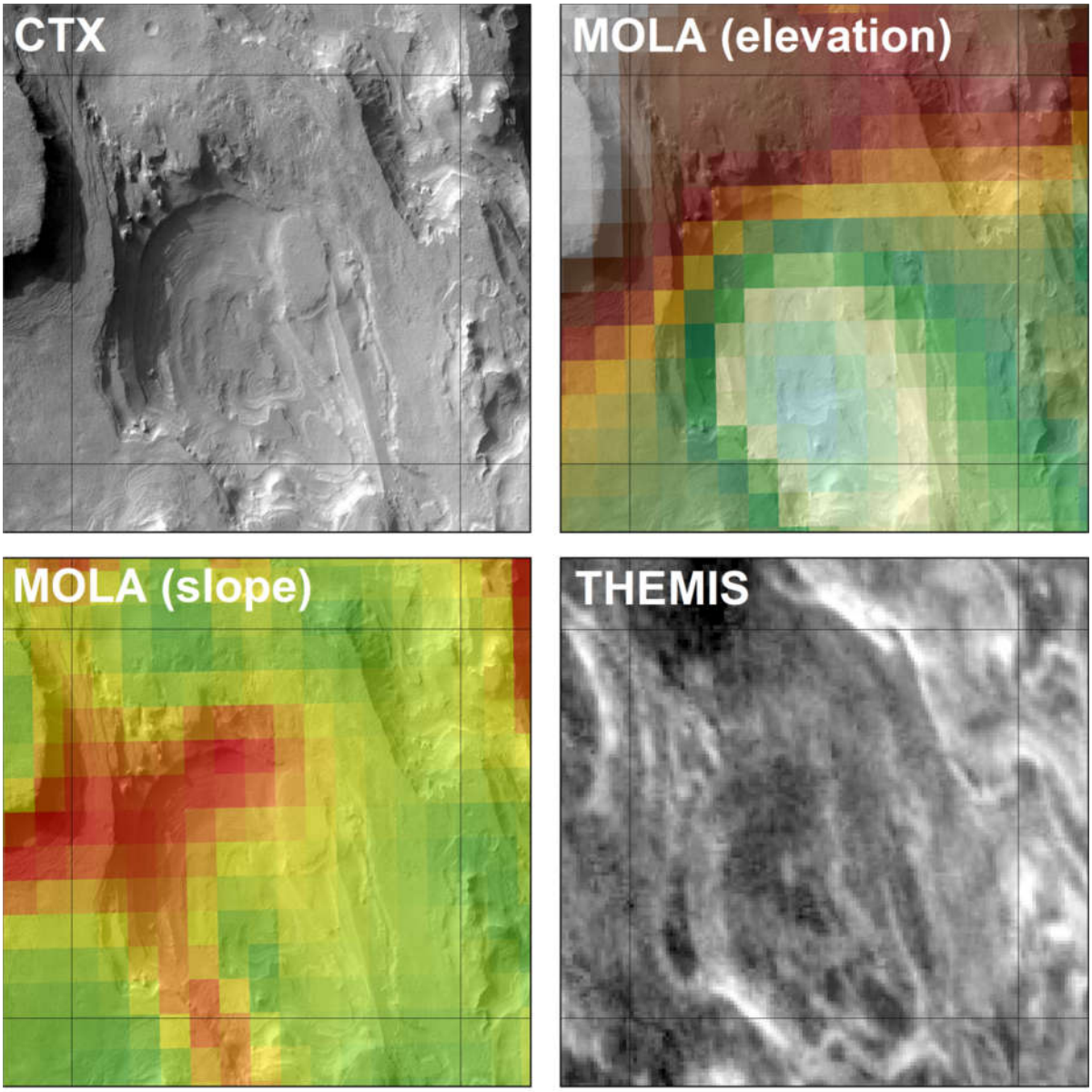

Fig. 7. *Multilayer coverage of an exemplary grid cell; 20 × 20 km, north is up (image is centered at 28.8°S, 67.0°E).*

2.2 Grid-mapping

The margins of the examined area are defined by the topography (mountain ranges along the rim) and an elevation of 5,500 m below the Martian datum (where no obvious rim is visible). The total area examined is about 8,000,000 km^2. The basic grid map has been generated automatically in a polygonal shapefile using the Repeating Shapes tool in ArcGIS 10.3 (Jenness, 2012). Thus, Hellas Planitia was separated into approximately 20,000 grids, each with a dimension of 20×20 km. For minimizing geometric distortion of geomorphological features a stereographic projection centered at λ=69°, φ=-49° was used.

The actual grid-mapping work has been carried out by photogeological interpretation. To balance between completeness and effective mapping, only every second grid was examined. The missing grids were later interpolated automatically (see below). The attribute table of the shapefile has been extended into several columns for the collected information. See *Table 2* for the gathered parameters. Each parameter has been categorized into one of the classes mentioned in *Table 3*. Additional parameters that have been gathered are information about CTX quality and coverage of the grid. More than 93% of all grids have a complete CTX coverage, and 99% are covered by more than two thirds, whereas 96% of all CTX covered grids have a medium to good quality.

For a sufficient resolution of the grid a 20×20 km raster has been chosen in order to (1) compare the results to the work done by Orgel et al.,2015; Ramsdale et al., 2017; Séjourné et al., and 2015; Hauber et al., 2015 in Vastitas Borealis, as these studies used the same grid size, and (2) as this mesh size is adequate for such an extensive study area. To ensure a consistent and uniform work only one mapper, the author of this text, has executed the grid mapping in Hellas.

Every grid has been mapped at a scale of 1:30,000 on the basis of CTX images (Context Camera onboard Mars Reconnaissance Orbiter; Malin, 2007). CTX images are the main data basis for producing a reliable map as they provide both a sufficient resolution (ground pixel size ~6 m) and spatial coverage. Parameters like elevation (*Fig. 1*), slope inclination (*Fig. 3*), and aspect were extracted from the MOLA dataset for each grid, as well as the average TI and DCI values by using the "Zonal Statistics" tool in ArcGIS.

After data collection the missing grids were interpolated by simple spreadsheet calculations. To ensure a reliable interpolation of an unmapped grid a weighting factor was used, including 12 surrounding mapped grids into the calculation (*Fig. 8*). "No data" values [4] have been excluded. Along the margins of the research area the weighting factor needed to be adjusted for preventing distortions caused by the unmapped grids of the rectangular shapefile outside of the circular study area.

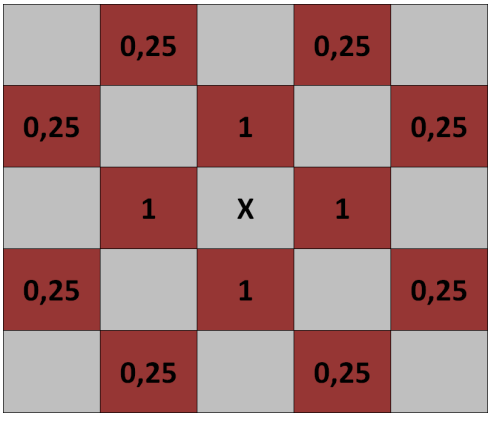

Fig. 8. *Weighting factors used for the interpolation of the grids. The dark grids represent values that have been mapped manually. The bright grids were originally empty. For interpolating the missing grids we multiplied and averaged the mapped grid, using the weighting factors as shown above. In order to prevent an impact of statistical outliers during interpolation, an extensive weighting key has been applied. Thus, adjacent grids were weighted by a factor 1, and more distant grids by a factor of 0.25.*

Table 2. *Gathered features and parameters for the study area.*

Ice-related landforms	Water-related landforms
Banded terrain	Channels
Gelifluction	Chaotic terrain
Large-pitted mounds	Fans
Latitude-dependent mantle (LDM)	Gullies
Layered-remnant deposits (LRD)	Light-toned deposits (LTD)
Lineated terrain (LT)	Sheet deposits
Polygons	Shorelines
Reticulate terrain	Viscous-flow features (VFF)
Scalloped terrain	
Other landforms	**Imagery**
Dunes	CTX coverage
Honeycomb terrain	CTX quality

Table 3. *Categories used in grid-mapping.*

Categories		
0	absent	landform not observed
1	possible	landform cannot be certainly determined
2	present	landform occurs but does not prevail
3	dominant	landform covers most of the grid
4	no data/not compiled	grid has no CTX coverage

The raster values of four external parameters (elevation, slope inclination, thermal inertia (TI), and dust cover index (DCI)) were averaged (mean) for each grid based on MOLA, THEMIS-nighttime or DCI datasets. It is important to mention that the values for slope inclination do not consider local slopes as their values average all slopes within one 20×20 km grid; this concerns especially the interpretation of small-scale landforms such as gullies. Thus, it is only possible to analyze their regional distribution. For aspect (azimuth) the majority function in ArcGIS 10.1. was applied. THEMIS-nighttime mosaics were used for relative comparisons of thermophysical surface properties, as the enormous dimensions of Hellas made it unpractical to process single THEMIS-nighttime swaths.

Statistic evaluations, diagrams, and graphs were carried out in a Python and spreadsheet environment. For these calculations only the values "present" and "dominant" were considered as

they ensure the presence of a landform; so "possible" values were strictly excluded and are only visible in maps. In order to compare the spatial distribution of the landforms regarding their elevation, slope angle, aspect, TI, and DCI box-whisker plots have been created in a Python environment. These plots also provide information about median, quartiles, interquartile range, and dispersion of each landform. It needs to be emphasized that these graphs can only show trends as the landforms are not distributed normally, e. g., regarding their elevation. However, it is possible to extract information in which conditions and environments each landform predominantly occurs.

Table 4. *Classification for each parameter for linear graphs. Parameter bins with a sample size (population) of less than 30 have been neglected in order to exclude a sampling bias.*

MOLA						THEMIS		TES	
Elevation	Total	Aspect	Total	Slope	Total	Thermal Inertia	Total	DCI	Total
[m]		[°]		[°]		[grey values]		[emissivity ε]	
≤ −7800	17	0	1878	0.00	39	0	572	≤ 0.941	59
−7600	98	25	1967	0.25	1279	10	97	0.942	53
−7400	326	50	1301	0.50	2564	20	85	0.943	63
−7200	470	75	914	0.75	3002	30	105	0.944	130
−7000	1239	100	969	1.00	2715	40	122	0.945	211
−6800	2476	125	1411	1.25	2313	50	105	0.946	352
−6600	3251	150	1832	1.50	1683	60	123	0.947	458
−6400	2881	175	2241	1.75	1344	70	172	0.948	619
−6200	2374	200	1779	2.00	991	80	303	0.949	761
−6000	1764	225	1227	2.25	787	90	676	0.950	912
−5800	992	250	717	2.50	513	100	1607	0.951	1148
−5600	700	275	612	2.75	432	110	3097	0.952	1157
−5400	600	300	696	3.00	398	120	4265	0.953	1267
−5200	458	325	1197	3.25	331	130	3927	0.954	1378
−5000	349	350	1358	3.50	244	140	2480	0.955	1308
−4800	274			3.75	200	150	1364	0.956	1319
−4600	253			4.00	162	160	590	0.957	1195
−4400	250			4.25	150	170	205	0.958	1059
−4200	164			4.50	101	180	69	0.959	988
−4000	167			4.75	111	≥ 190	26	0.960	883
−3800	183			5.00	90			0.961	772
−3600	141			5.25	83			0.962	621
−3400	118			5.50	66			0.963	614
−3200	92			5.75	53			0.964	505
−3000	53			6.00	58			0.965	477
−2800	66			6.25	27			0.966	365
−2600	51			6.50	28			0.967	320
−2400	39			6.75	32			0.968	229
−2200	53			≥ 7.00	194			0.969	210
−2000	31							0.970	169
≥ -1800	60							0.971	108
								0.972	95
								0.973	54
								0.974	44
								≥ 0.975	85

Each of the five parameters was subdivided into several classes (*Table 4*). According to the formula developed by Sturges (1926) at least 16 classes/bins (based on a sampling size of 20,099 grids) have to be generated for each parameter. In order to receive a higher data resolution, the amount of classes for each parameter was extended by establishing even figures (e. g. each bin in elevation is 200 m wide instead 475 m when applying 16 classes). To guarantee a sufficient statistical reliability for each normalized diagram, only classes/bins were considered that contain more than 30 samples (Bahrenberg et al., 1999). For TI and DCI only spatially extensive land-

forms have been considered (banded terrain, honeycomb terrain, LDM, scalloped terrain, sheet deposits, and light-toned deposits) as small or linear landforms, for instance gullies, are not sufficiently significant within a 20×20 km grid. For understanding the behavior of one landform, e. g., regarding a potential elevation-dependent distribution, the graphs were normalized in order to remove the sampling bias (absolute graphs are strongly dependent on the research area's topography, and thus, biased). Normalized values are based upon elevation, slope, aspect, DCI, or THEMIS (*Table 4*), giving the density of a landform by class; e. g., the density of channels at an elevation of -3,000 m is 0.3, and hence, 30%. This statistical correction is necessary for classes that are underrepresented in Hellas, e. g., grids with an elevation higher than -4,400 m always contain less than 200 grids (*Table 4*).

As the results of THEMIS only provide relative grey scale values, and hence a low information content, their plots were shifted to the supplements of this manuscript. However, the thermal inertia results of most of the landforms are presented in textual form in chapter 3.

It was also considered and discussed if the grid-mapping could be performed automatically, e. g., by supervised classifications. However, most of the landforms are either linear and therefore not suited for 2D classifications (e. g. dark pixelated channels might be confused with dark pixelated crests or dust devil tracks), diffuse (e. g. lineated terrain often has not clear margin), or request the interpretive skills of a human researcher (e. g., possible shorelines, alluvial fans).

2.3 Mapping of Sheet Deposits

In order to understand the geospatial, sedimentary, and stratigraphic behavior of sheet deposits, an area on the eastern Hellas floor has been mapped at a scale of 1:100,000 in a GIS-environment. The study area is confined to a plain at the terminus of Dao Vallis where lobate sheet deposits occur, and extends 165×125 km covering an area of 20,625 km².

Age determinations for units AHsd1, AHsd2, and Asd3-5 are based on crater counts on representative locations using CraterTools 2.1 (Kneissl et al., 2011). The resultant crater-size frequency distributions (CSFD) were analyzed with Craterstats II (Michael and Neukum, 2010). Crater counts were executed on CTX images using a mapping-scale of 1:18,000 (Platz et al., 2013). Only craters with more than 50 m in diameters were counted. In this study, the production function of Ivanov (2001) and the chronology function of Hartmann and Neukum (2001) have been applied.

The thicknesses of deposits are derived from the heights of the flow fronts. They were estimated with MOLA single shot data (Smith et al., 2001). In order to ensure reliable results each profile is

the mean value of two, usually parallel, MOLA tracks. The distance of both tracks is always less than 1,000 m. For each sheet deposit unit, three of these measurements were executed and eventually averaged again. Thus, minimum, mean, and maximum values for the thickness of each sheet deposit layer could be derived. For comparison, the thickness values of sheet flows of unambiguously volcanic origin (Hadriacus Mons, Elysium Mons, and Arsia Mons) were calculated too.

By combining thickness and area of each sheet deposit unit it is possible to derive their volume too. Preventing disputable statistic assumptions, merely the areas of each unit were considered being immediately visible. Hence, volumetric measurements are always conservative minima. Together with hydrologic values for the three sediment-laden transport mechanisms by Costa (1988), these numbers were also used for calculating the amount of the possible water content.

The study has been completed with the analysis of the surface mineralogy. Especially, the hyperspectral data set acquired by the OMEGA (Observatoire pour la Minéralogie, l'Eau, les glaces et l'Activité) experiment (Bibring et al., 2007) onboard the Mars Express spacecraft provides a sufficient coverage of the study area. OMEGA detects a wavelength range between 0.35 and 5.1 µm. In order to avoid the influence of the thermal signal dominating the OMEGA spectra in the 3–5 µm region, the analysis focuses on the wavelength region between 0.35 µm and 2.5 µm (Poulet et al., 2007). The observations have been radiometrically calibrated by the OMEGA team (Bibring et al., 2007) and effects of the atmosphere onto the spectral signal corrected following the algorithm of Mustard et al. (2007).

In order to compare the spectral mapping results to the region of interest, the OMEGA observation have been map-projected and combined into a mosaic. Previous studies showed that OMEGA is able to detect key surface materials of the Martian surface in the form of mafic iron-bearing silicates, hydrated minerals, ferric oxides, and ices (Poulet et al., 2005; Bibring et al., 2006). The appearance of these materials in the OMEGA spectra can be determined based on spectral criteria or parameters, whose identification and mapping is described in detail in Poulet et al. (2007).

In addition to the OMEGA data, four radiometrically calibrated MRO CRISM observations are available and have been map-projected and atmospherically corrected using the CRISM analysis tool (CAT) provided by the CRISM team. In order to be consistent with the results derived from the OMEGA data, the same parameter set was used for the analysis of the CRISM spectra.

Since the focus of this study lies on the discrimination between volcanic, fluvial, and glacial deposits, the analysis is based on spectral parameters sensitive for the presence of mafic minerals;

such as olivine and pyroxene, using their prominent relatively broad 1 µm- and 2 µm-absorptions, respectively (Gaffey et al., 1993). Hydrated minerals exhibit a distinct absorption near 1.9 µm (Gaffey et al., 1993). H_2O ice is well defined by its two prominent absorptions in the 1.5 µm- and 2 µm-region. Consequently, the spectra was investigated for any existing absorption and variations in the absorption depth, using the corresponding spectral parameters as defined in Poulet et al. (2007).

3. Results

3.1 Grid-mapping

3.1.1 Topography

For the research area in Hellas Planitia a differential hypsometric curve (*Fig. 9*) was created, which shows that 76% of the 20×20 km grids are at an elevation range between -6,000 and -7,500 m below the Martian datum line. Its low-point, which is also the lowest point on the Martian surface, is located in Badwater crater (33°S, 62°E) at an elevation of -8,194 m. The highest elevation of -12 m is an unnamed peak in the Hellespontus Montes on top of the western rim of Hellas Planitia. Despite the significant absolute relief, slope inclination is relatively low. 48% of all grids have an inclination of 1°, 21% show 2°, and further 20% show an inclination of 3° or higher.

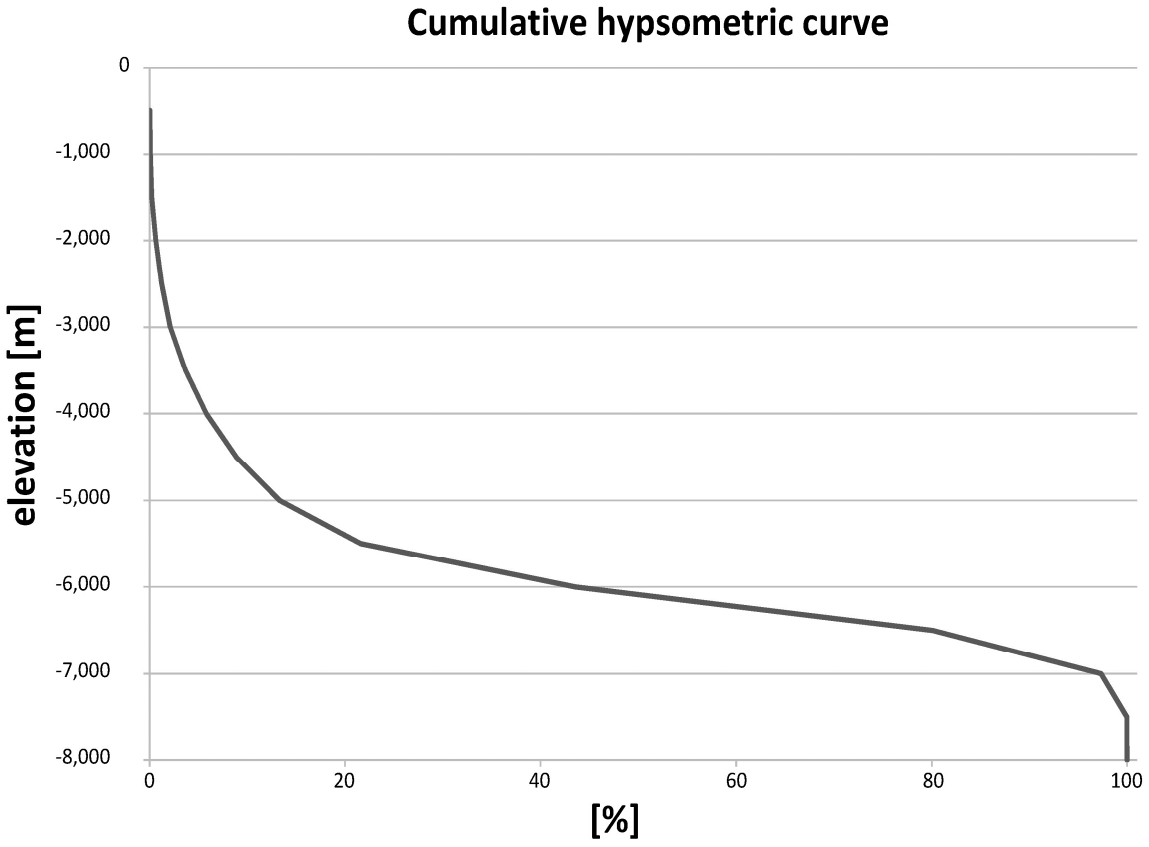

Fig. 9. *Hypsometric curve for Hellas based on MOLA and the 20×20 km grid.*

3.1.2 Ice-related Landforms

Due to its location in the southern mid-latitudes, Hellas Planitia is strongly affected by the latitude-dependent mantle (LDM), which is thought to be a mixture of ice and dust (Mustard et al., 2001; Kreslavsky and Head, 2002b; Schon et al., 2009, 2012; Kostama et al., 2006) and contains a significant amount of ice (46 – 94% by volume; Conway and Balme, 2014) below a des-

iccated surface lag (*Fig. 10* and *Fig. 11*). The thickness of this lag ranges between 0.25 m and 8 m, with a mean thickness of 3.2 m (Conway and Balme, 2014). This lag decreases in thickness with decreasing distance to the poles (Feldman et al., 2002; Mangold, 2011). The LDM appears to be a layered deposit. The evolution of each layer likely depends on factors like orbital excursions of the planet's axial tilt, precession, and eccentricity (e. g., Kreslavsky and Head, 2002b; Head et al., 2003; Kostama et al., 2006; Dickson et al., 2015). Especially during high obliquity periods surface ice remains stable at the mid-latitudes (e. g., Levrard et al., 2004; Mischna et al., 2003; Forget et al., 2006). Moreover, the atmosphere contains more dust during these phases. The dust particles act as condensation nuclei for the ice (Richardson and Wilson, 2002; Haberle et al., 2003), and as soon as these ice/dust particles grow big enough, they start to fall by gravitation and deposit. It is unclear if this process is still active on Mars or if it is just temporarily halted because of an ongoing interglacial period (Head et al., 2003, Madeleine et al., 2014). However, according to crater-size frequency distributions, the latest LDM was deposited in geologically recent times (0.1 – 2.1 Ma) (Kostama et al., 2006; Willmes et al., 2012). At certain environmental conditions, such as during high obliquity phases, high temperatures, and/or aeolian activities, LDM appears to be susceptible to sublimation (e. g., Mangold, 2011a and 2011b; Dundas et al., 2015) and/or melting processes, causing degradation or deformation, into several characteristic morphologies, e. g., scalloped terrain (Morgenstern et al., 2007; Lefort et al., 2009; Ulrich et al., 2010; Zanetti et al., 2010; Willmes et al., 2012; Dundas et al., 2015), the so-called lineated terrain, and possibly layered remnant deposits (LRD) (Morgenstern et al., 2007) within small craters. Another potential sublimation feature found in Hellas is the dissected terrain; a thin blanket of LDM perforated by small and erratically shaped sublimation pits. Its thickness varies between a few meters to tens of meters (Mangold, 2011). Mangold (2011) suggests that these sublimation pits are the result of ongoing active sublimation on Mars.

Because of its enormous size, depth, and hence, high air pressure, Hellas is a significant sedimentary trap for this atmospherically-derived deposit. Approximately 90% of the study area is draped by this mantling deposit, except for a region in northeastern Hellas, which extends from Talas crater (35.5°S, 75.5°E) to the lower termination of Harmakhis Vallis (*Fig. 10*). This NW to SE trending elliptical gap in LDM coverage extends over an area of 200×800 km. This observation is consistent with the roughness map of Kreslavsky and Head (2002b), because this area shows high roughness values, which independently indicates that the local small-scale relief is not muted or smoothed by the deposition of LDM. The gap also correlates to an area with less water-equivalent hydrogen (<3%) as compared to the rest of Hellas Planitia with 4-6% (Feldman et al., 2002).

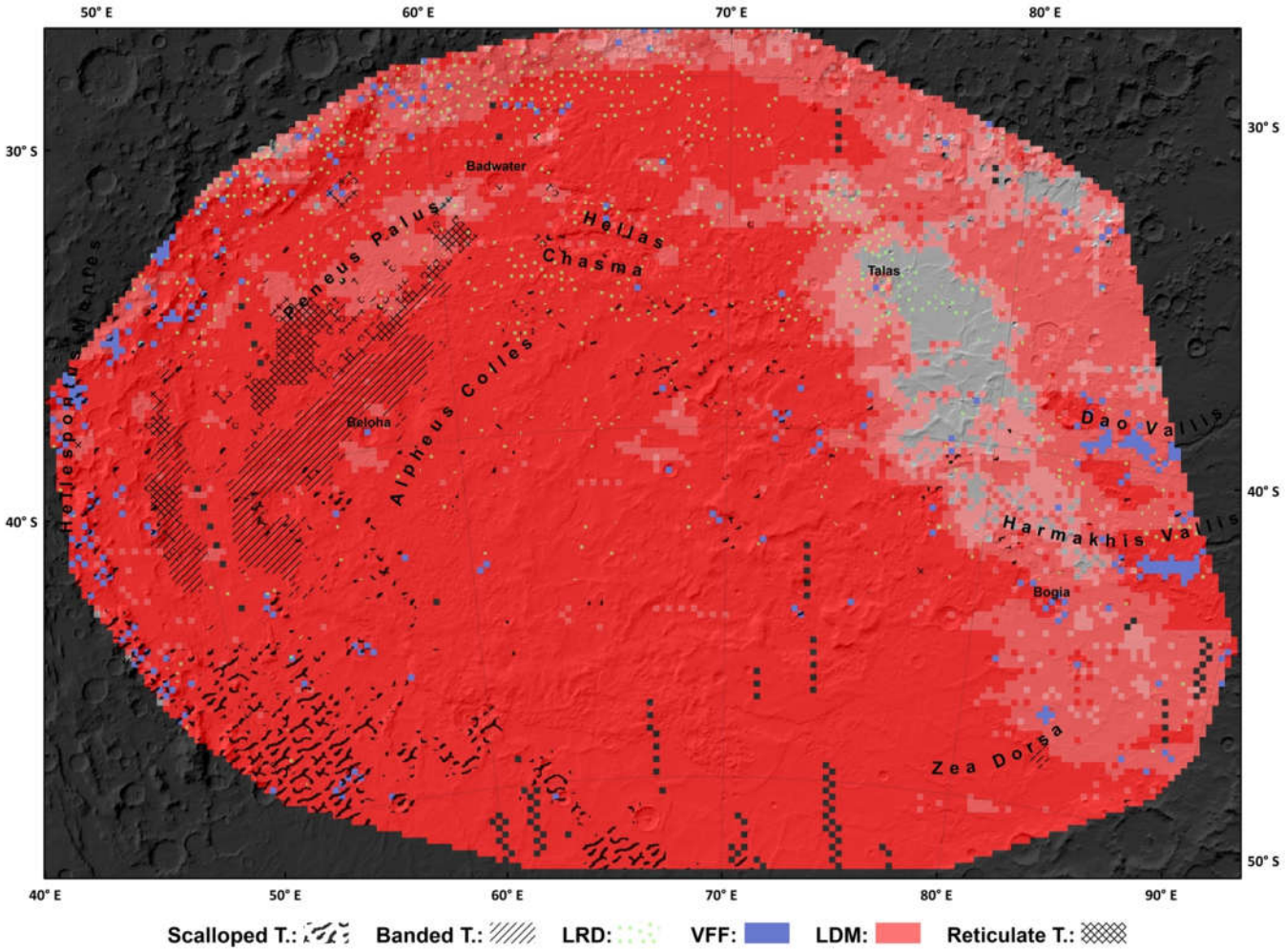

Fig. 10. *Gridmap showing selected ice-related landforms in Hellas Planitia. The intensity of the red color is a measure of the abundance or prominence of LDM. Note the gap of LDM in NE Hellas. Basemap: MOLA.*

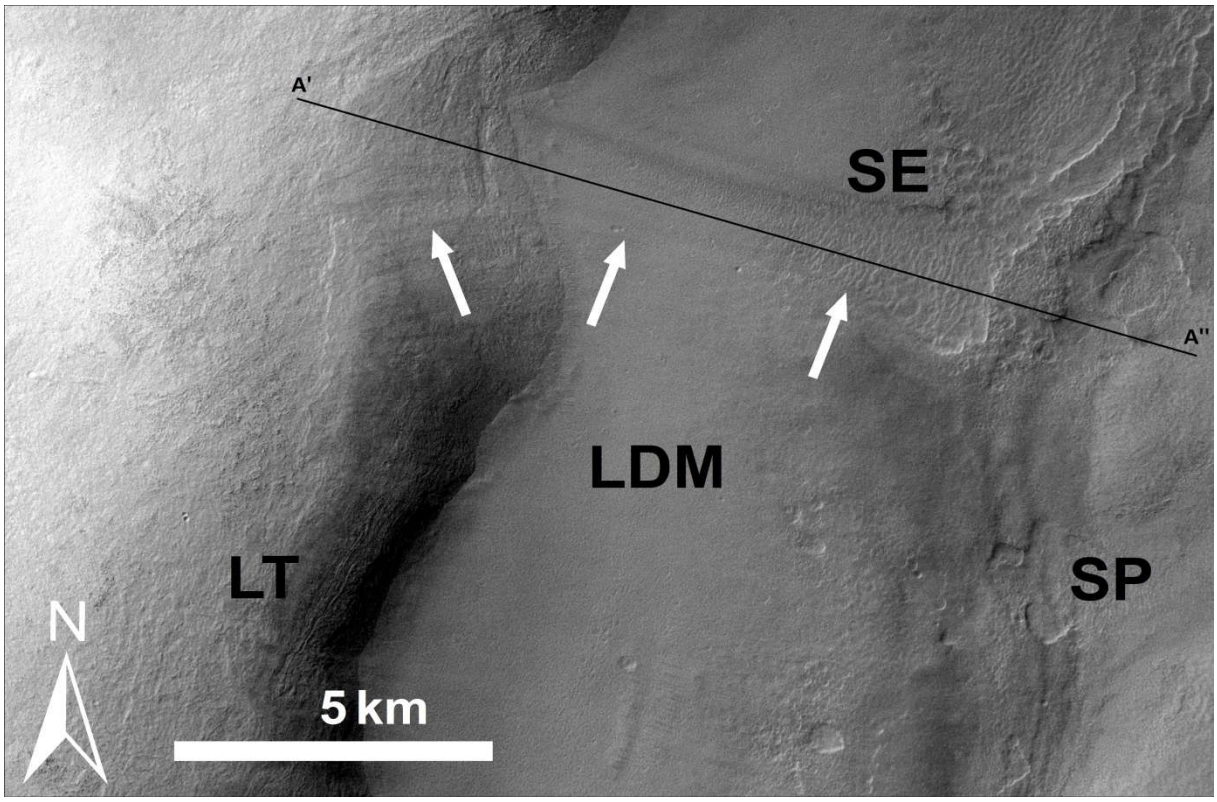

Fig. 11. *Various morphologic expressions of LDM in Hellas. To the left there is the stratigraphically oldest LDM layer termed lineated terrain (LT), showing linear patterns. The scalloped terrain occurs in two different types: the classic pitted and ovoid form (SP) and a more diffusively distributed form (SE). SP appears to be predominantly controlled by insolation and SE by wind activities (white arrows). Note the ramp of the ridge in the upper left part of the image, where probably aeolian wind streaks are passing through (CTX P14_006528_1412 at 38.8°S, 69.7°E).*

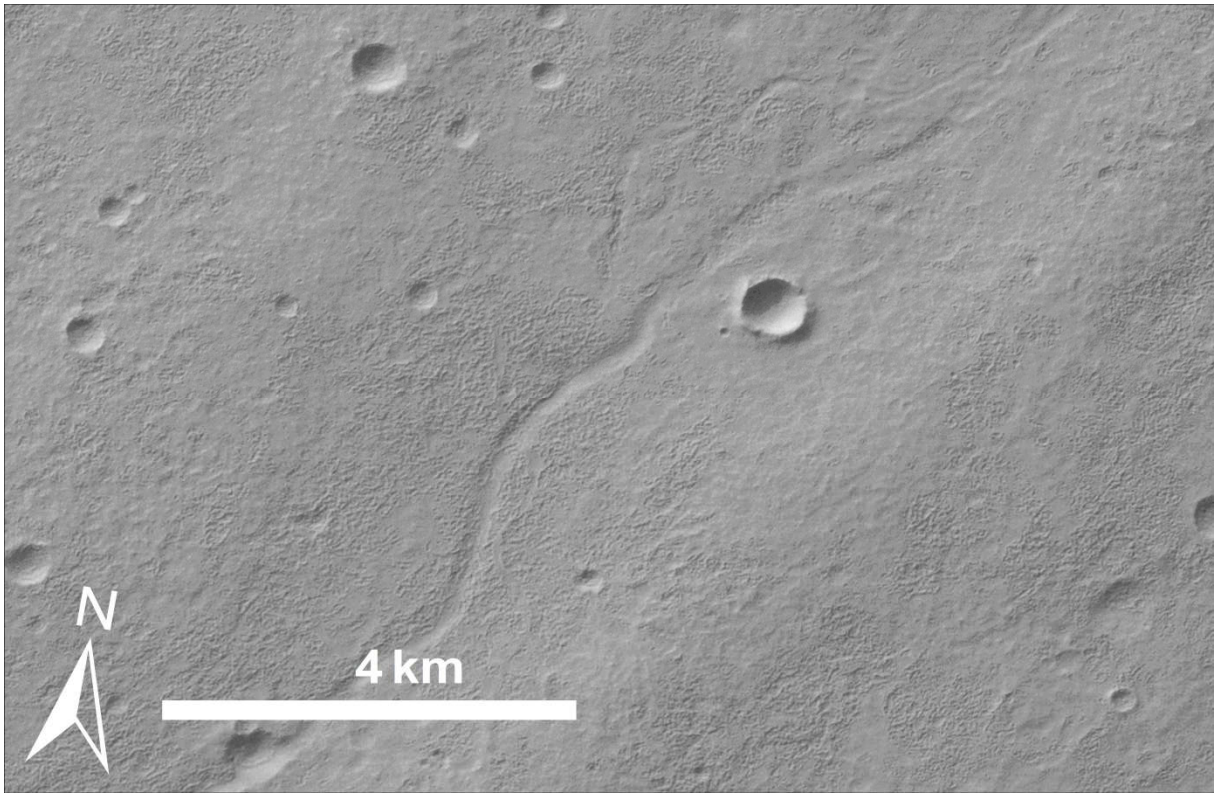

Fig. 12. *Muted and dissected LDM terrain north of Dao Vallis (CTX image P19_008426_1440 at 35.7°S, 83.9°E).*

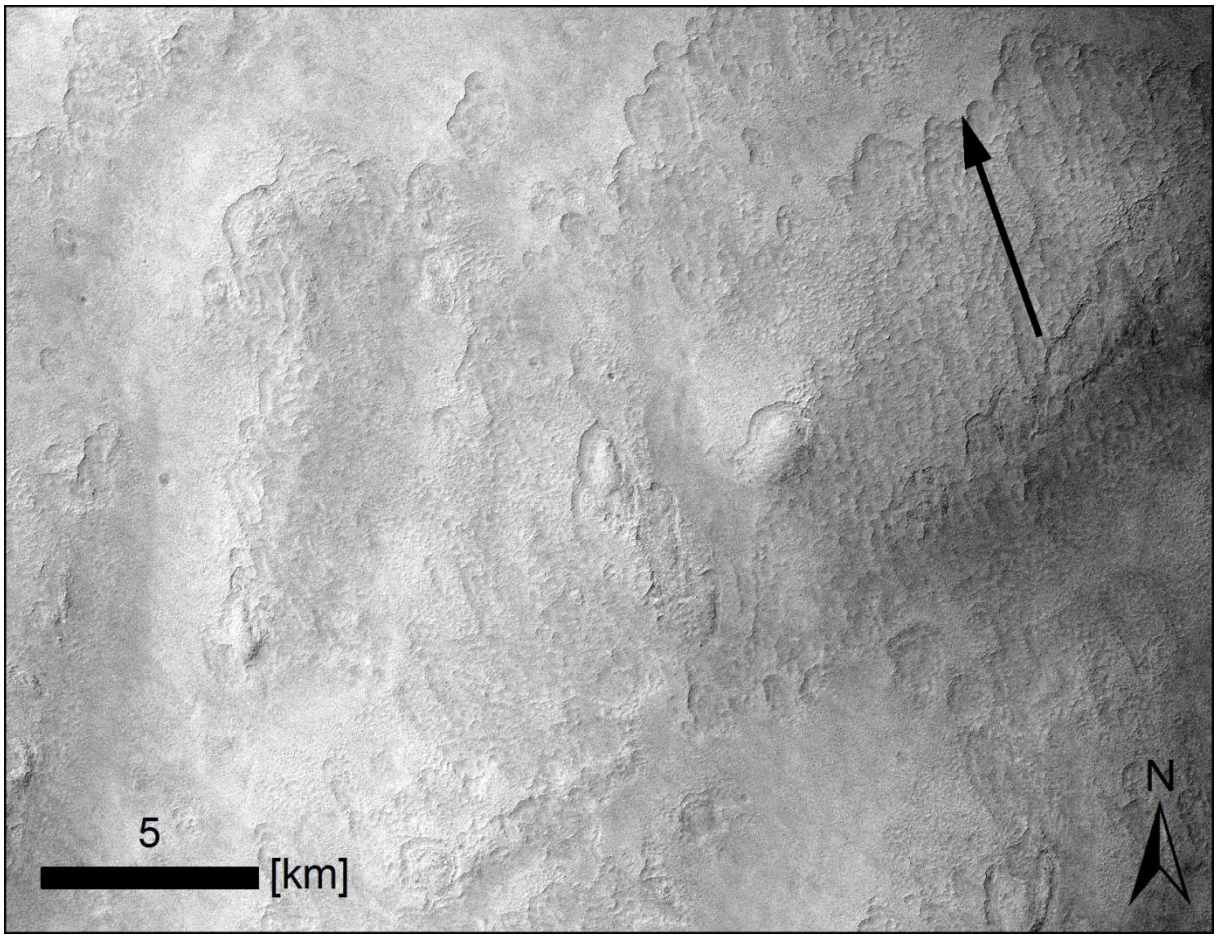

Fig. 13. *Deflected scalloped terrain at the southern rim of Hellas Planitia. Black arrows indicates the direction of wind at this point, and hence, the orientation of scallops too. Please note how far the scallops are orientated towards northwest, instead of north, where the most intense solar irradiation is expected (CTX image G14_023683_1273 at 52.0°S, 66.3°E).*

Immediately east of this gap is an area being covered by a thin coat of LDM (dissected terrain). Beneath this blanket there is clear evidence of underlying but muted volcanic and/or fluvial morphologies (*Fig. 12*), suggesting that this region has only been covered by a thin LDM sheet, possibly deposited during one of the last obliquity excursions. Other, but much smaller LDM-free regions are located along Hellas' northern rim (<30°S), as well as another elongated spot (70×100 km) in northern Peneus Palus. The rest of the basin is covered with LDM. However, there are areas showing a rougher texture of LDM than other parts. For example, LDM in the central and southern part of Hellas displays a relatively smooth texture, and appears to be young. In contrast, around this central area, in the southwestern, southeastern and northern part of the basin floor, the mantling deposit is often severely degraded. Especially north of 35°S LDM is characterized by a rough texture. THEMIS nighttime datasets show a slight trend of LDM covered grids to lower TI values.

Scalloped terrain is referred to line symmetric and rimless depressions within LDM (e. g., Morgenstern et al., 2007), measuring a few tens to several hundred meters in diameter (*Fig. 11*). Their depth ranges from a few meters to tens of meters. On the southern hemisphere they show a relatively steep (15° to 30°) pole-facing scarp and a smooth and gently inclined (2°) equator-facing slope. The steep scarp is stationary, while the smooth slope retreats progressively (Mangold, 2011; Séjourné et al., 2011). They occur isolated or in clusters. Scalloped terrain is especially common in Utopia Planitia and Malea Planum (Zanetti et al., 2010; Lefort et al., 2009). The two prevailing scenarios for the volume loss is either sublimation of the LDM material (e. g., Lefort et al., 2009; Zanetti et al., 2010; Dundas et al., 2015) or melting (Soare et al., 2007, 2008, 2011) of subsurficial ice, and hence, the collapse of the overlying material.

The scalloped terrain in Hellas Planitia occurs in scattered locations mostly south of 35°S (*Fig. 10*). It displays two shapes: the typical isolated or merged ovoid form as well as a widespread, irregular and ripple-like shape. Pits of the latter type are much smaller than the classic scalloped pits (*Fig. 11*). Both can occur next to each other. Extended populations are found in southwest Hellas close to the breached rim where the basin transitions into Malea Planum. This geomorphology is generally found on medium to high elevations and rarely in low elevations. It preferentially occurs on steeper slopes (*Fig. 17*). Its aspect maximum is towards north and the minimum towards south. TI values show no obvious correlation with scalloped terrain. The DCI values of scalloped terrain show a trend towards low dusty areas (*Fig. 21*).

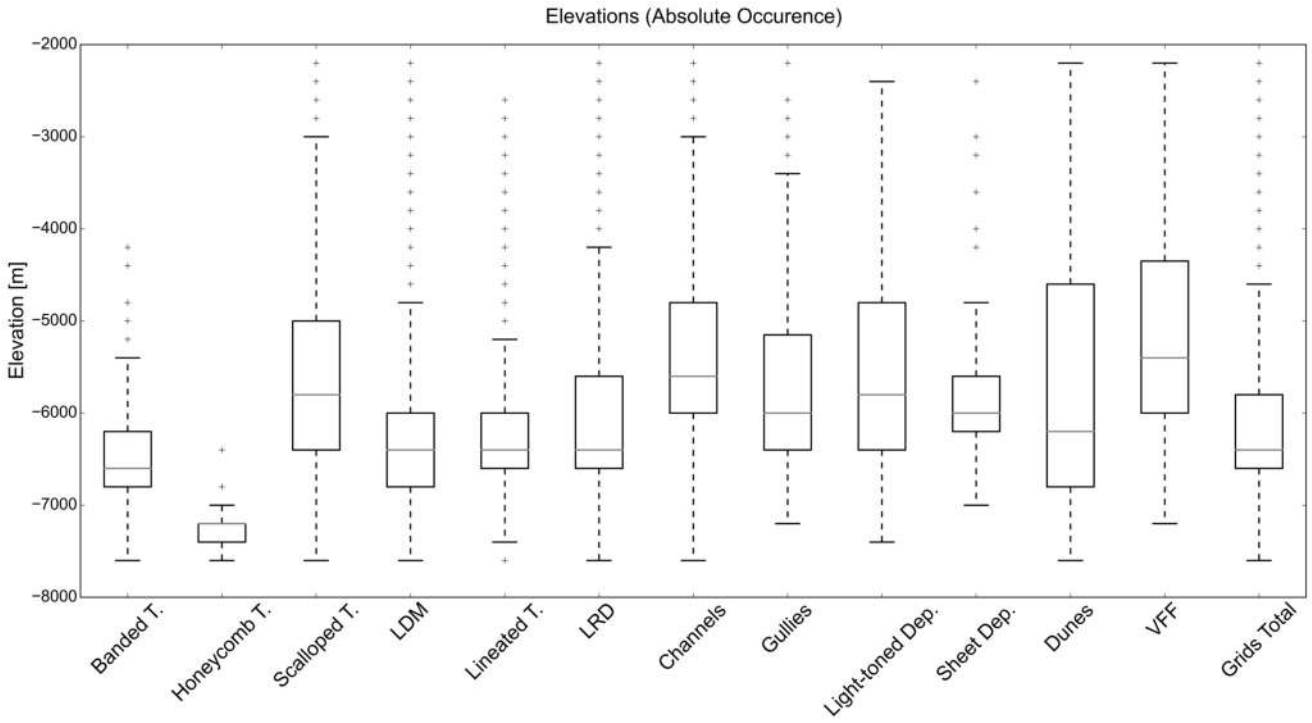

Fig. 14. *Box-Whisker plot showing the distribution of landforms regarding their absolute elevation. The upper and lower ends of the boxes represent the first and third quartiles. The grey line within the box is the median (second quartile). The whiskers/antennas display the 1.5 IQR (interquartile range). The plus marks show extreme values.*

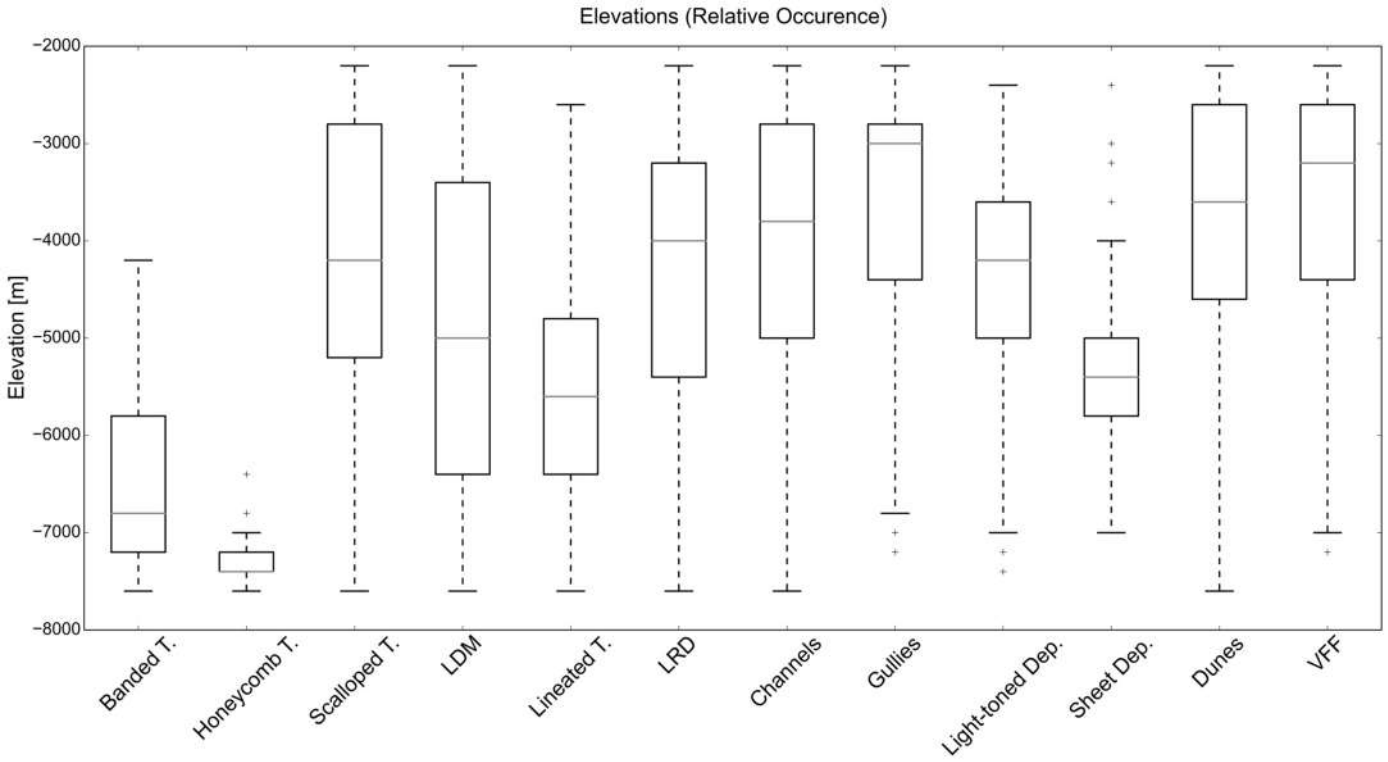

Fig. 15. *Box-Whisker plot showing the relative distribution of landforms regarding their elevation. For explanation of symbols see caption of Fig. 14.*

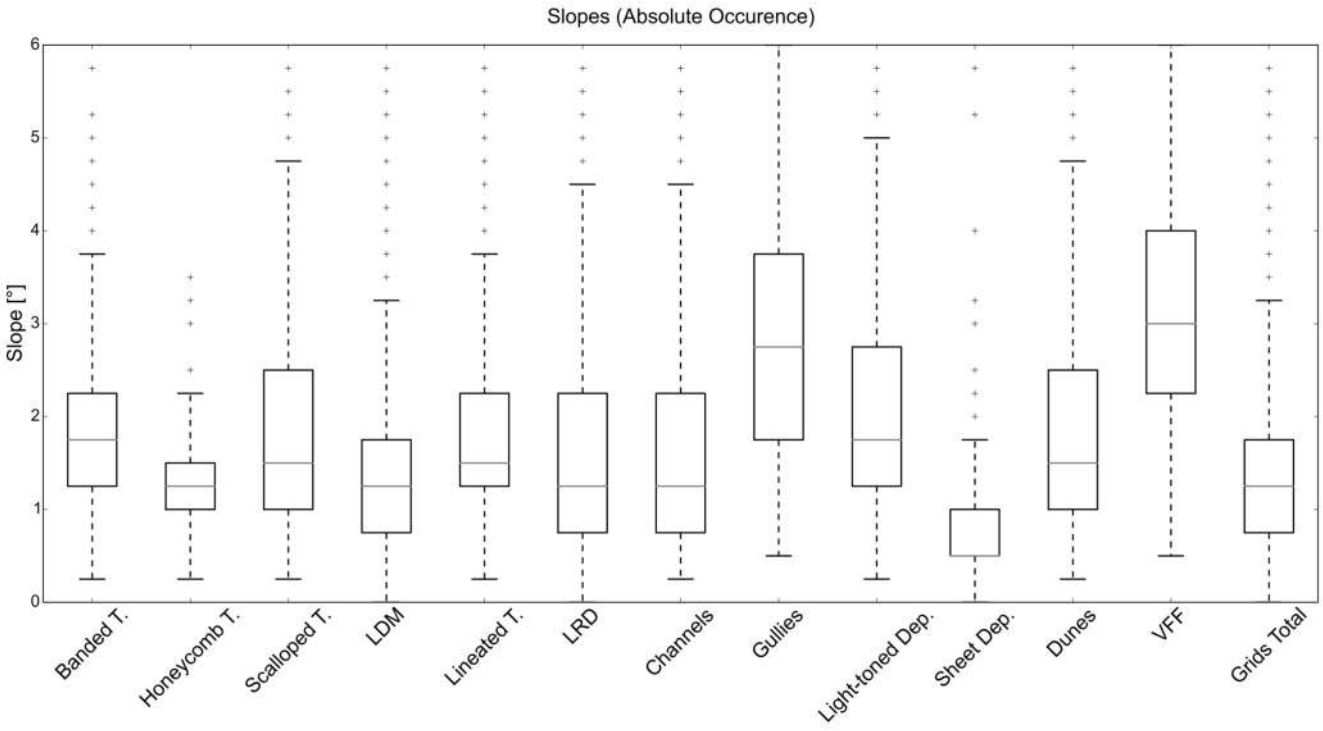

Fig. 16. *Box-Whisker plots showing the distribution of landforms regarding their absolute slope. For explanation of symbols see caption of Fig. 14.*

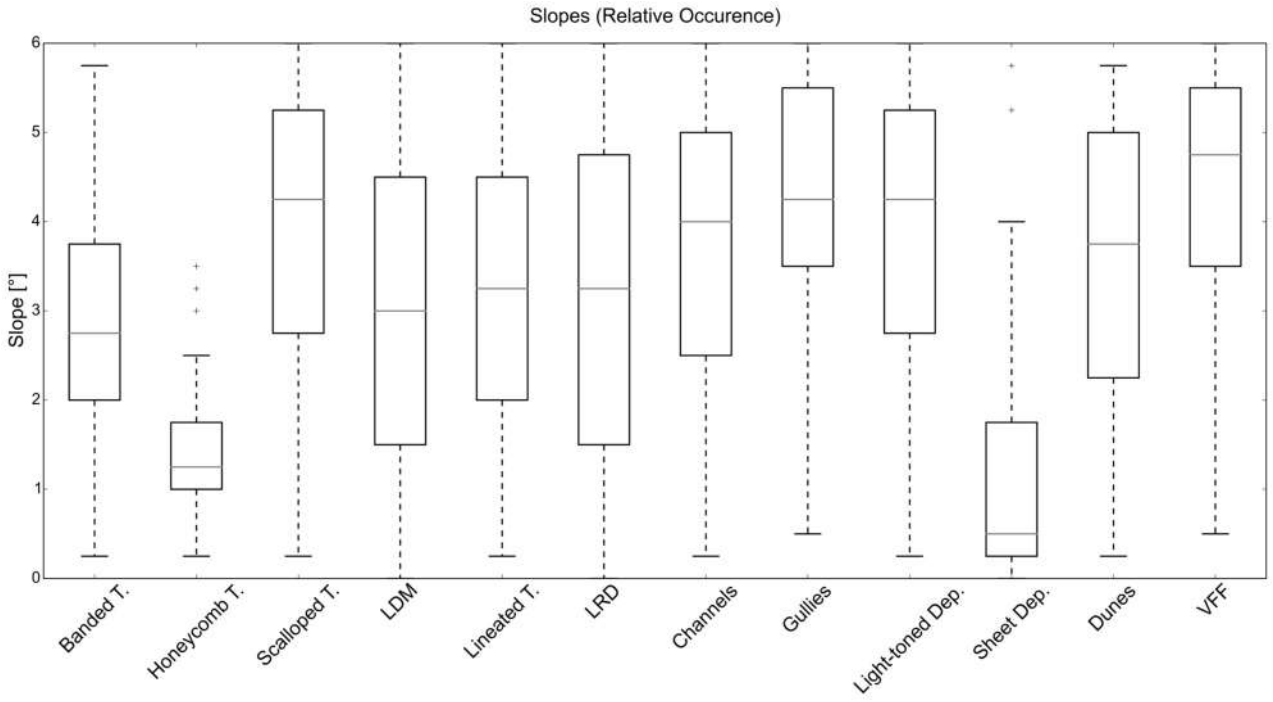

Fig. 17. *Box-Whisker plot showing the relative distribution of landforms regarding their slope. For explanation of symbols see caption of Fig. 14.*

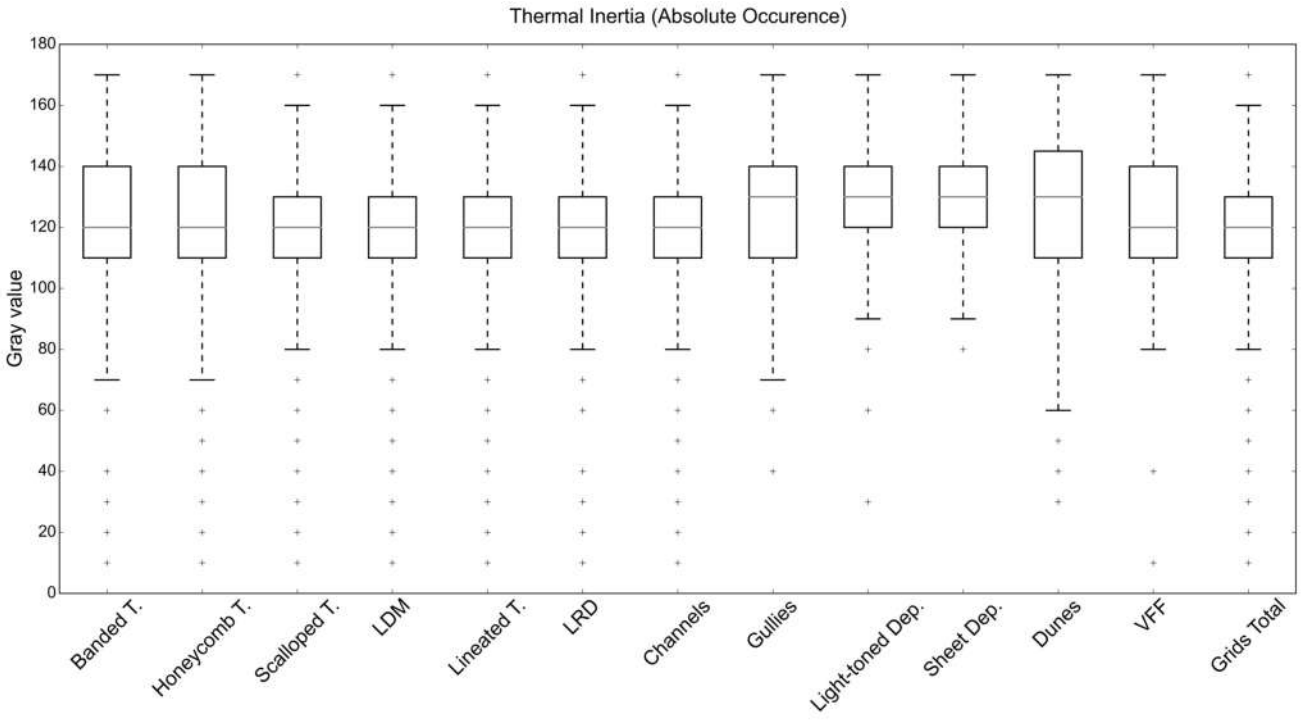

Fig. 18. *Boxplot presenting the absolute Thermal Inertia values of selected landforms. Note: The given numbers are grey scale values. For explanation of symbols see caption of Fig. 14.*

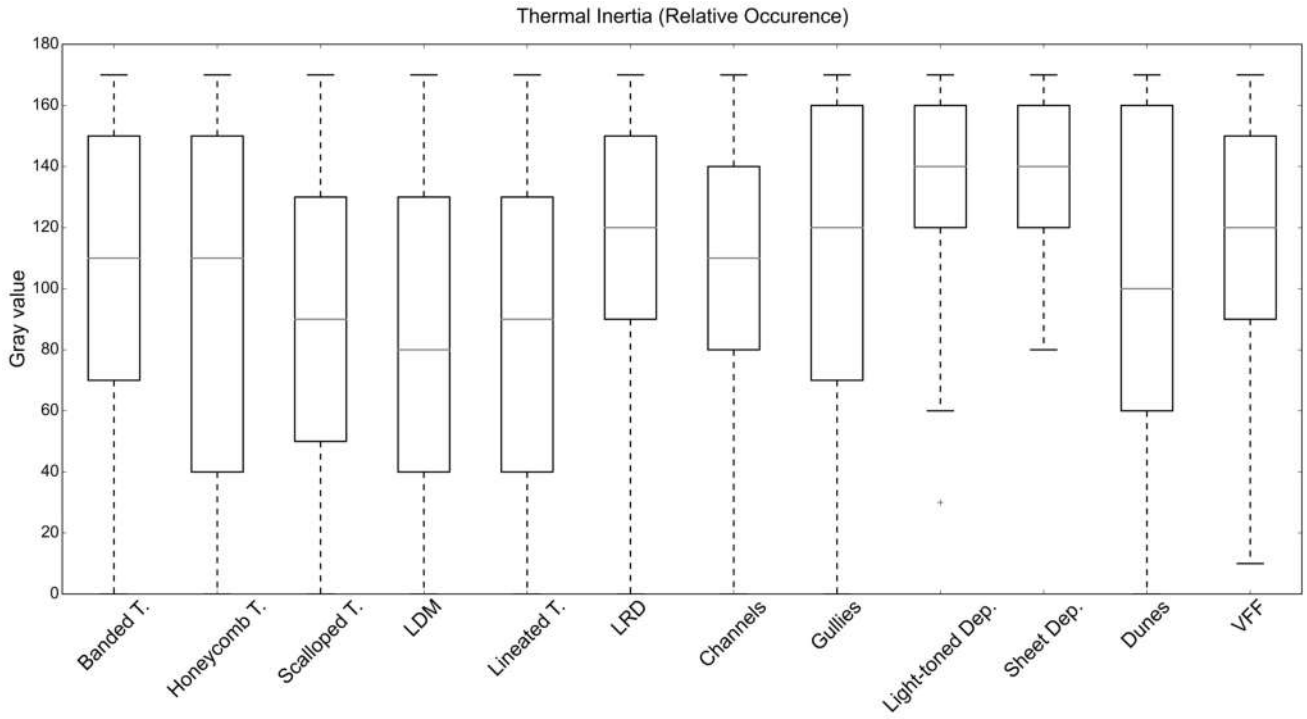

Fig. 19. *Boxplot presenting the relative Thermal Inertia values of selected landforms. Note: The given numbers are grey scale values. For explanation of symbols see caption of Fig. 14.*

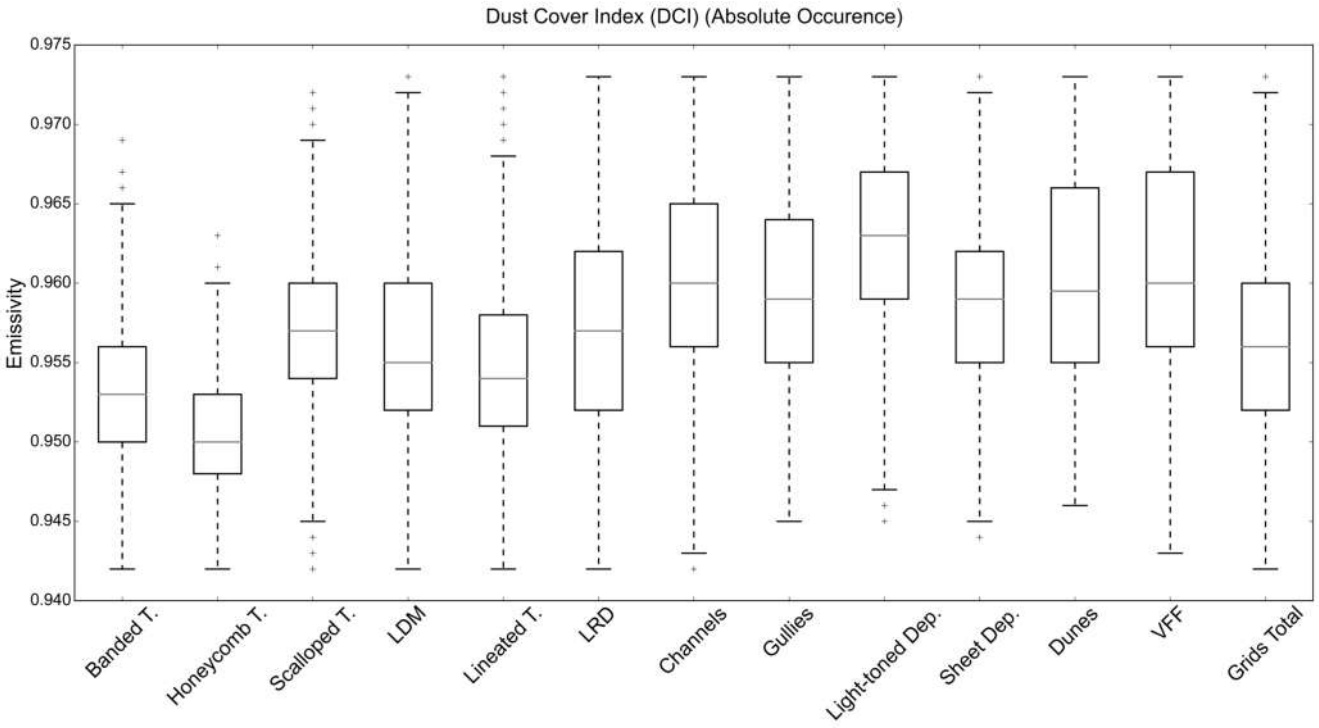

Fig. 20. *Boxplot presenting the absolute dust cover index values (DCI) of selected landforms. Note: the higher the values the less each landform is covered by dust and vice versa. For explanation of symbols see caption of Fig. 14.*

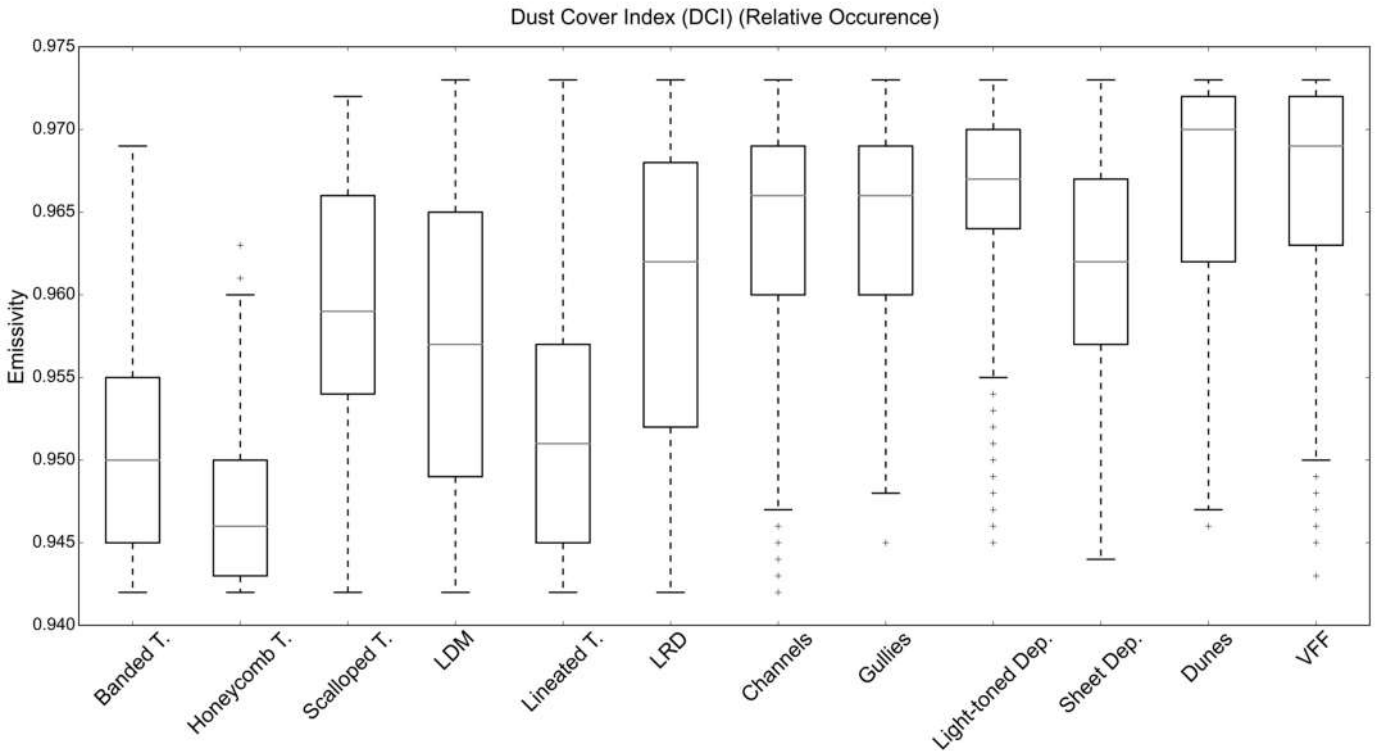

Fig. 21. *Box-Whisker plot showing the relative distribution of landforms regarding their DCI. Note: the higher the values the less each landform is covered by dust and vice versa. For explanation of symbols see caption of Fig. 14.*

The term banded terrain describes a smooth and two-dimensionally convoluted layered unit covering the landscape, caused by viscous flow of either ice-rich volcanic debris or an ice-dust mixture (Diot et al., 2015, 2016) (*Fig. 22*). Although not fully understood yet, the process that formed the banded terrain in the Amazonian (Diot et al., 2014) is one of the most recent surface processes in Peneus Palus, and probably affected larger parts of this lowland.

The banded terrain mainly occurs on top of the westernmost part of the Alpheus Colles plateau (*Fig. 10*). There are also minor occurrences along the inner western and southwestern rim of Hellas and within an isolated mountain range in the Zea Dorsa region. The relative frequency of the banded terrain is decreasing slightly from -7,500 to -4,500 m. Slope inclination tends to values between 2° and 4° and its maximum aspect values are towards E and NW. The banded terrain has a slight trend to higher TI values, and a significant trend towards strongly dust covered areas (*Fig. 21*). Moreover, there is no evidence that the banded terrain is susceptible to the formation of scalloped terrain.

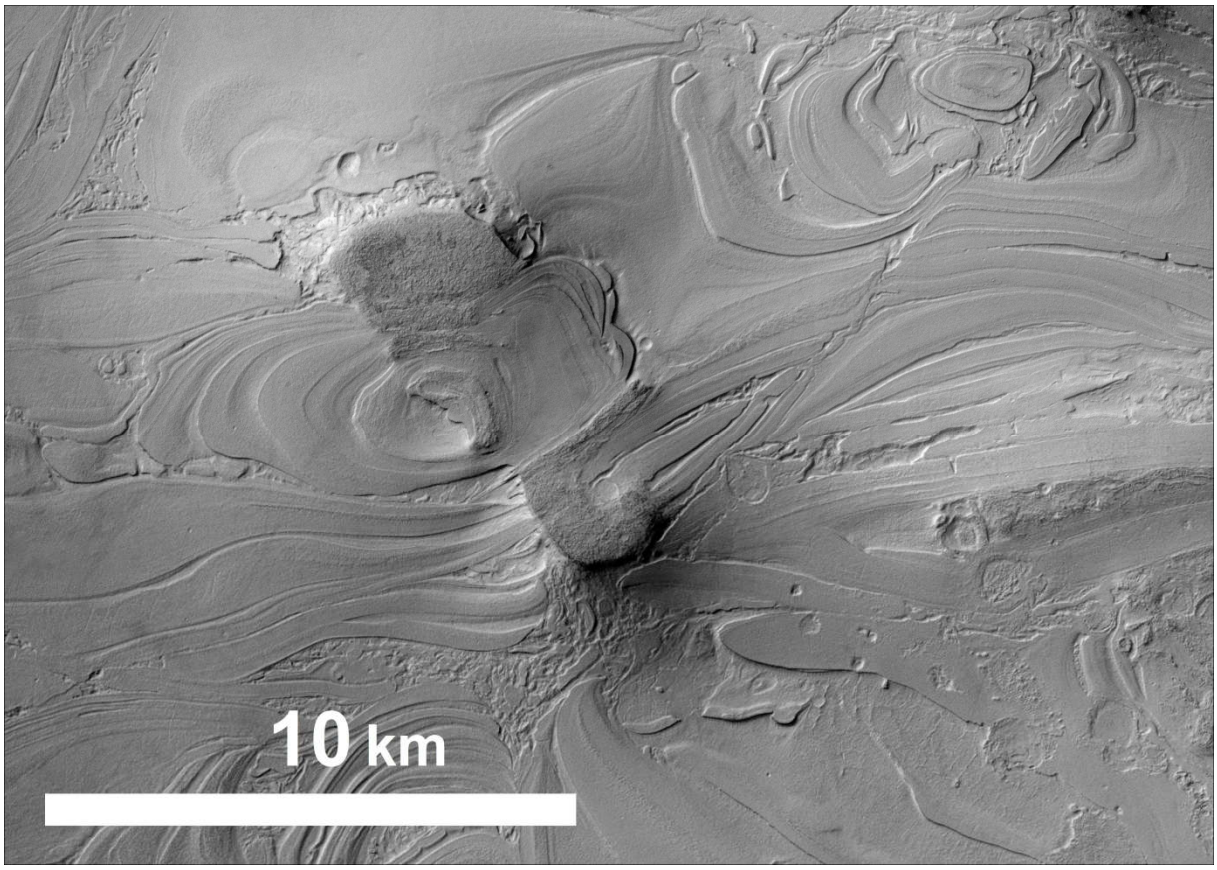

Fig. 22. *Banded terrain in the Alpheus Colles region (Cropped CTX image centered at P17_007636_1414 at 38.9_S, 55.7_E).*

Layered remnant deposits (LRD) were first described as layered material by Morgenstern et al. (2007) in Utopia Planitia. They suggested these subhorizontal deposits within craters are remnants of an older LDM that survived the removal of LDM in protected areas. This is why the term was extended into layered remnant deposits (LRD) (*Fig. 23*).

LRD are predominantly found at elevations higher than -5,000 m, and slightly tend to occur on slopes with an inclination of 2° and 5° in the normalized graphs (*Fig. 17*). At HiRISE resolution LRD seem to be a brittle and sometimes polygonally fractured material. They predominantly occur in small to medium-sized craters of less than 2 km in diameter, except in NE Hellas were they only occur in craters larger than 3 km. Interestingly, there are places where some craters contain LRD, but adjacent craters of the same size do not, despite appearing neither younger nor older. The grids containing LRD have a maximum aspect towards S and a minimum towards N. As they mainly occur in the northern latitudes of Hellas Planitia (<38°S), however, their large-scale aspect is strongly biased by the pole-facing interior slopes dominating the northern part of Hellas. Their preferred local aspect within each crater displays an opposite trend. LRD mostly occur on the inner north-facing wall of medium-sized craters, and in the center of small craters. A weak trend towards areas with low dust cover is visible in the DCI.

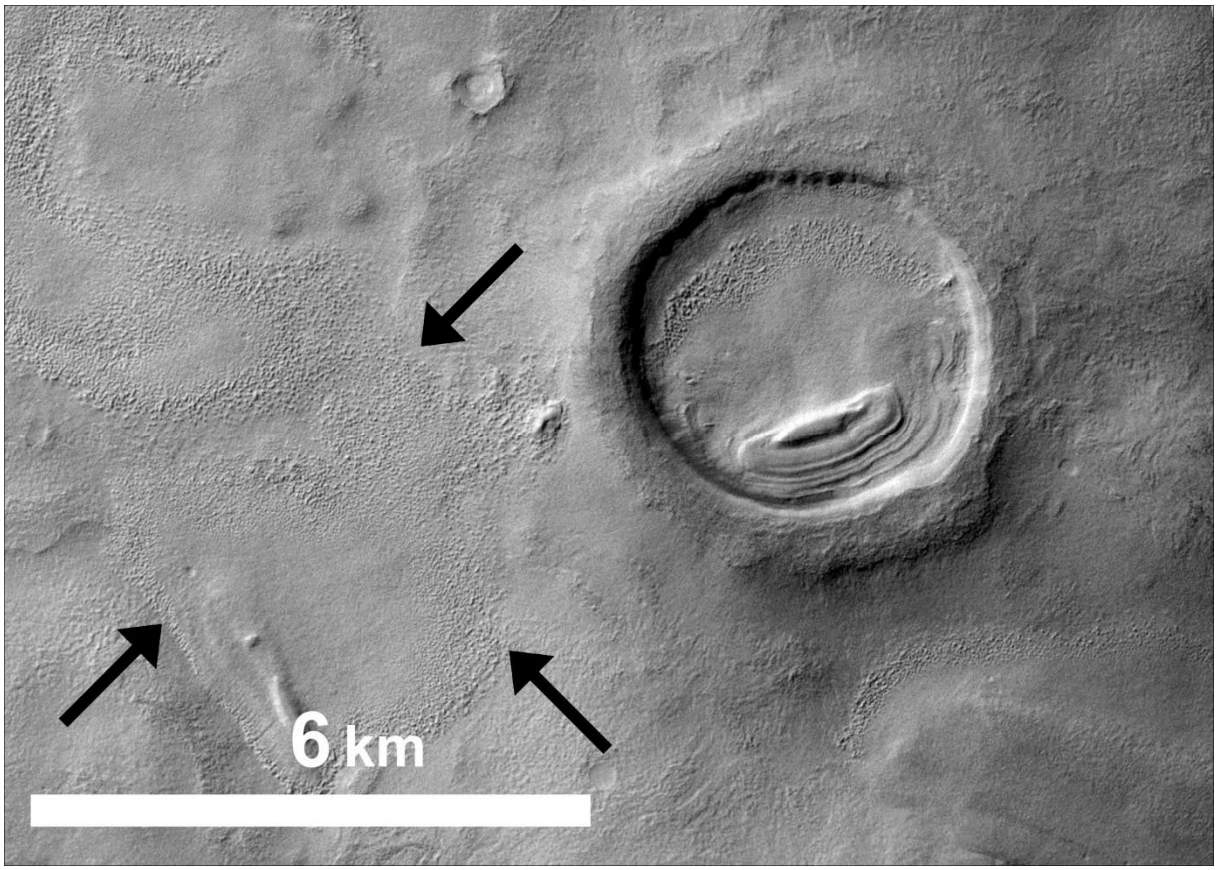

Fig. 23. *Crater filled with layered-remnant deposits (LRD). In the left part of the image, a younger, but marginally textured LDM (black arrows) is embedded into an older LDM layer (detail of CTX image centered at P18_008084_1461 at 35_S, 61.8_E).*

Viscous-flow features (VFF) are thought to be the result of creep processes of icy material (e. g., Milliken et al., 2003; van Gasselt et al., 2007a). Here all icy mass wasting deposits were classified as VFF (glacier-like flows, lineated valley fills, lobate debris aprons). Milliken et al. (2003) proposed that VFF's were formed in a ten meter-thick layer with high amounts of ice, which is currently being degraded. The global distribution of VFF is apparently linked to the distribution of LDM (Milliken et al., 2003; van Gasselt, 2010). The mapped VFF also include glacier-like features (Hubbard et al., 2014).

VFF mainly occur on elevations higher than -5,000 m; below this datum there are almost no VVF (*Fig. 15*) despite the presence of a significant relief at the basin floor (see *Fig. 3*). VFF are mostly observed on slopes steeper than 3° (*Fig. 16* and *Fig. 17*), with a preferred aspect peak towards E and a further but smaller peak towards W (*Fig. 24*). This aspect distribution is similar to that of the banded terrain. VFF tend to have higher TI values and low dust coverage (*Fig. 19* and *Fig. 21*).

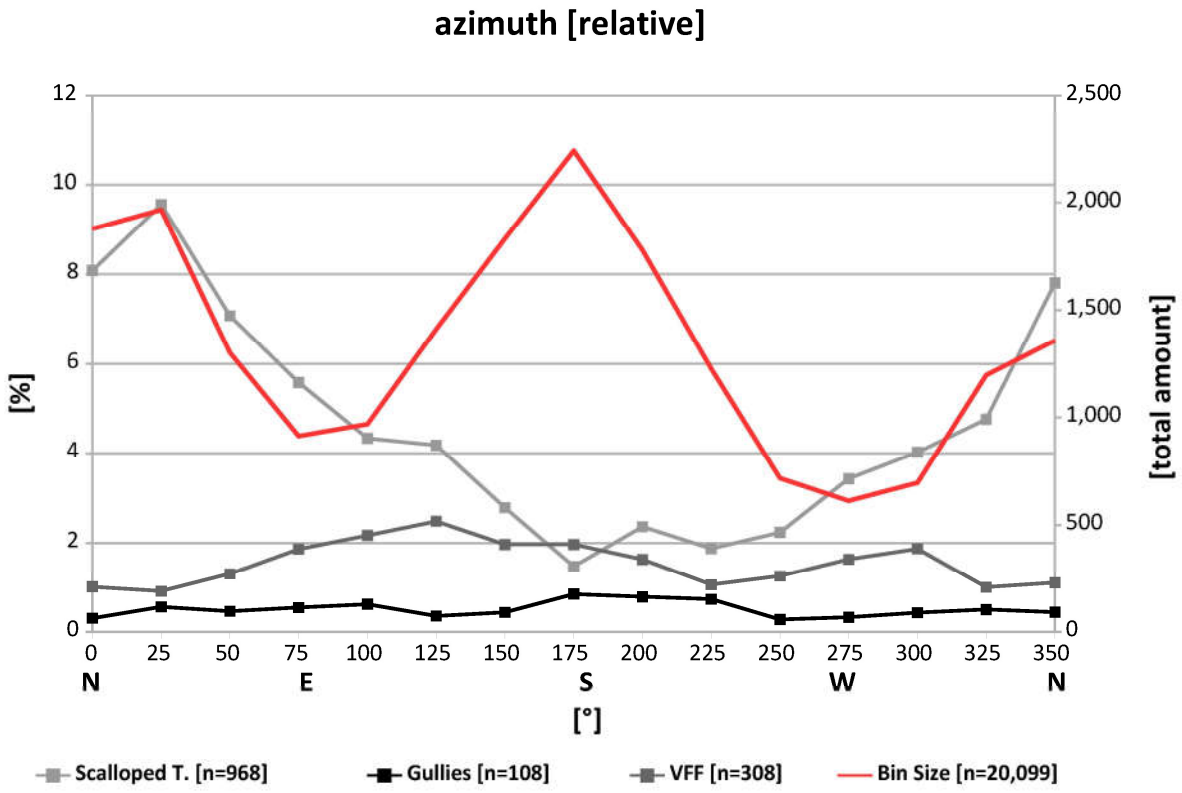

Fig. 24. *Normalized line graph contrasting the aspect behavior of scalloped terrain, VFF, and gullies in percent (left axis), as well as the bin size distribution of the grids (right axis).*

The informally named lineated terrain appears to be a degraded or deformed variation of LDM (*Fig. 11*). Its surface is rough, undulated, and furrowed. The furrows are arranged parallel to the slopes. Within Hellas Planitia, the LDM has two different forms: an older and deformed variety (here referred to as lineated terrain) is underlying a younger and smooth variety (here referred to as LDM). Lineated terrain is often exposed within smooth LDM, similar to nunataks (especially in Alpheus Colles region).

In Hellas, the lineated terrain is probably an older and degraded LDM deposit with a rough surface, and is widely superposed by the youngest LDM deposit. It mainly occurs at elevations between -6,500 and -4,500 m (*Fig. 15*). Its slope inclination maximum ranges from 2° to 4° (*Fig. 17*), and its aspect maximum is from E over N to W. Geographically, the lineated terrain concentrates in central Hellas, with smaller accumulations along the western and southwestern rim. In the Alpheus Colles region it is partially arranged in arcuate bands up to 300 km in length, and seems to be linked to the large pitted mounds (see paragraph for large-pitted mounds below). On the other hand, the lineated terrain and large pitted mounds apparently exclude each other; hence they both only occur adjacent to each other, but rarely together. Areas with a high density of lineated terrain are Coronae Planum, Alpheus Collesa, a rugged plain between Hellas Chasma and Talas crater, and the mountains at the terminations of Dao and Harmakhis Valles. In these areas this terrain type is severely lineated and possibly deformed. In THEMIS-nighttime data it has no preference for higher or lower TI values. However, the DCI shows a strong trend towards significant dust coverage (*Fig. 21*).

3.1.3 Water-related Landforms

Two types of channels are present in the study area: large outflow channels (*Fig. 1* and *Fig. 26*) and small (in some cases dendritic) channel networks. Several huge outflow channels drain into Hellas, i.e. Dao, Niger, Harmakhis, and Reull Valles. All of them are considered to be of late Hesperian to early Amazonian age, and they were probably formed by volcanic and/or tectonic processes (e. g., Leonard and Tanaka, 2001; Mest and Crown, 2001; Kostama et al., 2009). All of them are located at Hellas' eastern rim. The smaller channel networks (Navua Valles, Sungari Vallis, Mad Vallis, Axius Valles) show shallow and narrow valleys up to several hundreds of kilometers in length. They are also partially branched, and show no obvious source. Therefore, they may have either formed by surface runoff and/or ground-water sapping (Crown et al., 2005). Zuschneid and van Gasselt (2007) analyzed the age of the area around Sungari Vallis and found that the fluvial resurfacing events took place during the mid- to late Amazonian (~350 to 750 Ma).

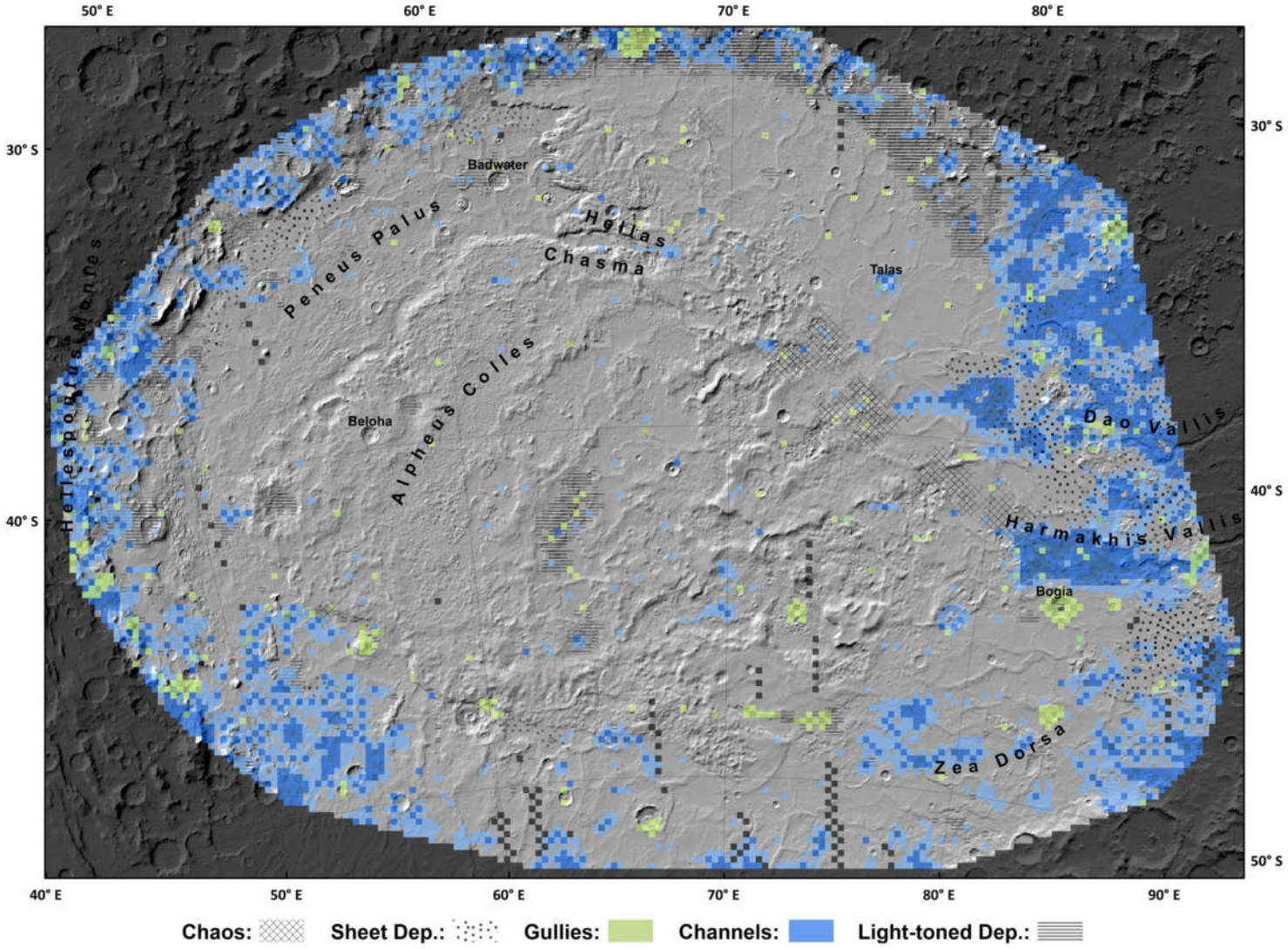

Fig. 25. *Gridmap showing the geography of potential water-related landforms (basemap MOLA).*

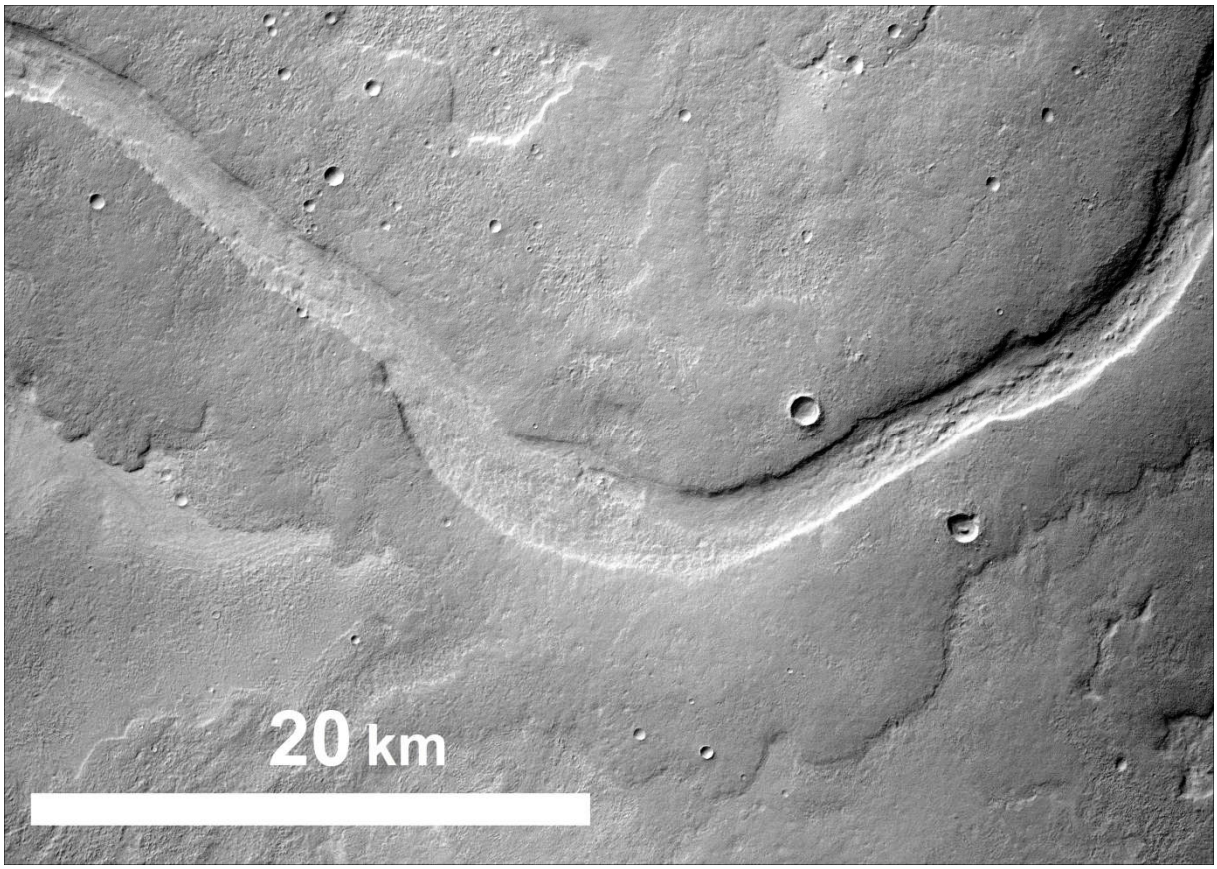

Fig. 26. *Extensive sheet deposits covering the banks of the lower Dao Vallis region (Cropped CTX image P19_008492_1423 at 39.9_S, 81.4_E, north is up). See Fig. 5 for location.*

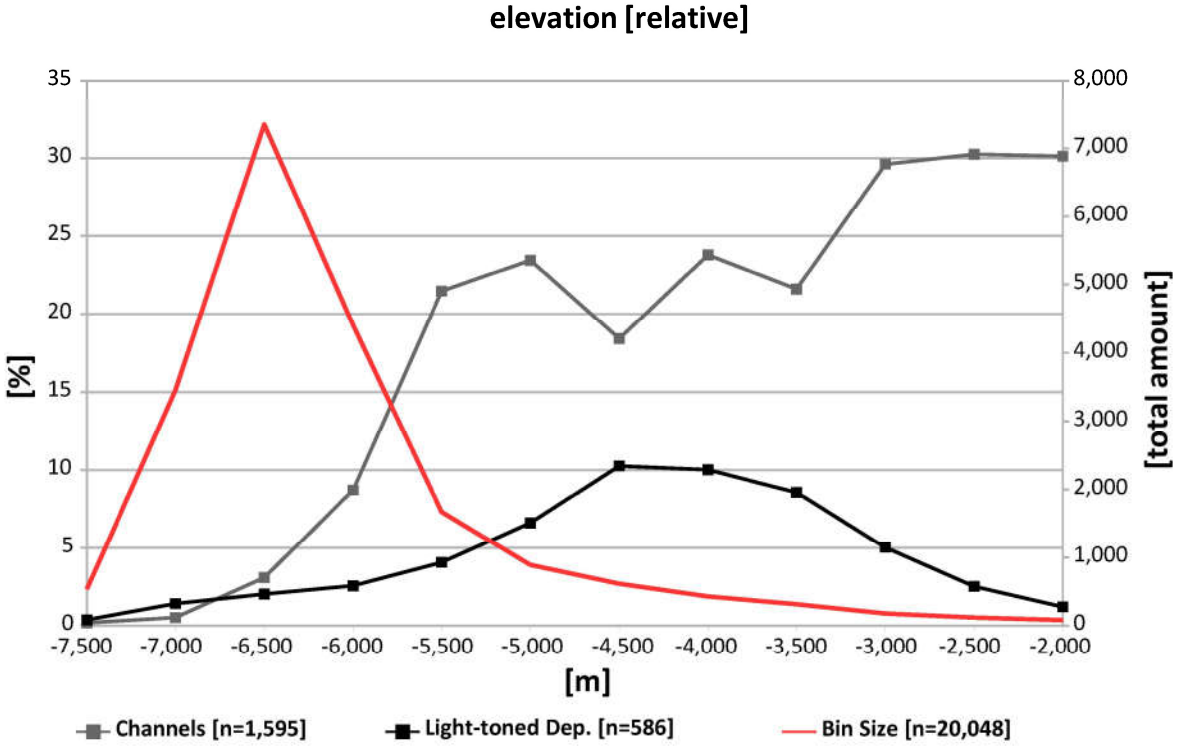

Fig. 27. *Relative elevation distribution of channels and light-toned deposits (left axis). The bin size (red line) presents the absolute frequency of analyzed grids (right axis).*

Channels are visible almost everywhere along the whole rim (*Fig. 25*). They are apparently linked to sheet deposits (see below). On the southern rim the density of channels is slightly lower. The highest densities occur along the eastern rim where the big outflow channels drain into Hellas Planitia. On the floor of the basin the spatial density of this type of landform is very low. Channels mainly appear at higher elevations (*Fig. 15* and *Fig. 27*) and steeper slopes. Their slope distribution mainly ranges from 3° to 5° (*Fig. 17*). Grids with channels generally have higher TI and DCI values, corresponding to a low dust coverage (*Fig. 21*).

Light-toned deposits (LTD) were already studied intensely in the Hellas region (*Fig. 27* and *Fig. 28*) especially along its northern and western rim and the high plains surrounding the impact basin (e. g., Wilson et al., 2007; Ansan et al., 2011; Carter et al., 2013; Bandfield et al., 2013; Chuang et al., 2015; Salese et al., 2016). The most prominent aqueous minerals in northern Hellas are Fe/Mg smectites of Noachian origin (Ansan et al., 2011). Moreover, chlorites, and opaline silica have been detected (Carter et al., 2013). Ansan et al. (2011) examined an extensive and thick sedimentary body in Terby crater, located on the northern rim of Hellas. They found evidences that the phyllosilicate-bearing LTD might be remnants of an ancient Noachian-aged fluvial deposit, which was eroded during the Hesperian. Furthermore, they hypothesized that these LTD might have been deposited as a delta in a subaqueous environment. Just north of Hellas, Salese et al. (2016) studied phyllosilicate-bearing intercrater plains that suggest a wet and depositional milieu during the Noachian. They also calculated relatively high erosional rates of these deposits (~1,000 nm/yr-1), suggesting an ancient sedimentary cycle in the northern Hellas region. During the Hesperian, these sediments have been partially covered by younger volcanic deposits (Salese et al., 2016). Another extensive area within Hellas suggesting a former aqueous environment is located along Hellas' western rim, and consists of poorly hydrated crystalline silica (Bandfield et al., 2013). Hence, at least northern and western Hellas experienced an intense period of aqueous activity during the Noachian, causing the formation of phyllosilicates.

Based on the mapping in this study, LTD such as those observed in Terby crater appear to be part of an extensive sedimentary belt extending up to 1,000 km along Hellas' NE rim (*Fig. 25*). An even wider extent cannot be excluded, as such deposits can only be identified if there are exposed outcrops visible. Other possible LTD deposits along the rim can be found in the Hellespontus Montes region along the western rim. On the floor of Hellas there are some further scattered occurrences; especially in an unnamed crater SW of Beloha crater. Most of the LTD are located at an elevation between -5,000 and -3,500 m (*Fig. 14* and *Fig. 15*). They tend to occur on steeper slopes with inclinations of 3° to 5° (*Fig. 17*). The aspect distribution shows a strong peak towards SW, which is likely due to the extensive sediment bank on the inner slope in NE

Hellas. In THEMIS-nighttime infrared data, LTD show a significant trend to high TI values. They are generally characterized by a very low dust cover (*Fig. 21*).

The high-resolution mapping of the entire Hellas basin was also used to identify possible ancient *shoreline* relicts in Hellas, which were suggested by Moore and Wilhelms (2001). They described at least one continuous scarp encircling the inner basin, and hypothesized it being the remnant of an old shoreline of a possibly ice-covered lake.

The mapping has not revealed clear evidence for an ancient shoreline. Their geomorphic expression may either be too weak due to erosion, or there may have never been a body of water within Hellas. Only two locations on the floor of the basin were detected where possible shorelines suggest that at least small lakes existed on the lowest parts of Hellas Planitia (*Fig. 28*). The amount of grids containing possible coastal morphologies was too small for statistical analysis (n=19), therefore, they were excluded from plots and maps.

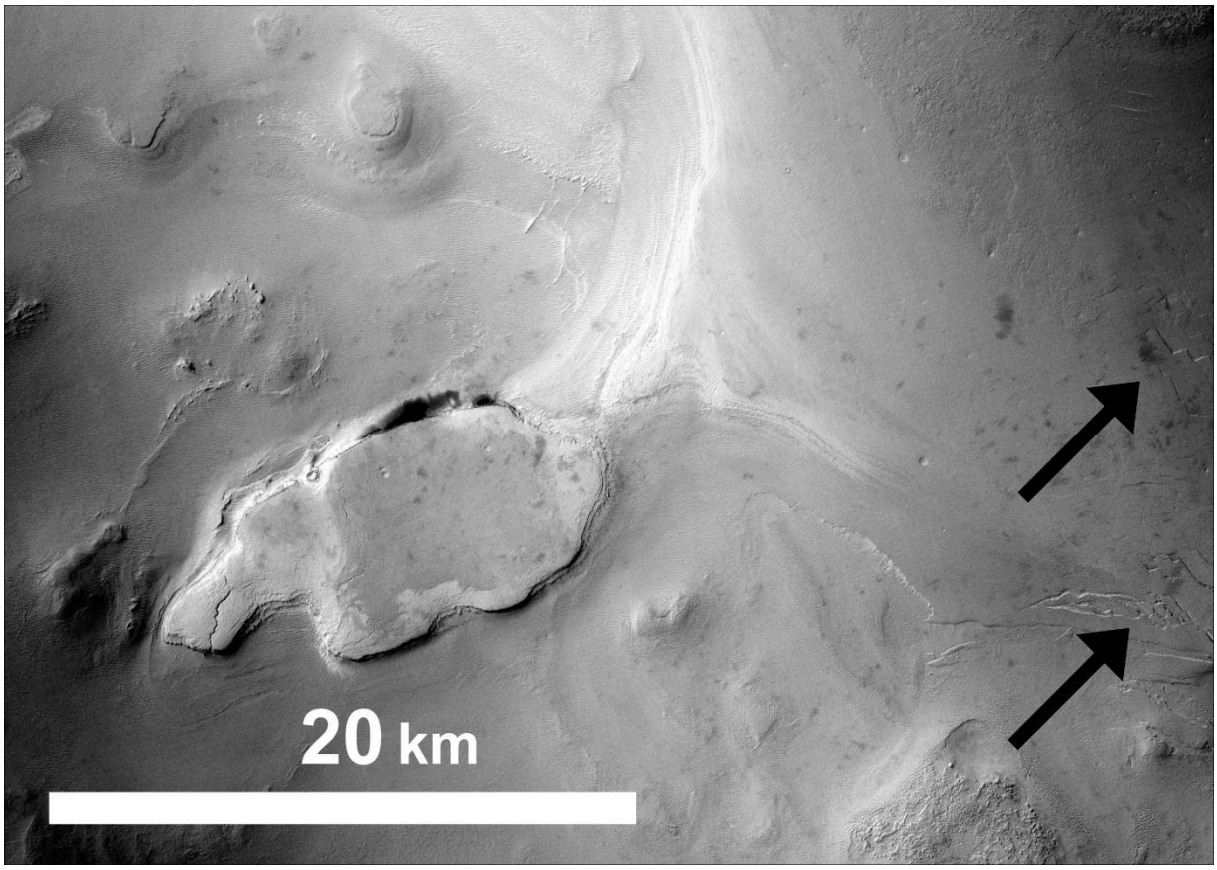

Fig. 28. *Light-toned deposits in a nameless crater on the western Hellas floor. The crater floor show extensive sedimentary bodies, obviously having a brittle behavior (note the young cracks and troughs indicated by black arrows). The curvilinear structure in the right part of the image might also be an ancient shoreline formed by wave refraction worth for discussion (CTX image P14_006700_1386_XI_41S306 W at 41.1_S, 53.2_E, north is up).*

Gullies are considered to be small and very local source-channel-fan systems. The length of typical gullies rarely exceeds 1,000 meters; their width ranges from several meters to a few decameters. They are found on steep, predominantly pole-facing, slopes, especially on crater walls or mountains, ranging from 24° to 30° inclination. They are mainly found in the Martian mid-to-high latitudes between 30° and 72° latitude (Harrison et al., 2015). First described by Malin and Edgett (2000) on basis of high-resolution MOC imagery, they were interpreted to be the most likely examples for possible liquid water activities on recent Mars, and thus, of high importance for potential astrobiological habitats. Today, there are three prevailing formation models; a wet, water-based origin, suggesting that either subsurficial water or melting ice formed gullies fluvially (e. g. Malin and Edgett, 2000; Christensen, 2003, Harrison et al., 2015), a CO2-based origin (e. g. Cedillo-Flores et al., 2011; Diniega et al. 2013; Dundas et al., 2015b), and simple gravitational dry mass movements of eolian sediments (Shinbrot et al., 2003; Treiman, 2003).

The density of gully distribution in Hellas is low compared to the surrounding highlands of the southern mid-latitudes (Harrison et al., 2015; *Fig. 25*). In this respect, the topographically low Hellas basin is similar to the northern lowlands, which also have a low gully density (Harrison et al., 2015). Within Hellas Planitia, most gullies were observed along the western, northern, and eastern rim as well as the southern basin floor. Gullies are mainly found along scarps or attached to the inner walls of medium- to large-sized craters. However, craters of a given size can display very different gully densities, e. g., in Bogia crater (75 km diameter) a high density of gullies could be confirmed, but in a similar-sized crater not far to the west of Bogia no gullies could be found. Even at Badwater crater, the lowest point on Mars, no gullies have been observed at CTX resolution. Other landforms displaying gully erosion are outcrops of light-toned deposits and LDM-covered mountains and hills. Despite of the low elevation of Hellas, there is much fewer gully activity than expected. The results show that gullies preferentially appear at higher elevations of >-4,000 meters (*Fig. 15*). In Hellas, most gullies occur on pole-facing slopes with high inclinations (see *Fig. 17* and *Fig. 24*); but it has to be noted that the slope values are averaged for 20×20 kilometers grids, which is too coarse to resolve the local slopes of gullies. Nevertheless, there seems to be a slight preference for gullies being located on pole-facing slopes even at large scale. Moreover, grids containing gullies show a strong shift towards higher TI values, in agreement to observations done by Harrison et al (2015). There is no correlation with respect to the DCI.

Sheet deposits are extensive, thin (meters to tens of meters thickness), and high-thermal inertia deposits covering areas with gentle slopes (*Fig. 17*). Morphologically, they must be related to the outflow channels. There are two possible origins of this landform: volcanic and/or fluvial. Lava sheet flows show a very rough, folded, and/or undulating texture, and are also interpreted as

inflated lava flows (Zimbelman et al., 2011; Leverington, 2011). Alternatively, they might also be of fluvial origin. In this case, they show a smooth and even surface and appear interconnected to channels. Voelker et al. (2013 and 2017b) described them as possible cryofluvial sediment flows. Thus, these sheet deposits would be the sedimentary remnants of ancient floods.

Most sheet deposits occur on the floor of Hellas Planitia close to its rim and channels (*Fig. 25*). There are prominent examples along the banks of the big eastern outflow channels of Hellas, but also in Peneus Palus. Most of these deposits are located at an elevation of -6,000 to -5,000 m within gently inclined and SW-exposed grids (*Fig. 15*). In THEMIS data, they exhibit a strong trend toward high TI values. Grids containing sheet deposits show a thin dust cover according to DCI data (*Fig. 21*).

3.1.4 Other Landforms

The honeycomb terrain is a unique landform on Mars and only occurs on the bottom of Hellas Planitia close to the lowest elevations of the planet. It is characterized by cell-like depressions that are separated by narrow ridges. Several hypotheses have been proposed to explain the formation of this peculiar landform. Moore and Williams (2001) suggested that these features might be imprints of grounded icebergs, molding these forms into the sediments. Mangold and Allemand (2003) hypothesized their evolution by endogenous convection cells. Salt diapirism (Mangold and Allemand, 2003; Bernhardt et al., 2016) and ice diapirism (Weiss and Head, 2017) have also been proposed.

The honeycomb unit is only observed in the Peneus Palus region. No other evidences for honeycomb terrain in the Hellas region were found. Honeycomb terrain is located along the transition zone between Peneus Palus and Alpheus Colles, and predominantly occurs on extremely low elevations of -7,000 m or less and on gentle slopes ranging between 1° to 2° (*Fig. 17*). It occurs mainly on slopes with aspects towards SE and NW. THEMIS data do not show a trend of grids containing honeycomb terrain towards low or high TI values. However, in DCI there is a strong trend towards a thick dust cover (*Fig. 21*).

Because of its enormous depth, and hence, its dense atmosphere the investigation of dunes in Hellas Planitia is of special interest. The formation of dunes requires a source area, a sufficient amount of lose material, and an active wind regime. On Mars, dunes preferentially occur in topographical depressions such as impact craters or valley floors, but also around the north polar cap. However, the Mars Global Digital Dune Database (Hayward et al., 2014) shows a scarcity of dunes for the Hellas region. Most dunes on the planet are of mafic composition, suggest-

ing that they have a similar origin (Tirsch et al., 2011). An intracrater dune field on the southern basin floor of Hellas Planitia was studied by Tirsch et al. (2011), who found spectral evidence for pyroxenes.

In Hellas Planitia, most dunes occur south of 40°S in impact craters and other topographic lows. There is one extensive dune field in Hellespontus Montes on the rim of Hellas. Surprisingly, there are almost no dunes in the deepest parts of the basin, e. g., in Peneus Palus. Most dunes appear at elevations higher than -5,000 m (*Fig. 15*). Regarding slope inclination, dunes mainly occur on inclinations of 2° to 5°. Most of the grids containing dunes are exposed to the southeast. THEMIS infrared data has a relatively high dispersion, while DCI data shows a tendency towards low dust coverage (*Fig. 21*).

3.2 Sheet Deposits

The study area (165×125 km) is located at the rim of eastern Hellas Planitia along the lower reaches of Dao Vallis. The majority of the area consists of interior Hellas plains of Hesperian origin (Leonard and Tanaka, 2001; Bernhardt et al., 2016), which are interpreted as low-viscosity lavas (Leonard and Tanaka, 2001). Other surface units are Noachian to Hesperian rim terrain and channel material of Hesperian to Amazonian origin (Leonard and Tanaka, 2001). Most of the plains are dissected by wrinkle ridges. The elevations range from -6,600 to -4,400 m with respect to the Martian datum, and the relief is generally flat, except for some rugged mountains in the northeastern part of the study area. The most prominent physiographic feature is the large, E-W-trending outflow channel, Dao Vallis. After reaching the plains of Hellas the channel is very narrow and shallow as compared to its upstream parts. Its width ranges from 1.7 to 2.2 km, and its depth is around 50 m. In the central part of the study area the channel becomes wider (up to 16 km) and deeper (up to 170 m), but a smaller channel continues on the bottom. The big section finally bifurcates into four branches. The banks of the channels are covered by a thin sheet of lobate deposits, hereafter called sheet deposits (*Fig. 26*).

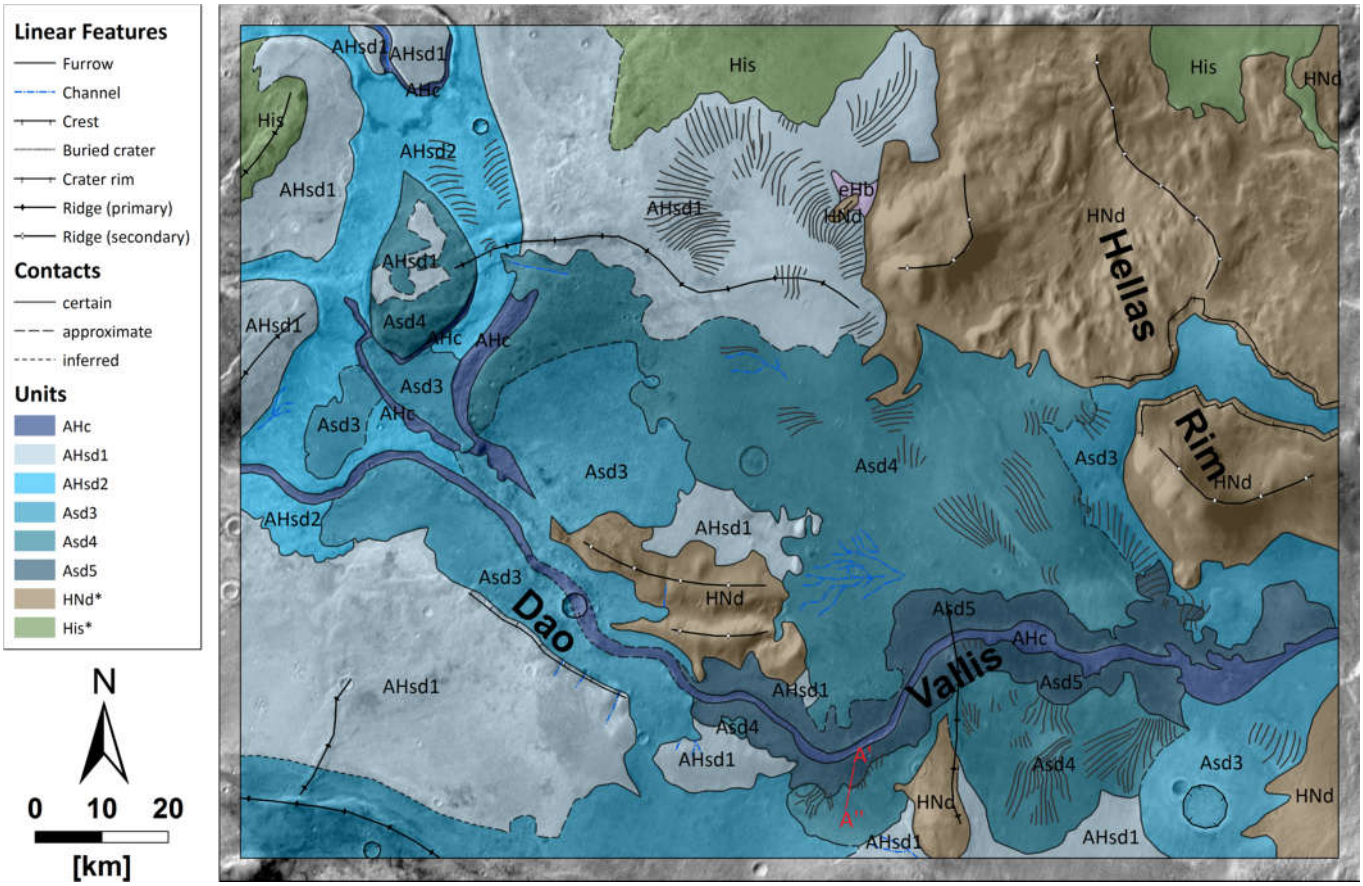

Fig. 29. *Geological and geomorphological map provides information about the geospatial behavior of sheet deposits in the study area in eastern Hellas Planitia (Basemap: THEMIS). *derived from Tanaka et al., 2014. Red line indicates the location for the topographical profiles shown in Fig. 35.*

3.2.1 Geography and Physical Properties

All of the sheet flows are related to Dao Vallis, covering its banks and adjacent plains respectively. They are only found on level plains and very low inclinations (see also Voelker et al., 2017a). They also flow around topographical obstacles. Besides, their flow fronts are often arranged in lobes. Topographical analyses have revealed a significant extent of each sheet deposit layer within the study area. More than 14,500 km² of the research area are blanketed by five sheet deposit units (*Fig. 29*).

AHsd1 (Amazonian-Hesperian sheet deposit 1) – Oldest and most extensive sheet deposit unit covering 5,069 km² (only the visible part!). Its mean thickness is 18.9 m (see *Table 5*), making it the least thick of the sheet deposit units. In some parts this unit shows conically arranged ridges and grooves (*Fig. 30*). Their length varies from a few hundred meters to several kilometers, and their widths/wave lengths range from 5 to 15 m. Their spacing and relief is too narrow and subtle, respectively, to be resolved in MOLA or HRSC DEM's; so the elevation difference between the ridges and furrows does very likely not exceed more than a few meters. In some parts this unit is deformed by large wrinkle ridges; up to many tens of kilometers in length and 5 km width, up to a height of 100 m. Compared to all other sheet deposit it has also the lowest thermal inertia.

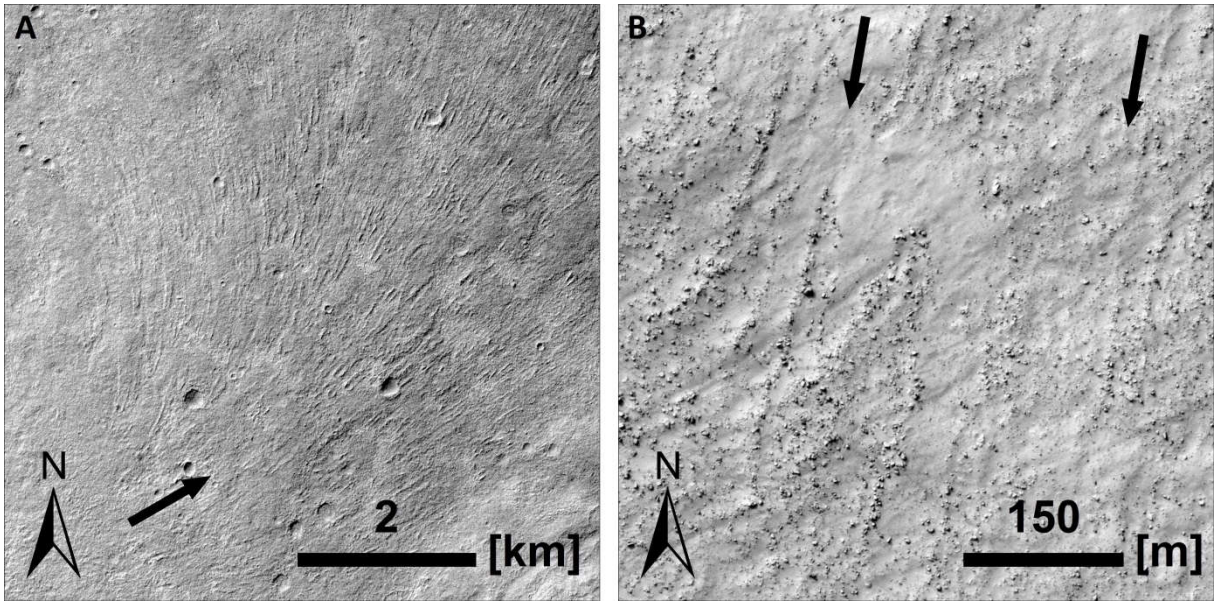

Fig. 30. *Conically shaped lineations on top of a sheet deposit. Left: CTX imagery presents the geographical arrangement on a large-scale (P19_008492_1423; centered at 81.2 E, 38.3 S). Right: HiRISE datasets show the composition and small-scale composition of the lineations (PSP_007200_1395_RED; centered at 82.4 E, 39.8 S). See Fig. 5 for location.*

AHsd2 (Amazonian-Hesperian sheet deposit 2) – The unit is mainly found within the wide parts of the Dao Vallis channel, but also covers rarely the overbanks. Its mean thickness is 29.4 m. Like unit AHsd1 it is partially covered by conically-shaped ridges and grooves, and is also affected by large wrinkle ridges.

Asd3 (Amazonian sheet deposit 3) – This unit is found in both the wide channel floors and the adjacent plains. Its mean thickness is 26.1 m. In very few areas this unit is deformed by small to medium wrinkle ridges, being several tens of kilometers long and 3 km wide. Their height cannot be reliably measured in MOLA datasets.

Asd4 (Amazonian sheet deposit 4) – This unit covers wide parts of the plains adjacent to Dao Vallis. It clearly flowed around obstacles like hills (*Fig. 31*). The unit shows clear signs of conically arranged lineations. Its mean thickness is 29.1 m. The surface of Asd4 is also characterized by a unique distributive channel network having a length of ~15 km and a width of 10 km (*Fig. 31*). Using MOLA single shot data, each channel has a depth of only a few meters. The channels follow the topographic gradient (mean inclination approx. 0.3 %) towards west, but there is no distinctive source visible. The source region is located on top of Asd4, close to the margin of the overlying unit Asd5. Moreover, there are distinctive polygonal features on top of the flow with a mesh size of less than 10 m. Asd4 shows little deformation by wrinkle ridges. Only in its southernmost part it is affected by a large wrinkle ridge.

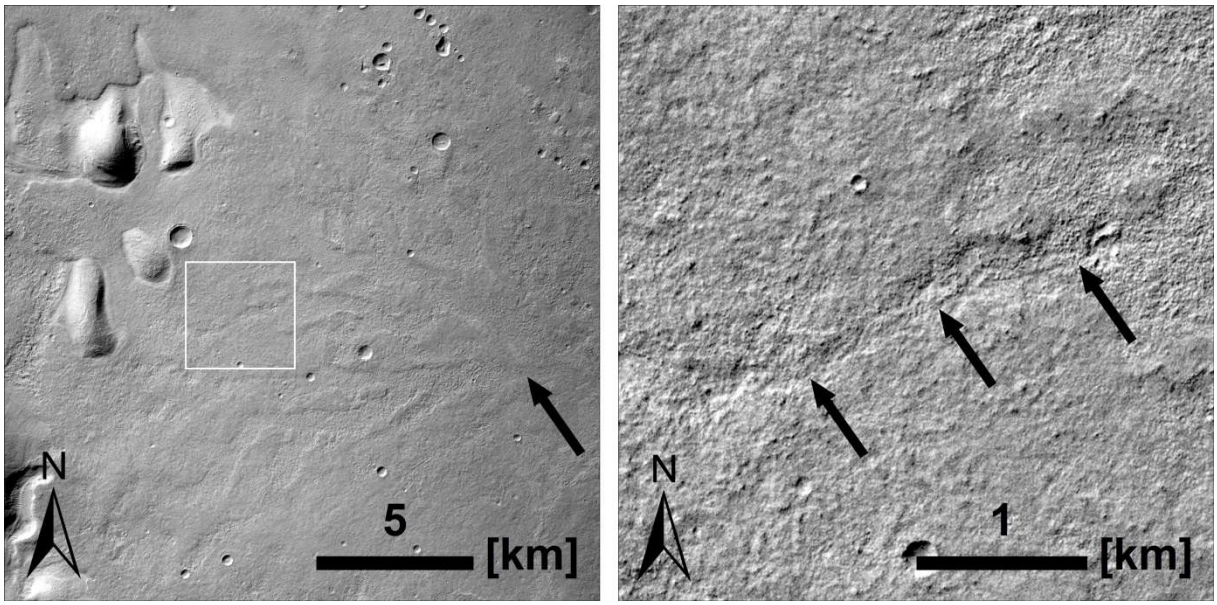

Fig. 31. *Left: Dendritic channel system on top of sheet deposit unit Asd4. The black arrow indicates the origin of this distributive network. Note also the topographical obstacles in the upper left engulfed by sheet flows. The white box indicates the location of a close-up view of one of the channels visible on the right. Right: Narrow channels of fluvial character are clearly visible; here, black arrows indicate the alignment of a possible fluvial channel (both images: CTX P19_008347_1382, centered at 81.4°E, 39.5°S). See Fig. 5 for location.*

Asd5 (Amazonian sheet deposit 5) – This is the least extensive of all sheet deposit units covering 954 km². It is confined to two narrow swaths north and south of Dao Vallis and extends up to 14 km from the Dao Vallis main channel. Partially, there are small polygons (mesh size up to 10 m) visible (*Fig. 32*). In THEMIS-nighttime datasets it shows the highest thermal inertia values compared to all other sheet deposit units. The unit is mainly free of wrinkle ridges. Only in its central part a large wrinkle ridge is cross-cutting the deposit.

For older underlying units are not relevant for the understanding of sheet deposits, the descriptions of Tanaka et al. (2014) were adapted.

eHb (Early Hesperian basin unit) – The unit is immediately underlying most of the sheet deposits. Its thickness has been estimated several hundred meters. Tanaka et al. (2014) interpreted them as basin fill of volcanic, lacustrine, or aeolian origin, likely dissected by fluvial erosion and tectonic activities.

lNh (Late Noachian highland unit) – In the study area this unit corresponds to the rugged basin rim of Hellas. The unit has been interpreted of undifferentiated material of either fluvial, volcanic, or impact-related origin. The material is lightly to severely degraded or deformed (Tanaka et al., 2014).

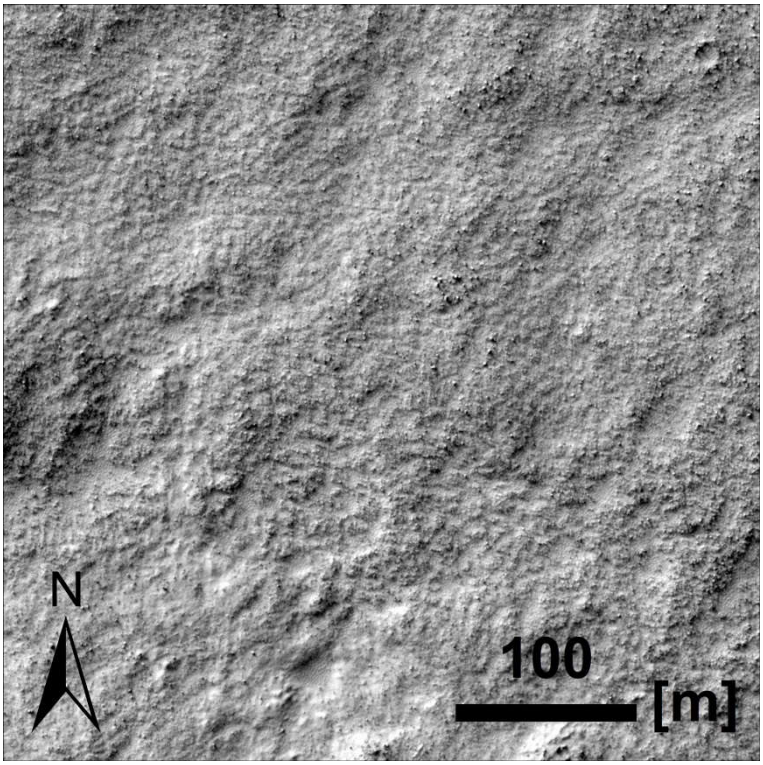

Fig. 32. *Polygonal structures are only visible in high-resolution HiRISE images. The polygons are located on top of unit Asd5. Note that the hexagonal shape of the polygons is hard to distinguish, and the troughs are widened and shallow; probably due to degradation processes (PSP_008492_1400 _RED; centered at 81.5 E, 40.0 S). See Fig. 5 for location.*

Unfortunately, OMEGA observations covering the area of interest are highly dominated by dust and reveal no clear evidence for hydrothermal alteration within the flows. OMEGA and CRISM derived spectra display the typical featureless 'dust' signature (Mustard et al., 2007; Poulet et al., 2007). Hints for hydration of the surface material have been found 400 km upstream of Dao Vallis outside of the study area due to distinct absorptions near 1.5 and 2 µm in the OMEGA spectra (Zalewska et al. 2013). However, it cannot be excluded that the observed signature is caused by H_2O ice aerosol features rather than hydrated minerals (Wiseman et al., 2016). These absorptions have been detected only in OMEGA observations acquired during the southern winter and slightly deepen with increasing latitude. They appear strongest within the channel, which corresponds to the geological unit AHc in the study area. But this might be caused by more aerosols surviving in shadows of the low lying topography of this area.

3.2.2 Stratigraphy and Age Determinations

The map (*Fig. 29*) indicates 5 distinctive layers of sheet deposits AHsd1-2 and Asd 3-5 superposing each other. Unit AHc covers the floor of Dao Vallis and is very likely composed of the same material as the other sheet flow units; but it cannot be linked to one of the other five layers. Unit eHb (Tanaka et al., 2014) is one of the major interior units within Hellas Planitia of early Hesperian origin. The oldest unit in the study area is lNh (Tanaka et al., 2014) being the ancient rim of Hellas, evolved during the late Noachian.

According to previous studies, the eastern plains in Hellas are of Hesperian age (Leonard and Tanaka, 2001; Tanaka et al., 2014; Bernhardt et al., 2016). As these authors mapped the whole Hellas basin at large scale, they did not differentiate between areas that are covered by sheet deposits and those which are not; hence, we defined the counting areas at a smaller scale for each unit. The results revealed an Amazonian to Hesperian origin of the sheet deposits. These ages of the oldest units (AHsd1 and AHsd2) fit approximately into the Hesperian time frame suggested by Leonard and Tanaka (2001), Tanaka et al., (2014), and Bernhardt et al. (2016). However, the three youngest units Asd3 to Asd5 show a clear Amazonian origin, and are significantly younger than the surrounding Hesperian plains (*Fig. 33*, *Fig. 34*, and *Table 5*). These ages result in the stratigraphy presented in *Fig. 34*. The ages of the units eHb and lNh are derived from Tanaka et al., (2014).

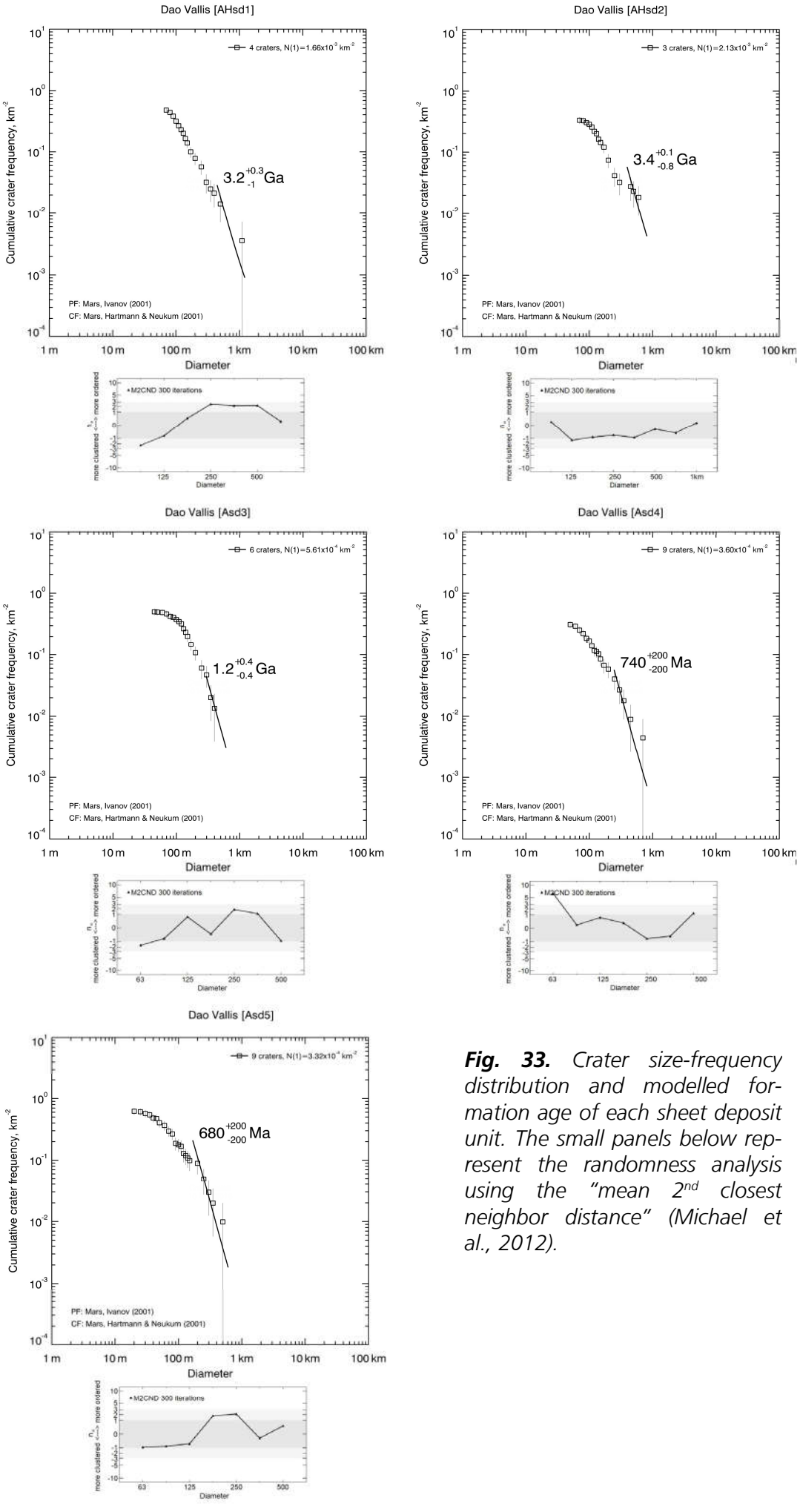

Fig. 33. *Crater size-frequency distribution and modelled formation age of each sheet deposit unit. The small panels below represent the randomness analysis using the "mean 2nd closest neighbor distance" (Michael et al., 2012).*

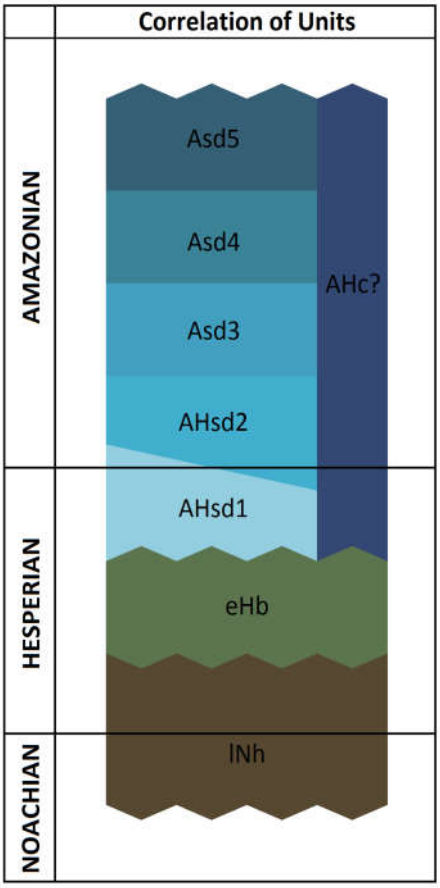

Fig. 34 (left). *Correlation of units in the study area. The age of AHc could not be reliably determined. But it must have been deposited and/or modified during each flood event. Hence, we located it generally in the same ages of the sheet deposits. The ages of His and HNd were obtained from Tanaka et al., 2014.*

Fig. 35 (below). *Plot presenting the averaged profile of two parallel MOLA single shot datasets (Orbits 13,480 and 16,687) of a flow front of unit Asd5; see red line A' – A'' in Fig. 29 for location. The mean deviation of both profile is 2.29 m. Thickness has been calculated manually between top point T and bottom point B. In this case the depth of the flow front totals 28.96 m (black line) and 33.39 m (grey line).*

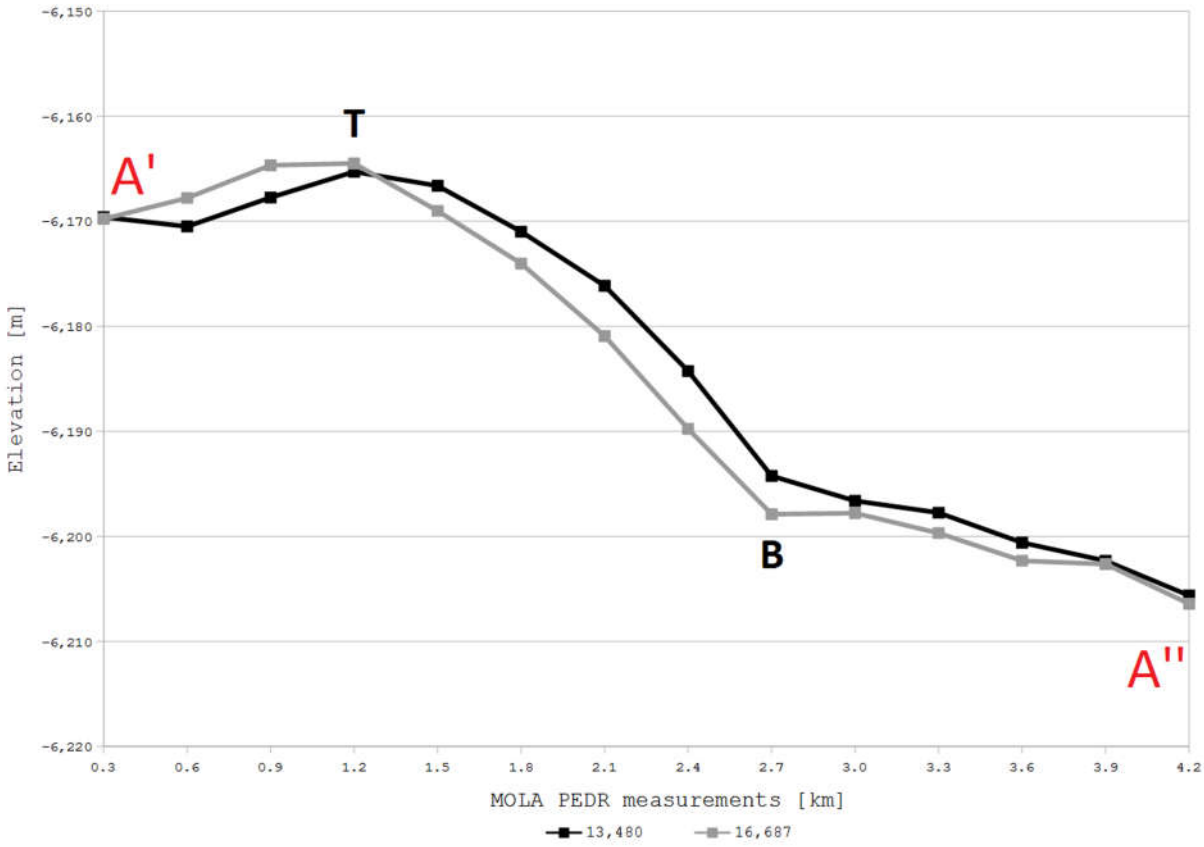

3.2.3 Thickness and Volume of Sheet Deposits

In contrast to the areal extent of each sheet deposit unit, its thickness can only be derived from the topography of each flow front. Due to the lack of thickness information of the interior of the sheet deposits, these thickness values of the fronts were extrapolated to the whole visible extent of each unit. Moreover, crater outcrops have been examined within the sheet deposits in order to derive further thickness values (Basilevskaya et al., 2006), but no distinctive layers could be observed. As a result, the presented numbers may have large uncertainties. The values range from 18.9 (AHsd1) to 29.6 m (Asd5) resulting in an overall average thickness of sheet deposits of 26.6 m (see *Table 5*). The volume of sheet deposits is in the range of several tens of cubic kilometers (*Table 6*).

Table 5. *Morphometric properties of each sheet deposit unit of the study area and selected volcanic flows (based on MOLA single shot data). [1]Giacomini et al. (2009), [2]Pasckert et al. (2012), [3]Williams et al. (2007), [4]Thordarson and Self (1998). For representative comparisons of the Martian volcanoes we only used ages of emplaced lava flows afar from the caldera.*

	Max [m]	Mean [m]	Min [m]	Area [km²]	Volume [km³]	Model age [Ma]
AHsd1	24.4	18.9	13.4	5,069.0	67.9 – 123.7	3,200 (+300/-1,000)
AHsd2	44.6	29.4	14.2	1,210.5	17.2 – 54.0	3,400 (+100/-800)
Asd3	38.1	26.1	14.0	3,665.2	51.3 – 139.6	1,200 (±400)
Asd4	42.8	29.1	15.4	3,689.0	56.8 – 157.9	740 (±200)
Asd5	36.9	29.6	22.2	953.7	21.2 – 35.2	680 (±200)
Arsia Mons	37.9	29.1	20.3	-	-	260[1]
Elysium Mons	76.1	63.6	51.1	-	-	1,810 (+230/-240)[2]
Hadriacus Mons	100.4	86.8	73.3	-	-	3,700 (+100/-200)[3]
Roza Member, Earth[1]	67.0	36.0	11.5	40,300	1,300	-

3.2.4 Comparison with Volcanic Sheet Flows on Mars

The thickness values, length, and volume of the studied sheet deposits in Hellas correspond to those described for the terrestrial Roza Member formation of the Columbia River Basalt Group. However, no morphologies were confirmed indicative for lava flows.

Besides morphometric analyses the sheet deposits in eastern Hellas were tested for characteristic lava features (Keszthelyi et al., 2004). Keszthelyi et al. (2004) compared volcanic flows in Iceland to those on Mars (preferentially in Athabasca Valles region). They described five geomorphological characteristics for lava sheet flows. (1) Longitudinal ridges on top of the flows (a few meters wide to several hundred meters in length). (2) Plates measuring several hundred meters to kilometers in diameter "floating" on the surface of the flows; the plates are surrounded by ridges. (3) Convex polygons on top of the flows several meters across. (4) Parallel grooves on the lava flow extending several kilometers in length; occurring behind engulfed obstacles. (5) Inflated lava flow margins and a smooth texture (pahoehoe).

The sheet flows in eastern Hellas were inspected for the five volcanic morphologies defined by Keszthelyi et al. (2004). However, no clear evidence for most of these morphologies was found; i. a. no compression ridges could be detected. The parallel grooves of Athabasca Valles (Keszthelyi et al., 2004; Fig. 10 therein) are genetically not related to the sub-parallel/conic lineations of eastern Hellas shown in *Fig. 30*. While those of Athabasca Valles occur in the lee of obstacles in lava flows, the grooves and ridges in Hellas are not related to any obstacles and are often arranged conically in plan view. Moreover, no platy morphologies on the sheet deposits in Hellas were found.

The sheet deposits of the study area were compared to flows of three Martian edifices of unambiguously volcanic origin (*Table 5*). This was necessary to provide a sufficient variety of volcanic flow morphologies in order to compare them with sheet deposits found in Hellas Planitia.

Volcanic sheet flows of the Amazonian Tharsis and Elysium provinces extend several hundred kilometers in length and several tens of kilometers in width. In contrast, the older Hesperian highland volcanoes (e. g., Hadriacus Mons) are lacking such extensive sheet flows. Instead they show relatively narrow and short deposits of probably pyroclastic origin in proximity to the caldera (Wilson et al., 2007).

The surface of volcanic flows near Arsia Mons is severely degraded presenting an extremely rough texture (*Fig. 36*). The flows are covered by yardang-like knobs indicative for widespread aeolian erosion. The flow margins are also dissected and eroded. Today's thickness values of the flows range from 20.3 m to 37.9 m; compared to the flows of Hadriacus Mons and Elysium

Mons they are relatively thin. However, it might be possible that they were once much thicker before erosion took place. In THEMIS nighttime datasets the flow fronts are very distinctive too, and thermal inertia is low compared to the underlying material. Tanaka et al. (2014) determined an Amazonian-Hesperian age for the flows of Arsia Mons.

The flows of Elysium Mons show clear lobate flow fronts indicative for effusive volcanism (Tanaka et al., 1992). Their surface is generally smooth and partially streaked by troughs and grooves. Moreover, there are many small pits visible; up to a few decameters in diameter (*Fig. 36*). As the determined flow is located in the northern mid-latitudes at ~35°N the pits might be sublimation pits within an overlying volatile-rich Amazonian latitude-dependent mantle ranging from 30° to 70°N (e. g., Kreslavsky and Head, 2002b). Thickness values of the measured flow range from 51.1 m to 76.1 m. In THEMIS nighttime datasets it has a high thermal inertia. In HiRiSE imagery there are almost no rocks visible on top of the flow; only along the flow fronts are several accumulations of rocks. The age of the flows around Elysium Mons has been described Hesperian (Tanaka et al., 2014).

Unlike Arsia Mons and Elysium Mons, Hadriacus Mons only shows disputable flow fronts very close to its caldera (*Fig. 36*). It could not be determined if these morphologies are flows or the scarps of a retrogressively eroded layer. Crown and Greeley (1993, 2007) and Williams et al. (2007) determined these lobes as eroded pyroclastic deposits, and confined effusive volcanism only to the caldera of Hadriacus Mons. The surface is undulating and scarcely covered by small rocks (<3 m in diameter). The layer thickness ranges from 73.3 m to 100.4 m. In THEMIS-nighttime imagery the layers do not contrast to their surroundings.

3.2.5 Hydrologic Assessment

Assuming the deposits visible today are the sedimentary remnants of fluvial floods (see chapter 4.2.2.3), it was possible to recalculate the required total water volume by combing the current sedimentary volume with the water-sediment ratio for each fluvial scenario as reported by Costa (1988); see *Table 1*. The assumption that at least five flood events took place is based on the five distinctive units in the study area. Their lobate margins allow a reliable stratigraphical reconstruction (*Fig. 34*). The work also comprised the search for terraces along the side walls of the main channel, in order to reconstruct possible episodes of flooding, but no clear evidence for terraces was found.

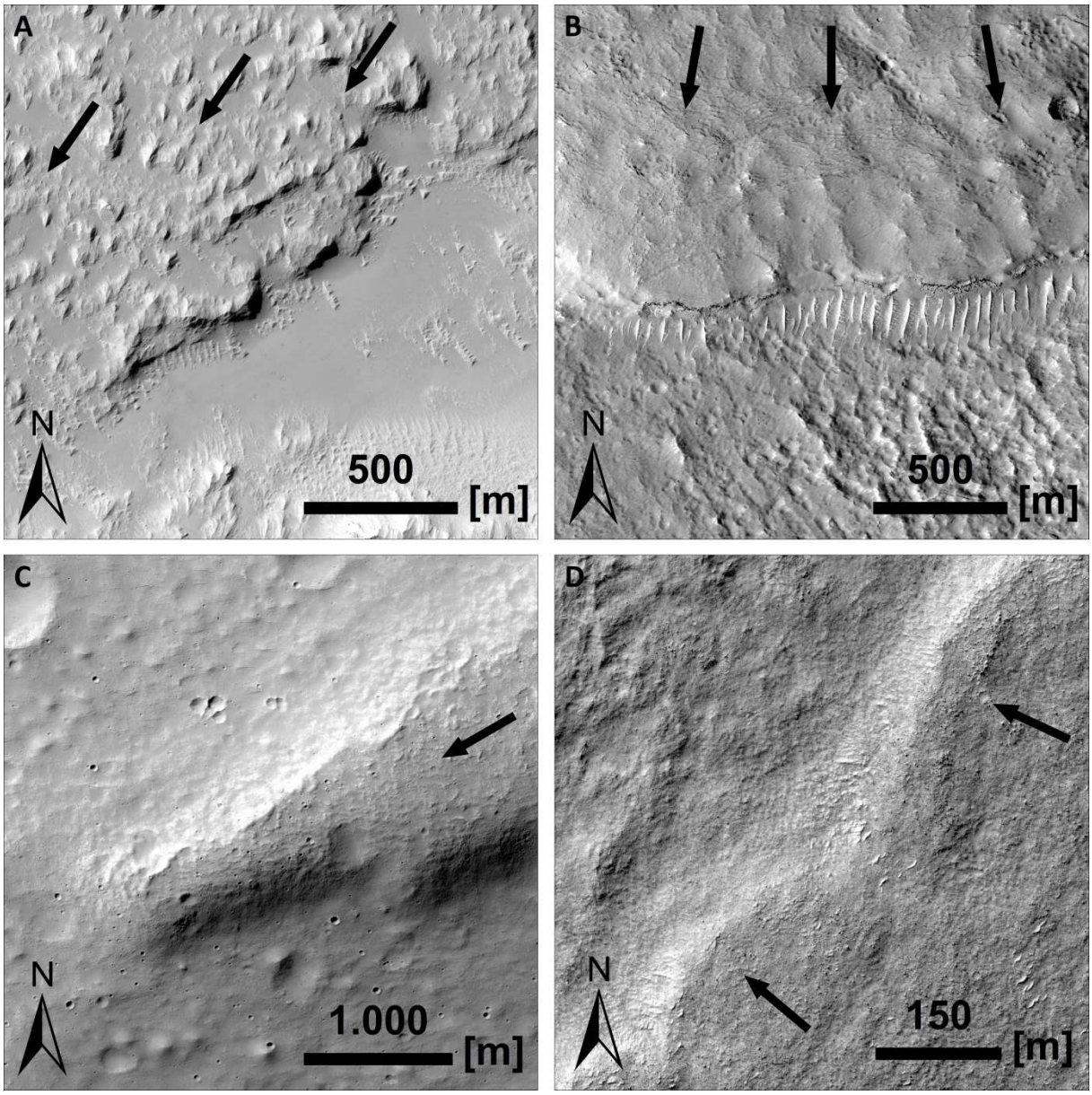

Fig. 36. *HiRISE imagery of volcanic flows and the examined sheet deposits in Hellas. Black arrows indicate the direction of flow. A: Southwestern flank of Arsia Mons (ESP_017176_1600_RED, centered at 232.5°E, 19.9°S). B: Northern flank of Elysium Mons (ESP_037499_2160_RED, centered at 141.9°E, 35.4°N). C: Western flank of Hadriacus Mons close to its caldera (PSP_008452_1400_RED, centered at 91.9°E, 30.6°S), note the different scale. D: Sheet deposit in the study area of eastern Hellas Planitia. The visible lobe is the flow front of unit Asd4 (right) superposing the older unit AHsd1 (left) (PSP_007200_1395_RED, centered at 81.4°E, 39.8°S); see Fig. 5 for location.*

Table 6. *Water volumes implied from sediment volumes for different transport types (see chapter 2.3 for data basis and calculations). Assuming a fluvial origin this table presents the additional volume of water required to develop the sheet deposits of the study area. For details of each flood type see text. Maximum values are based on both maximum thickness values (Table 5) and maximum water content for each flood type (Table 1) and vice versa.*

Unit	$Volume_{water}$ [km³]								
	Water Flood			Hyperconcentr. Sed. Flow			Debris Flow		
	Max	Mean	Min	Max	Mean	Min	Max	Mean	Min
AHsd1	30,797.4	15,534.6	271.7	494.7	285.7	76.6	139.5	79.9	20.3
AHsd2	13,442.6	6,755.7	68.8	215.9	117.7	19.4	60.9	33.0	5.1
Asd3	34,771.7	17,488.5	205.3	558.6	308.2	57.9	157.5	86.4	15.3
Asd4	39,314.1	19,770.7	227.2	631.6	347.8	64.1	178.0	97.5	17.0
Asd5	8,762.3	4,423.5	84.7	140.8	82.3	23.9	39.7	23.0	6.3
Total	*127,088.1*	*63,972.8*	*857.6*	*2,041.6*	*1,141.7*	*241.8*	*575.6*	*319.8*	*64.0*

3.2.6 Terrestrial Analogues

For a better understanding of the fluvial hypothesis of sheet deposits, similar deposits on Earth were evaluated; especially those within arid and cold environments (however, in a much smaller scale). The detected morphologies and key features that could be used as analogues are longitudinal lineations and distributive dewatering networks similar to those found in Hellas Planitia (*Fig. 30* and *Fig. 31*). These observations support that fluvial processes are able to evolve such widespread deposits and morphologies.

In the Mjezzem sabkha (salt pan) in western Libya the deposits of a mudflow have been identified (*Fig. 37*), which were deposited between 2012 and 2016 in an endorheic basin by floods from the Wadi Awwal. The deposits appear to be very thin (very likely <1 m thickness, as they are easily overrun by car tracks and do not show distinctive shadows). They also show lobate flow fronts in plan view, which are subdivided into much smaller flow lobes or "toes". On top of these deposits are extensive longitudinal grooves (>100 m in length) that might be caused by dewatering processes. The grooves display a radial pattern and diverge from the source of the flow. In contrast to the Martian lineations there are no distinct ridges between the grooves; instead there is a smooth blanket. Moreover, the surface is lacking any boulders within the given image resolution. At field work in 2010 only fine-grained material has been detected within the salt pan assuming that this material is the main compound of these flows.

On Svalbard small-scale dewatering morphologies on top and at the flow front of a small mud flow were found. Their length ranges from several tens of meters to one hundred meters (*Fig. 38*). The mud flow itself was still active but very slow moving during inspection in summer 2016. The flow had a thickness of a few decimeters at the flow front, and up to at a meter within the main body and consisted mainly of clay and silt.

In both terrestrial analogues the main compound of the sheet flows are small grain-sizes (clays to sand). Furthermore, evidences for dewatering processes could be detected. But in contrast to the sheet deposits in Hellas, no boulders have been detected on top of the flows, suggesting that the formation of these morphologies has been enhanced by a high amount of clays: As clays and silts are able to fill most of the pore volume, the sedimentary body is quickly saturated with water, resulting in a positive pore water pressure, and hence dewatering activities.

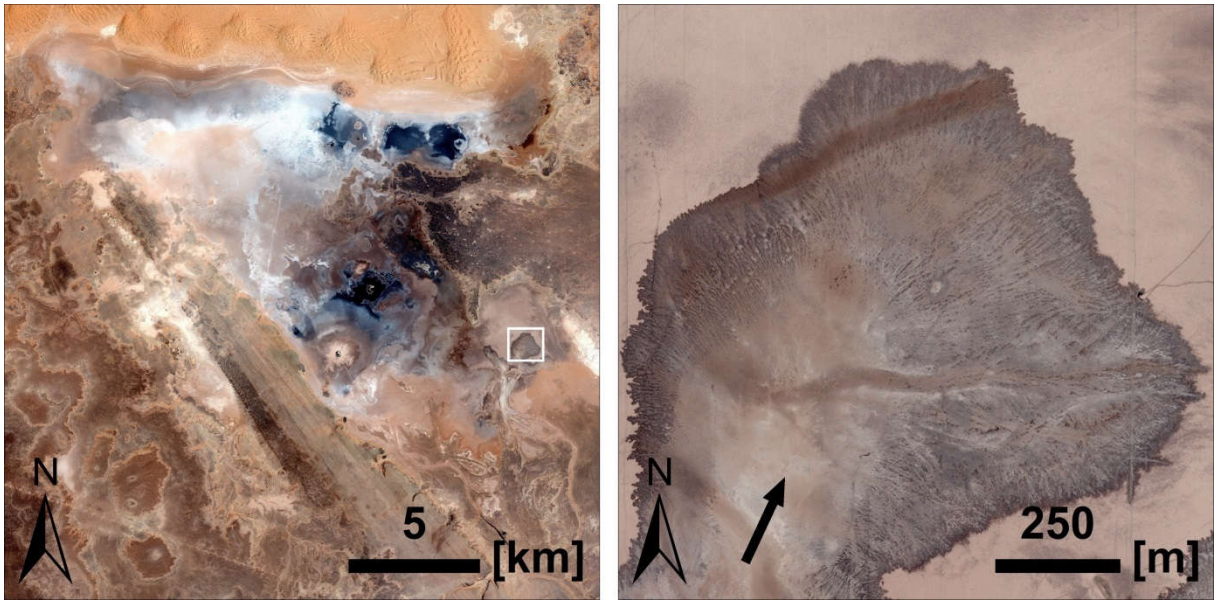

Fig. 37. *Left: Context image of the Mjezzem salt pan 35 km northeast of Ghadames, Libya. White box indicates the location of a mud flow emerged around 2014 from endorheic Wadi Awwal (right). The black arrow indicates the flow direction of the flow (Imagery ©2014 European Space Imaging).*

Fig. 38. *Small-scale mud flow on Svalbard at Kongsfjorden in summer 2016. The width of this very slow moving flow is around 4 m. Black arrows indicate dewatering morphologies on top of the flow (M. Voelker).*

4. Discussion

4.1 Geography of Hellas Planitia

4.1.1 Ice-related Landforms

Hellas Planitia is located within the southern latitude-dependent mantle belt (Schon et al., 2012). Despite most of Hellas is covered by LDM, the results show an extensive gap of LDM in the northeastern part of the basin. Subsequently, possible climatic scenarios how this gap might have evolved are presented. The dense atmosphere of the study area as well as high temperatures (Millour et al., 2015 and Forget et al., 1999) are able to cause more intense winds (Greeley et al., 1980) and absorbing higher amounts of water than other more elevated regions of the planet (Weischet, 1994). Dense air (Kieffer et al., 1992) and high wind speeds (Siili et al., 1999) in Hellas condition transport/removal of solid particles as well as a higher absorption of water. Both processes are important factors in eroding and/or subliming LDM.

The most important evidence for sublimation of LDM is the scalloped terrain and the rough texture on its surface; both are likely the result of ice removal. There are three extensive areas in Hellas where LDM is either strongly textured (i.e. degraded) or not existent:

1) The highly textured LDM north of ~35°S is probably the result of changing solar insolation caused by the variable obliquity of Mars` rotational axis (Laskar et al., 2004). Today, solar insolation, and hence, temperatures, are higher in the northern part of Hellas as compared to the southern part (Millour et al., 2015 and Forget et al., 1999), leading to an increased degradation of the LDM in northern Hellas. It is assumed that the highly textured LDM in northern Hellas is the remnant of an older LDM layer that has been deposited during high obliquity excursions, when the temperatures at these latitudes where significantly lower.

2) An inclined area at the southwestern inner rim of Hellas displays LDM which appears both significantly textured and scalloped. This region is located adjacent to a wide gap of the rim called Malea Planum, connecting the Hellas basin to the south polar highlands. According to existing wind circulation models (Ogohara and Satomura, 2008; Howard et al., 2012) winds drain through this southwestern gap towards north and into Hellas. Siili et al. (1999) and Howard et al. (2012) suggest that these winds might be caused by polar air masses moving down into Hellas Planitia by katabatic processes (cold winds caused by gravitational forces). The high wind speed at this inclined gap may be able to remove the protecting surface lag of the LDM (Head et al., 2003), and hence, facilitate the sublimation of the ice content of the LDM resulting in a rough texture.

3) The wind circulation models for Hellas might also explain a complete gap of LDM in NE Hellas (*Fig. 2* and *Fig. 10*). The winds originating from the south polar highlands are rotating clockwise within Hellas (Howard et al., 2012). When they have reached the northern rim of Hellas, they first turn east, and later south again, suggesting that these air masses heat up at the northern-most part of Hellas, due to the higher solar insolation at these latitudes (<35°S), before they move south again. The high temperatures cause a decline of the relative humidity, advancing desiccation of soils. The area in NE Hellas where these dry air masses would interact with the surface corresponds to the location of the gap of LDM. Consequently, it can be assumed that the dry air either eroded a former LDM blanket or completely prevented its formation at this place.

In Hellas two different types of scalloped terrain located within LDM were found: (1) distinctive pitted depressions (SP in *Fig. 11*) and (2) an extensive rugged morphology like the scalloped depressions, however, at a much smaller scale and areally widespread (SE in *Fig. 11*). Hence, their shapes provide information that both morphologies have been evolved by the same process.

Following, evidences are presented that the development of scalloped terrain not only depends on solar insolation but also on aeolian processes. They appear to be geospatially linked to regions with a strong wind regime. Moreover, their axes are often orientated along the wind direction.

Siili et al. (1999) calculated wind patterns on the southern slopes of Hellas and found evidence for very high wind speeds up to 30 m/s. The geospatial and geomorphic characteristics of scalloped terrain supports the hypothesis of wind currents originating from south polar highlands (Siili et al., 1999; Howard, 2000; Howard et al., 2012, Ogohara and Satomura, 2008; compare for discussion on LDM above); i. e., the longitudinal axes of the depressions are orientated into the direction of the wind, and not directly north toward the sun. Furthermore, the small ridges are also located transverse to the wind (similar to ripples), suggesting that these ripple-like ridges developed in a unidirectional wind regime. As the wind generally comes from the same direction it probably caused very shallow ridges in the loose material covering the surface, e. g., dust or the LDM itself. Thus, a small-scale relief of ripples could evolve. In turn, this relief caused little variations of the wind speed near the surface, and hence, different intensities of erosion. On top of these ripples the wind was most intense, and could erode LDM easier than in between. As a result, the protecting lag of LDM has been removed along the tops of ripples, and wind currents could excavate the volatiles beneath, especially along the side opposed to the wind, leaving transversal ridges behind (see *Fig. 11*and *Fig. 39*). Similarly, the dominant wind direction may have been responsible for the deflection of the scallop orientation from N-S (expected if only

insolation were responsible) to NW-SE, caused by a mixture of solar insolation and wind. As their steep side is located against the wind, the volatiles exposed at the steep scarp are subject to intensified degradation by wind-driven sublimation. There are dense populations of these deflected scalloped depressions and ridges in SW Hellas directly adjacent to the Malea Planum gap (*Fig. 10*), where strong unidirectional winds have been proposed (Siili et al., 1999; Howard et al., 2012).

On the other hand, no such scalloped depressions and ridges occur on similarly inclined slopes in SE Hellas, where the same northern exposition and amount of insolation is given. This leads to the idea that wind, besides solar insolation, may be a prominent factor in the development of the scalloped terrain in SW Hellas. This notion is consistent with other models suggesting an aeolian origin of the scalloped terrain (e. g., Costard and Kargel, 1995; Zanetti et al., 2010; Ulrich et al., 2010; Séjourné et al., 2011). Hence, strong winds (Siili et al., 1999) might have triggered or at least supported the removal of the dusty surface lag (Head et al., 2003) by aeolian erosion, and hence, entailing desiccation processes (Mustard et al., 2001), causing the development of the scalloped terrain.

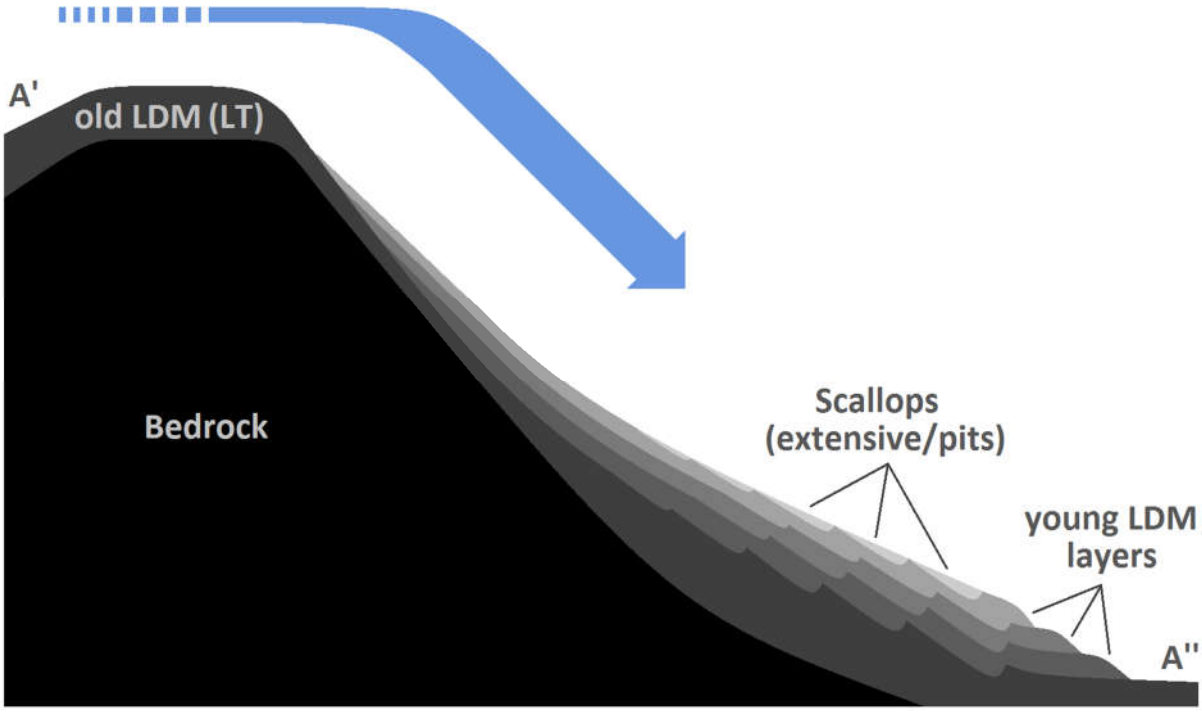

Fig. 39. *Sketch illustrating the erosion of LDM by wind (for the location of A'-A'' please take a look at Fig. 11). The underlying bedrock (black) is covered by several generations/layers of LDM (shades of grey). The volatile-rich LDM material is successively eroded by winds (blue arrow), eroding the protective surface lag and enhancing sublimation. Thus, a distinctive scalloped terrain evolves.*

The large-scale distribution of layered-remnant deposits (LRDs) within craters over all of Hellas Planitia appears to be controlled by a latitude-dependent process, as they mainly occur north of 37°S. On the other hand, their small-scale distribution remains paradox and difficult to explain. At local scale, they predominantly exist on the equator-facing wall of impact craters, i. e. on the part of the crater that receives the highest amount of solar insolation. However, if they consist of the same material as LDM, as proposed by Morgenstern et al. (2007), they would be subject to increased sublimation in relatively warm or dry local environments.

Although their large-scale distribution appears to be latitude-dependent, the maps suggests that LRDs are more or less independent from the distribution of LDM, as they occur in areas with both thick and absent LDM cover. For example, they also occur in the region in NE Hellas that probably never has been blanketed by LDM (see discussion above on LDM). Besides the assumption that their evolution and composition is not linked to LDM, three different scenarios can be distinguished:

Enhanced aeolian processes might have caused sublimation and/or excavation of LDM material. But wind does not explain the consistent location of LRD in the southern half of craters over such a huge area, as the currents in northern Hellas are generally west-oriented. If LRD were eroded by wind, they are expected to be located on the wind-protected western lee side of the inner crater bowl.

As they predominantly occur north of 37°, solar insolation, and hence, thermal sublimation, could explain the latitude-dependence of this landform. But it does not explain why LRD-layers consistently "survived" in the southern part of craters that (currently) receives the most intense solar radiation. This hypothesis might be conclusive if LRDs were located in the shaded northern half of a crater, where volatiles are protected of sublimation. Due to Mars' permanently changing obliquity of up to 47° within the last 20 Ma (Laskar et al., 2004), it is possible that the northern parts of the crater interiors once received a high amount of solar insolation even at these latitudes. Thus, any volatile-rich material could have been removed there.

Another explanation for this paradoxical location might be that LRDs are a result of relief inversion. In this scenario, today's LRDs were once hollows within a volatile-rich layer (LDM). The origin of the hollows might be caused by enhanced sublimation of a thin LDM layer draping over the topography of an impact crater. This would preferentially remove LDM in the southern half of the crater bowl, were the incoming insolation is highest, leaving a hollow. Subsequently, this hollow may have been refilled by a younger material poor of ice (e. g., dust). When the remaining LDM material around and beneath this younger material vanished later, it remained as a LRD in this crater. Considering all these aspects, the last two scenarios (or a combination of

both) can be assumed as most likely, as only these scenarios can explain the continuous location of the LRDs within impact craters and their latitude-dependence.

Viscous-flow features (VFF) form by gravity-driven processes, so by definition they can only form in the presence of inclined topography (slopes). In Hellas, VFF seem to be absent at low elevations of less than about -5,500 m, despite of the presence of relatively rough topography, and hence, slopes, on the basin floor (*Fig. 3*). The terrain of the floor may not be as steep as the surrounding rim, but there are also chasms (Hellas Chasma), chaotic terrains (Hellas Chaos), big craters (e. g., Badwater, Talas, Beloha), cliffs, tall mounds and peaks rising up to 1,200 m above their surroundings, as well as extensive hummocky terrains with hills rising more than 300 m above the plains (Alpheus Colles). The question is then, why are there no VFF observed on the slopes of the deepest parts of Hellas? As discussed above, it appears possible that the high air pressure and wind activities at these low elevations are able to absorb even more moisture than at higher elevations, and hence, desiccate the regolith. These conditions may have prevented the development of VFF in Hellas.

A further observation indicates that VFF might be genetically linked to gullies. Van Gasselt (2007b) already suggested such a relation, as VFFs might have been able to contain a sufficient amount of water necessary for the development of gullies. In Hellas, they often share the same locations too. Moreover, both preferentially appear on elevations higher than -5,500 m and steep slopes. Milliken et al. (2003) found that gullies and VFFs on the southern hemisphere also share the same poleward exposition; however, in Hellas Planitia their aspect values differ from each other: VFFs are mostly exposed towards E and W, in contrast to the preferred aspect values of gullies, tending slightly towards S (*Fig. 24*). Both landforms rarely occur on highly insolated and, hence, warmer, north-exposed slopes. Whereas gullies are dominantly located on shaded south-facing slopes, VFFs mainly appear on slopes receiving medium solar insolation. Based on the 20×20 km grid map resolution, gullies and VFFs probably do not occur on north-exposed slopes as ice may long have disappeared or may never have accumulated on these relatively warm slopes.

The banded terrain, so far only detected in Hellas, is hypothesized to be a mobilized viscous flow of an ice-rich material, similar to the VFF (Diot et al., 2014, 2016). Based on the analysis of HiRISE images it has been suggested that banded terrain represents near-surface ice deposits that are subject to viscous downslope flow (Diot et al., 2014, 2016). The mapping results enabled comparisons between the large-scale geographical distribution of the banded terrain and the VFF. Based on these results both landforms display different characteristics regarding their elevation, slope inclination, and DCI. In contrast to VFF, the banded terrain occurs at much lower

elevations and on shallower slopes. Moreover, the banded terrain has a higher dust cover; probably caused by its low elevation, and thus, higher atmospheric activities.

As VFF, a landform requiring volatiles, seem to avoid low elevations in Hellas, it is likely that desiccating environmental conditions on the low-lying Hellas floor are caused by a dense and warmer atmosphere. However, banded terrain is also interpreted to be related to the deformation of ice-rich material and predominantly occurs at these lowest elevations (Diot et al., 2014, 2016). This observation presents a paradox, as one type of ice-rich landforms (banded terrain) occurs on the floor of Hellas, whereas another one (VFF) is lacking.

Putting all possibly ice-related landforms in context it can be suggested that several climatic cycles caused deposition and degradation of LDM, and hence, the formation of LT and LRD (*Fig. 11* and *Fig. 23*). As both landforms often appear as layered features, each layer could be the result of one LDM episode. Most recently, the development of scalloped terrain is evidence for degradation of the volatile-rich LDM blanket. Scalloped terrain is hypothesized to be an early stage of the geomorphologic process eroding LDM that leads to the development of LT and LRD. Moreover, VFF and the banded terrain seem to be inactive today, as no deformed craters on top of their lobes in Hellas have been detected.

4.1.2 Water-related Landforms

Despite there is a high morphologic diversity of *channels* in Hellas Planitia, their general density in the study area is comparatively low. Besides the big outflow channels in the east (i. e., Dao and Harmakhis Vallis), very young and extensive channel systems along the rim (e. g., Navua Valles), and older, more eroded or muted, short channel networks were detected too. The distribution of channels along the rim of Hellas Planitia provides information for three different environmental conditions for their development.

The big eastern outflow channels are comparable with other outflow channels on the planet triggered by volcanic activities resulting in the release of subsurface water. Their dimensions which require enormous water volumes might suggest theories of a former lake within Hellas (e. g., Moore and Wilhelms, 2001). However, the valleys have been determined of Hesperian/Amazonian age (Leonard and Tanaka, 2001; Crown and Greeley, 2007), hence, Hellas would have contained a lake at the same time. But this appears to be unrealistic as the Martian climate at this time was already too cold (Schuster and Weiss, 2005) and the atmosphere too thin, in order to maintain such an extensive and deep body of water, even in Hellas.

Small and typically dendritic valleys are widespread along the rim. They were probably unable to transport high amounts of water because of their narrow and shallow profiles. Some of the small valleys, e. g., Navua Valles, show very pristine morphologies suggesting an Amazonian age (Hargitai and Gulick, 2017).

Along the southern rim the density of channels is very low, indicating that either climatic conditions prohibited their development at these (colder) latitudes, or these channels have been significantly eroded (e. g., by aeolian processes). Furthermore, a later superposition by other materials, e. g., volcanic deposits from the adjacent Malea Planum volcanoes (Williams et al., 2010) is also possible. The lack of channels on the basin floor is still unclear.

Extensive thin deposits (hereafter referred to as *sheet deposits*) on the floor of eastern Hellas are apparently associated with the big outflow channels, suggesting that they are either of volcanic or fluvial origin.

If they are of volcanic origin they might be deposits of magmatic sheet flows, similar to those in other big provinces of Mars (e. g., Tharsis or Elysium). If so, their likely source was Hadriacus Mons ~800 km to the east, as there is no other obvious volcanic edifice in their vicinity. However, the surface of the sheet deposits in eastern Hellas lacks typical volcanic features like a platy-ridged morphology (Keszthelyi et al., 2004). Please see also chapter 4.2.

Another scenario suggests a fluvial genesis. Kostama et al. (2008) reported evidence for the extensive release of subsurficial ice-bearing layers around the head regions of the big outflow channels (e. g., Dao Vallis). These layers were covered, and hence, protected by younger volcanic layers probably originating from Hadriacus Mons. After then, subsurficial magmatic intrusions may have triggered the melting and runoff of these ice-rich layers. When the ice melted, this ice-dust mixture (together with the overlying volcanic layer) converted into a liquid mixture with a high amount of sediments and began moving downward towards the Hellas basin as a so-called hyperconcentrated sediment flow or debris flow (Costa, 1988). At this time, the morphologies of the outflow channels had not yet developed. Thus, the sediment flow covered extensive parts of the eastern Hellas floor and deposited widespread sheet deposits. When the flow continued, the relative amount of sediments decreased by two processes; first, the sediments from the eroded overlying volcanic layer in the channels' source region had been washed out and deposited first, and second by kinetic sieving processes. When the flow became clearer it turned from a depositional into an erosional mode, commencing to incise the channels into the sheet deposits themselves. Thus, the lower and much narrower parts of the big outflow channels might have evolved on the basins floor (~250 km north of Bogia crater). Moreover, it is likely that fur-

ther sedimentary flows drained through these channels later, covering the banks of these valleys with additional layers of sheet deposits (*Fig. 26*).

The results have shown that there are no obvious *shoreline* morphologies along the rim of Hellas, which could indicate an extensive and long lasting body of water as suggested by Moore and Wilhelms (2001). If there was indeed a body of water, it may not have existed long enough to form distinct coastal morphologies, or such easily degradable morphologic signatures may have been eroded over the last ~3 Ga. Ghatan and Zimbelman (2006) already detected a general paucity of coastal morphologies on Mars and found five possible scenarios why there is a lack of such landforms. (1) There was never an ocean/large standing body of water on Mars. (2) An ocean existed but wave intensities were too small to form distinctive shorelines (see also Kraal et al., 2006). (3) An ocean existed but the influx of sediments was too small to form coastal morphologies. (4) There was a frozen ocean that was unable to form shorelines. (5) There was an ocean that formed shorelines; however, these morphologies have widely been eroded over the last 3 Ga. So if there was an ocean on Mars, it more likely that it existed during the Noachian instead of Hesperian or Amazonian (Ghatan and Zimbelman, 2006).

Despite the lack of possible shorelines indicating a large lake within Hellas, there is evidence for coastal morphologies in association with LTD in small closed depressions at low elevations on the floor of western Hellas, (*Fig. 25* and *Fig. 28*), e. g., in two craters northeast and southwest of Beloha crater. The southwestern crater shows arcuate lineations behind a sedimentary obstacle typical for littoral erosion morphologies caused by wave refraction (Panizza, 1996). The waves of a hypothesized lake might have eroded the sedimentary layers, which were deposited in the crater when the lake level was higher. Moreover, *Fig. 28* shows some cracks in the uppermost layer on the far right. This might be a hint that a material in the subsurface (water?) has been removed, causing contraction or even lateral movement of solidified sediments downslope. Most of these fissures appear to be recent, as their edges are still pretty sharp. Therefore, an alternative hypothesis to a Hellas-wide paleo-sea is that Hellas might have hosted at least some smaller lakes.

The extensive *sedimentary bank* along Hellas' western to northeastern rim, consisting of light-toned deposits (LTD), has been mapped as a Noachian subdued cratered unit (Npl2) as well as a Hesperian ridged plains unit (Hpr) by Leonard and Tanaka (2001). These authors interpreted the Noachian subdued cratered unit as a thin blanket of aeolian, fluvial, or possibly volcanic origin. The younger Hesperian unit was interpreted as volcanic flood material consisting of low-viscosity lavas (Leonard and Tanaka, 2001).

Ansan et al. (2011) and Salese et al. (2016) suggested a sedimentary origin for the layers along the northern Hellas rim of Noachian age. Here, the presented grid-mapping results, based on high-resolution imagery, supported theories made by Ansan et al. (2011) and Salese et al. (2016) that these bright deposits would not be consistent with mafic lavas. OMEGA and CRISM spectra reveal extensive Fe/Mg phyllosilicates deposits in this region (Carter et al., 2013). The observed phyllosilicates along the rim are evidence for water activity in Hellas during the Noachian, comparable to the sedimentary bank in the circum-Chryse Planitia region (Carter et al., 2015). As these sedimentary deposits are mainly found at an elevation ranging from -5,000 to -3,500 m along the rim, this sedimentary bank might support hypotheses of a former sea within Hellas (Moore and Wilhelms, 2011). But this hypothesis is opposed by the lack of coastal morphologies in Hellas Planitia (see above).

There are two possible scenarios for this sedimentary bank. (1) The area now occupied by the sedimentary bank might once have been the contact line between land and the hypothesized sea, and hence, an environment for deposition of aqueous sediments. A possible hypothesis for the formation of the sedimentary belt, are proximal alluvial deposits, formed allochthonously by the fluvial influx of water. Thus, both the water and sediments might originate from the adjacent highlands of Tyrrhena Terra. The deposits are only observed along Hellas' western to northeastern rim and some very scattered places in the research area. Along the southern rim there are no LTD visible, correlating with a low density of channels in the same area. This asymmetric distribution might be caused by different climatic conditions; in northern Hellas (at lower latitudes) the Noachian climate was probably warmer and wetter than on the much colder southern basin rim (at higher latitudes). Hence, less or no fluvial activities in southern Hellas prevented the deposition of sediments there. Moreover, no clear evidence of former shorelines supporting a submarine deposition of LTD was found (see above). (2) Instead, the results of this work suggest that these deposits might also be the eroded/dissected remnants of subaerially deposited alluvial fans (similar to terrestrial bajadas). In this case, the alluvial sediments were transported by fluvial channels, and deposited at the base of the basin's rim. This scenario does not require a large lake, but is still able to explain the existence of hydrated sediments modified by water.

As LTD can only be determined when they outcrop, an even wider extend of that sedimentary bank around Hellas cannot be entirely excluded. Salese et al. (2016) suggested that Noachian LTD in intercrater plains north of Hellas are covered by stratigraphically younger volcanic deposits of Hesperian origin. Related to the Hellas basin, there is clear evidence for Hesperian volcanic activities along its eastern and southwestern rim where this hypothesized sedimentary ring might be completely covered by younger volcanic deposits (e. g., Leonard and Tanaka, 2001).

Although *gullies* are relatively rare and scattered on the basin floor, they are still of significance. They mostly occur in craters of almost every size in that area. However, whereas some craters display gully morphologies, other similarly-sized craters nearby do not display them (e. g., compare 37 km-diameter Bogia crater with an unnamed crater of comparable size about 150 km to the west). Bogia appears to be younger and has a high density of gullies all around its rim; in contrast, not a single one evolved in the older unnamed crater.

Although there is sufficient topographic relief energy on the basin floor (*Fig. 3*), gullies seem to avoid low elevations similar to the VFF. This observation is consistent with the hypothesis of low humidity values, and hence, desiccated soils in Hellas (see discussion above about VFF). This observation is also consistent with theories that gullies are formed by processes involving volatiles, whereas it is inconsistent with hypotheses that gullies form by gravitational mass movements (e. g., Shinbrot et al., 2003; Treiman, 2003).

Treiman (2003) observed that gullies occur on all substrates, slopes, and terrains of all ages. Together with the abundance of aeolian sediments and wind circulation patterns, both Shinbrot (2003) and Treiman (2003) postulate that gullies consist of aeolian sediments formed by gravitational granular flows. But this hypothesis opposes the observations made in Hellas. There are significant evidences that gullies prefer or avoid certain environments regarding elevation, slope and aspect. Applying the results of Treiman (2003) to Hellas, a high density of gullies within the basin would be expected. Its dense atmosphere and high wind activities make it a perfect trap for aeolian sediments. However, a high density of gullies could not be detected in the study area.

Another peculiar observation is the irregular distribution of active gullies in craters of similar size and location. Some craters contain large densities of gullies (e. g., Bogia; *Fig. 40a*), while others do not show any gullies or their rims are dissected by larger channels (e. g., Talas; *Fig. 40b*). Despite some of the craters with and without gullies appear to be of similar age, even a small temporal offset (of a few million years) may be enough to eradicate or cover gully-morphologies. Hence, gullies might only be visible for relatively short geologic time on Mars before they get muted or eroded. This scenario means that gullies are only temporarily active before they cease, and that their water content cannot be of atmospheric origin, as it is not "recharged" by atmospheric deposits containing ice (e. g., LDM). Instead, the origin of gully-water is more likely to be found either by a frozen aquifer, or by the impactor of the crater itself. The impact event exposes the subsurficial aquifer at the rim. As a result, the frozen aquifer starts melting/subliming under atmospheric conditions. This process is active until the remaining aquifer has become too deep for further release. Subsequently, the gullies cease and are finally eroded

(e. g., by aeolian processes) or muted (e. g., by LDM). The other scenario considers the impactor itself as the main source of water. While some asteroids have low water ice content, other consist almost merely of ice (see Schorghofer, 2008 and references therein)). If the ice does not completely sublime during the impact, the remaining ice will be integrated into the subsurface in and around the crater. A warm atmospheric environment could trigger the melting of ice, forming gullies; while those craters caused by a "dry" impactor remain without any gully morphologies. Both scenarios also fit into the observation that the high atmospheric pressure in the basin enhances sublimation, and hence, desiccation.

In summary, most of the water-related landforms in Hellas (channels and LTD) were formed during the Noachian and Hesperian, but there are also some apparently young Amazonian channels along the rim of the basin. They are characterized by young and distinct fluvial morphologies like braided channels, bars, or deltaic deposits (Hargitai et al., 2017). The most recent fluvial landforms in the study area are irregularly distributed gullies of late Amazonian origin.

4.2 Sheet Deposits in eastern Hellas

4.2.1 Geomorphology

4.2.1.1 Longitudinal Lineations

Longitudinal lineations (grooves and ridges) are generally oriented in flow direction, and rarely transverse or oblique to it. Hence, a genetic relation of these features to the development of the sheet flows seems likely. On Mars, three possible causes for the evolution of such lineations can be described; (1) by mass wasting/landslides, (2) by shear movements in a liquid (e. g., lava or mud), or (3) by a combination of both.

Longitudinal lineations are found on large mass wasting deposits, e. g., in Valles Marineris landslides (Lucchitta, 1979) (*Fig. 41*). However, there are some important differences between these lineations and those on top of the sheet flows analyzed in this study. In eastern Hellas, lineations are mainly sequences of grooves and ridges. In contrast, the lineations on top of the landslides in Valles Marineris are only composed of ridges and grooves, respectively. Moreover, their wave length is much higher in a range of several hundred meters contrasting the wave lengths of the ridges and grooves in the study area of only a few decameters. Unlike the landslides in Valles Marineris where furrows begin to occur in the central part of the slide and increase toward its terminus (De Blasio, 2011), the furrows and ridges on top of the sheet deposits in eastern Hellas Planitia occur irregularly along the flow. They could not be detected along the termini of the flow.

Despite there are differences in these types of lineations caused by landslides there are still genetic similarities too. The lineations found on either landslide type provide information about the propagation of the flow. If they developed simultaneously to the sheet flow/landslide, there must have been lubrication in order to provide a basal slip. If there is no lubrication the lineations would be destroyed by turbulent distortions during the formation of the flow (De Blasio, 2011), e. g., like in lava currents. As a possible lubrication material for the landslides in Valles Marineris, De Blasio (2011) suggests ice or evaporates that were already located on the floor before the landslide came down. Applying this hypothesis to the sheet flows of Hellas, there are two possible scenarios for lubrication; (1) the pre-existing surface was covered by an ice layer (e. g., snow or a mixture of ice and dust (like the latitude-dependent mantle today; Kreslavsky and Head, 2002b), or (2) the flow itself slid on a fluid layer originating from the flow itself by drainage effects allowing shear (see shear strength of debris flows in *Table 1*).

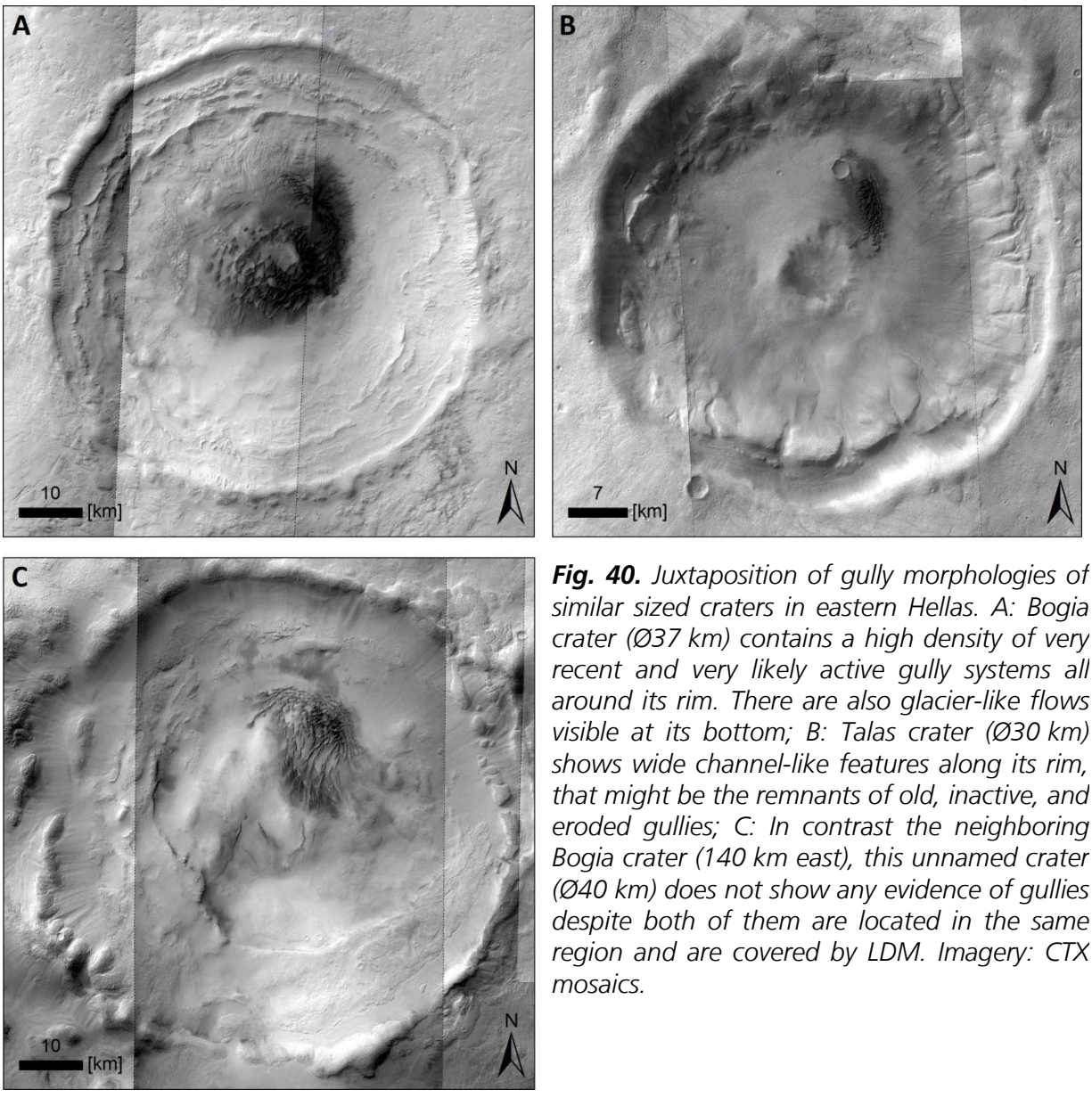

Fig. 40. *Juxtaposition of gully morphologies of similar sized craters in eastern Hellas. A: Bogia crater (Ø37 km) contains a high density of very recent and very likely active gully systems all around its rim. There are also glacier-like flows visible at its bottom; B: Talas crater (Ø30 km) shows wide channel-like features along its rim, that might be the remnants of old, inactive, and eroded gullies; C: In contrast the neighboring Bogia crater (140 km east), this unnamed crater (Ø40 km) does not show any evidence of gullies despite both of them are located in the same region and are covered by LDM. Imagery: CTX mosaics.*

The propagation and deposition of liquids may also result in a groove-and-ridge structure. Fluid lava currents usually have a shear penetrating the whole fluid body, hence, its surface is often distorted; especially in the distal parts of the flow where the surface already solidifies. Hence, lava flows are likely not able to develop such lineations. In contrast, the sheet flows in Hellas apparently slid over the surface preserving groove and ridge morphologies. Assuming a fluvial evolution the accumulation of boulders on top of the flow can be explained by kinetic sieving too. This process would involve floating, buoyancy and shear-and-tear zones within the upper (indurated?) layer of the sheet flow. As a result the floating blocks may got accumulated along these shear zones which today appear as blocky ridges.

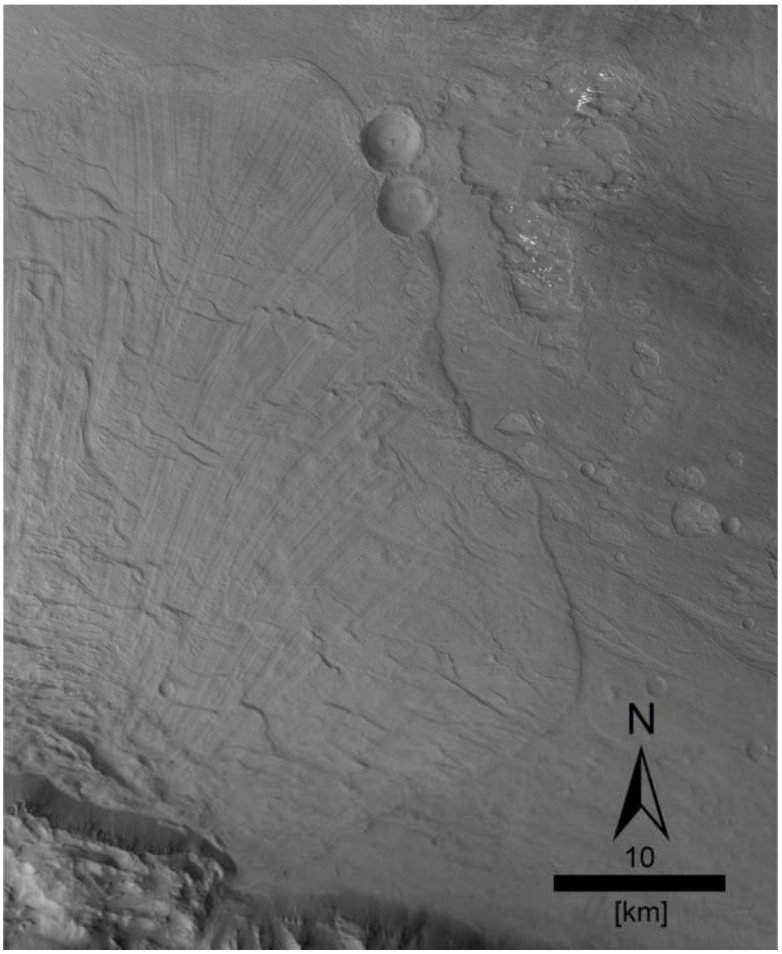

Fig. 41. *Lineations on a dry landslide in Valles Marineris (Coprates Chasma). In contrast to the lineations found in Hellas, the gaps between the ridges are much wider. Moreover,the ridges and grooves extend up to the flow front (HRSC image h2017nd).*

4.2.1.2 Polygons

For the evolution of the small polygons (*Fig. 32*) there are three possible scenarios; (1) outcrops of basaltic columns if a magmatic origin of the sheet deposits is assumed (i. e., columnar jointing in plan-view; Milazzo et al., 2009), (2), thermal-contraction polygons formed by modern periglacial processes; e.g., ice- or sand-wedge polygons (Seibert and Kargel, 2001; Mangold, 2005; Soare et al., 2005; Levy et al., 2009; Ulrich et al., 2011) or (3) desiccation polygons (El-Maarry et al., 2010). Despite using HiRISE imagery, the resolution is too low in order to make reliable statements based on visual analyses. Hence, only contextual interpretations can be made.

The polygon size of around 10 m is too small for platy-ridged morphologies which are up to a kilometer in length (Keszthelyi et al., 2004) caused by the cooling and tearing of the uppermost layer of a volcanic flow. Instead, if the sheet flows are of volcanic origin they might be the result of columnar basaltic joints visible in plan view. Milazzo et al. (2009) discovered the existence of columnar joints on Mars, generally within craters located on a volcanic and fluvially deformed plain; i. e., in Marte Valles. They suggest that the entablature occurred when lava flows were quickly cooled down by the inundation of fluid water (running water or precipitation). In contrast to their findings, the polygons of the study area are not immediately located within a possible channel bed. Instead, they are located on top of high standing overbank deposits. So if the polygons of eastern Hellas are columnar jointing of volcanic origin, only intense inundation could have formed those (Milazzo et al., 2009). Despite a lava origin cannot completely excluded, this scenario is believed to be less likely. The unfavorable high-ground position and the lack of fluvial landforms caused by precipitation/flooding do not support this hypothesis sufficiently.

The latitude and local geomorphologic environment could allow the formation of thermal contraction polygons. On Mars, this type of polygons is mainly found on top of a latitude-dependent and ice-rich mantling deposit (LDM) and is assumed to be of late Amazonian age (Seibert and Kargel, 2001; Mangold, 2005; Soare et al., 2005; Levy et al., 2009; Ulrich et al., 2011). In eastern Hellas, a thin to medium LDM cover supporting the evolution of polygons has been recently described (Voelker et al., 2017a). Most of the late Amazonian hypothesized thermal-contraction polygons appear to be very young with little or no erosion. In contrast, the polygons observed in the study area seem to be of a certain age, as they show clear signs of degradation; e. g., the hexagonal shape of the polygons is hard to distinguish, and the troughs appear broad and shallow (*Fig. 32*). Levy et al. (2009) described so-called subdued thermal contraction polygons with a very similar appearance; but they detected none of these polygons at the given latitude of the study area. It can, however, not excluded that these polygons are thermal contraction polygons, but if so, they must have developed on top on an older and now degraded LDM cover.

The development of polygons in the study area could also have been caused by desiccation processes. El-Maarry et al. (2010) described this type of polygons at one location in eastern Hellas. Despite they analyzed desiccation polygons within craters (as the result of dry lakebeds) this scenario might also work for sheet deposits. If the deposits are of wet, fluvial origin they might have evolved desiccation polygons too when material dried.

4.2.1.3 Distributive Channel System

Besides the main channel of Dao Vallis in the study area, there are further shallow channels arranged in a distributive pattern similar to an alluvial fan (*Fig. 31*). Hence, it is possible that a fluid drained out of unit Asd5, developing this pattern on top of unit Asd4 by dewatering processes.

On Earth, such drainage and dewatering patterns are unknown for lava flows; as young basalts show a high permeability (e. g., Saar and Manga, 1999 and references therein). But the observed channels in the study area are confined to one location, hence, it can be excluded that they were formed by precipitation, and assume a magmatic origin of the sheet flows less likely. Instead, a water-related formation of these channels is preferred. In this scenario the water originates from the sheet flow itself. Assuming a fluvial origin for the sheet flows in form of e. g., debris flows, the currents were a mixture of water and sediments with negative pore water pressure. This negative pore water pressure keeps the cohesion of the sheet flow at a high level. Thus, the current could move as a plastic flow being able to form stable flow fronts or transport large boulders. However, at the source of the dendritic channel system, the pore water pressure became positive, because of the settling, and hence compression of the sediments, causing drainage of water. This water, in turn, drained out of unit Asd5 and eroded the fluvial channels into unit Asd4. Similar patterns at much smaller scales have been found in mud flows on Svalbard Island and a salt pan in Sahara desert (see *Fig. 37* and *Fig. 38*).

4.2.2 Evolution

The sheet deposits were analyzed in a representative study area in eastern Hellas Planitia. Their geography, and hence, evolution seems to be closely related to the formation of the outflow channel system of Dao and Niger Vallis. The main question is: What processes have formed these deposits, and which environmental changes have stopped them? Three different scenarios for the development of sheet deposits are discussed below; volcanic, aqueous, or an ice-related origin.

4.2.2.1 Volcanic Origin

The morphology of the sheet flows in eastern Hellas differs significantly from the *lava flows* evaluated on Arsia Mons, Elysium Mons, and Hadriacus Mons (*Fig. 36*). Their surfaces are generally smooth and their front lobes are very distinctive. Except for the Arsia Mons flows, the depths of all other lava flows are more massive than the flows found in the Hellas study area (*Table 5*). This difference could be caused by different viscosities. The viscosity of the sheet flows in Hellas must have been very low; corresponding to a very liquid material.

The sheet flows of the study area are neither comparable to the flows found on Arsia or Elysium Mons nor to most of the morphologies of pristine flows (e. g., Keszthelyi et al., 2004; Gregg, 2016) in the Cerberus plains. The lineations of the Cerberus region do only occur behind obstacles. In contrast, the lineated terrain in Hellas is evenly distributed (independent of obstacles) and arranged conically. Moreover, there are no plates, polygonal floes or pressure ridges on top of the flows; only small-scale polygons have been determined in Hellas. Theoretically, the lack of floes and pressure ridges may be explained by the different ages of both deposits. While those in Cerberus are assumed to be extremely young (only a few tens of million years; e. g., Plescia, 2003) the sheet deposits in Hellas are at least 680 (±200) Ma old. This time difference may have been sufficient for the erosion of morphologies indicative for lava flows. But it is assumed to be unlikely, that all of these Amazonian features have been completely eroded without any remnant morphologies. Amazonian erosion rates widely vary depending on latitude and process. While low-latitude, non-glaciated areas of Mars show relatively low rates between ~1–4×10^{-6} m/Myr (Golombek and Bridges, 2000), erosion rates of higher latitudes and glaciated areas are comparatively high (10^{-2}-10^{1} m/Myr; Levy et al., 2016). The sheet deposits described in this study are located in the higher mid-latitudes, but are very likely not of glacial origin. However, it cannot be excluded that (peri-)glacial processes have reshaped these deposits (e. g., by LDM), even if they are of volcanic origin. Hence, the higher erosion rates of Levy et al. (2006) appear more likely. In this case, even the lowest erosion rate of 10^{-2} m/Myr is able to degrade the deposits by up to 6.8 m (Asd5) to 34 m (Asd2); depending on the age. This amount is sufficient for eradicating subtle volcanic morphologies.

Besides lava flows, *pyroclastic flows* as a possible transport mechanism has also been tested. In contrast to Arsia Mons and Elysium Mons, the flanks of Hadriacus Mons (*Fig. 36c*) mainly consist of pyroclastic deposits (Crown and Greeley, 1993, 2007; Williams et al., 2007) without any distinctive aeolian morphologies on top of its flows. The plan-view flow shape and morphology differ from the flow behavior of the sheet deposits in Hellas. The flow fronts of Hadriacus Mons are often cuspate, contrasting the wide and lobate flow fronts of Hellas Planitia. Williams et al. (2007) assume that the pointy flow fronts are the result of aeolian and/or fluvial degradation of

pyroclastic deposits. Moreover, they determined maximum runout distances for pyroclastic flows of up to 170 km emanating from the caldera. In contrast, the sheet deposits of eastern Hellas extend at least 800 km from the caldera of Hadriacus Mons, hence, a pyroclastic origin as a possible mechanism for their development is supposed to be unlikely.

4.2.2.2 Possible Water Sources

In an attempt to reconstruct the history of the outflow channels in the eastern Hellas region, Kostama et al. (2010) proposed the formation of multiple ice deposits on the northeastern Hellas rim, caused by a successive deposition of both ice-bearing deposits (caused by atmospheric air fall) and subsequent lava flows. Later, the ice-bearing layers would have been heated and consequently molten by ongoing magmatic activity. As result, the release of ice and/or water formed Dao Vallis and the adjacent outflow channels (e. g., Kostama et al., 2010; Kukkonen and Kostama, 2018; *Fig. 42*).

This scenario is consistent with the presented interpretation of the sheet flows (*Fig. 43*). The mobilization of buried ice-bearing deposits could explain the high sediment content of the flows, proposing that the ice-sediment mixture became liquefied and began to flow as a viscous flow unit following the topographic gradient towards the Hellas basin. As a result, the overlying deposits collapsed, and were incorporated into the flow, increasing the sediment-water ratio even more. Moreover, the Amazonian-Hesperian age for the Dao and Niger Vallis system (Crown and Greeley, 2007) correlates to the ages of the sheet deposits. Finally, the flows ceased when either the aquifers were depleted or the volcanic activities of the triggering highland volcanoes (e. g., Hadriacus Mons) terminated.

4.2.2.3 Aqueous Origin

Based on combined observations, a water- or ice-related origin of the sheet deposits seems more plausible than a volcanic origin. The smooth surface lacking typical volcanic features, the distributive channel network, and the longitudinal lineations are closer to fluvial water-laden sediment flows than lava currents.

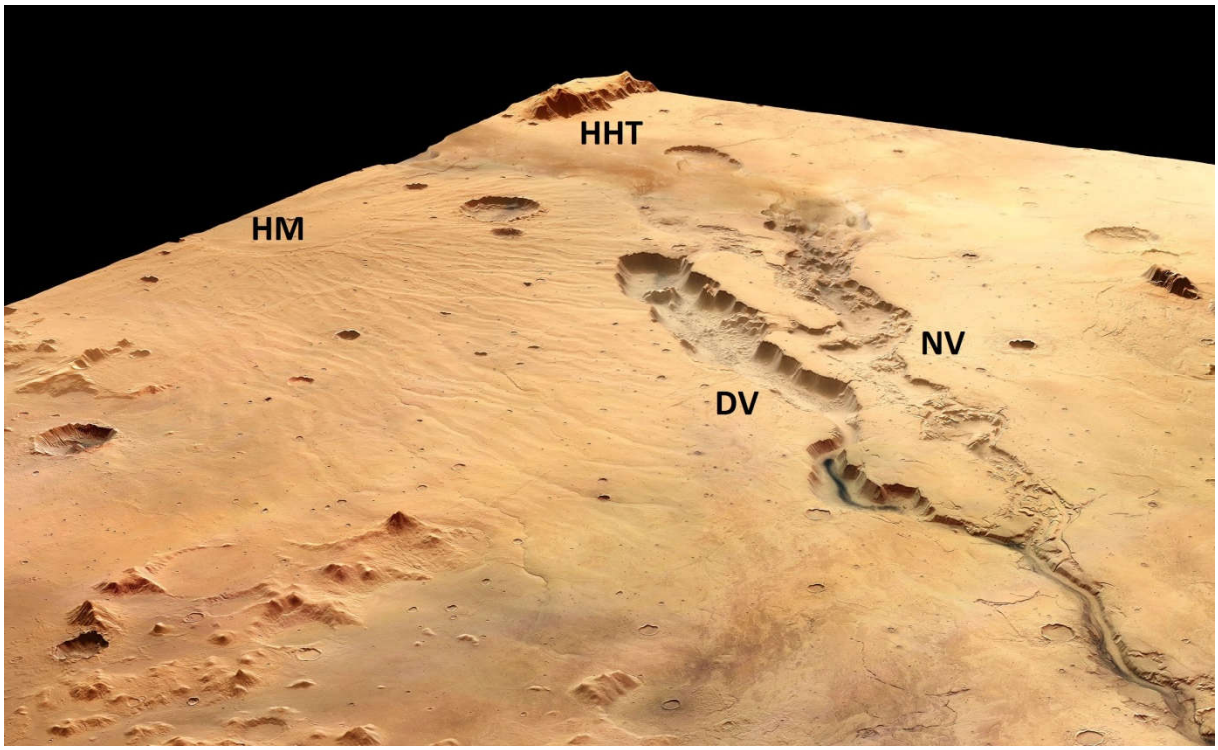

Fig. 42. *Oblique view of Hadriacus Mons (HM), as well as the source regions of Dao Vallis (DV) and Niger Vallis (NV). In the upper part of the image is the Hesperian Hellas trough (HHT) visible. Note the depressed darker region just below HHT, indicating the removal of subsurficial material by hydrothermal activities as suggested by Kostama et al. (2010). Imagery ESA/DLR/FU Berlin.*

Leaving such massive deposits behind, the flows must have entrained a high sediment concentration. Realistic values for hyperconcentrated flows are only found, if a maximum of 47% sediment content is given (see *Table 1*). Only then, adequate flow thicknesses of 28.5 to 47.2 m during their formation can be determined. In contrast, the recalculated flow depths of debris flows provide even more realistic values ranging from 17.4 to 28.8 m.

The bulk density of hyperconcentrated flows is lower than the density of debris flows (Costa, 1988). A high density of the currents would support the transport of large clasts as those found on the surface of the sheet deposits (*Fig. 30* right and *Fig. 36d*). This viscoplastic behavior of debris flows is able to relocate large clasts over far distances (Costa, 1988). Distinctive terminal lobes might be an indication for a high viscosity of the material, being more indicative for debris flows than hyperconcentrated sediment flows. However, terrestrial debris flows commonly have a high aspect ratio in plan view and extend up to a maximum of several tens of kilometers in length (e. g., Iverson, 1997 and references therein). In contrast, the flows in eastern Hellas are significantly longer and have a low aspect ratio. This difference might be caused by two reasons; a lower gravity causing a decrease of sedimentary compression, and/or a rheological behavior between that of debris flows and hyperconcentrated flows.

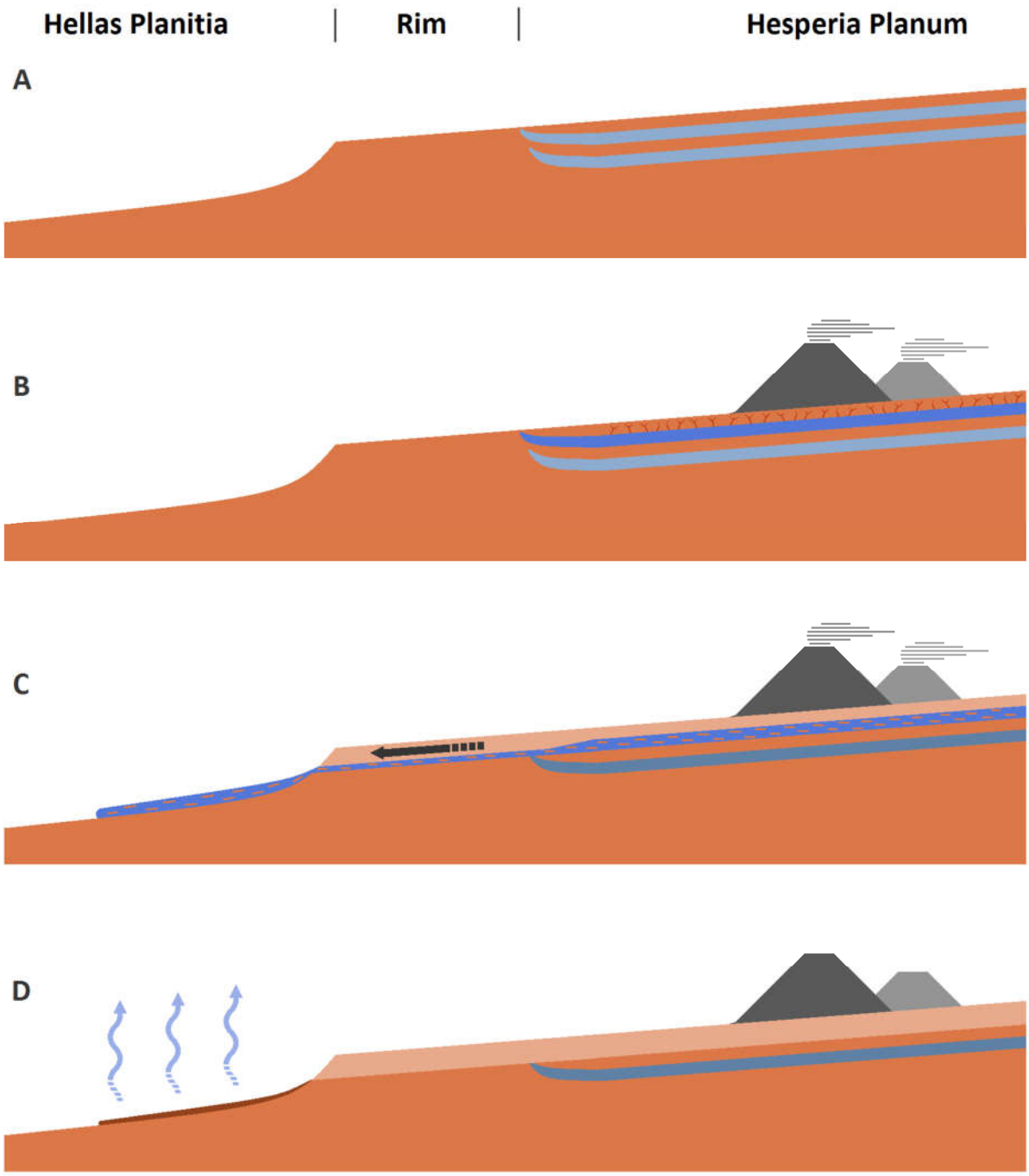

Fig. 43. *Fluvial evolution of sheet deposits in eastern Hellas. A: The Noachian geologic setting as suggested by Kostama et al. (2010). The bright blue bands indicate frozen and subterrestrial layers. The topographic gradient is given by Hellas Planitia. B: Beginning with volcanic, and hence, hydrothermal activities, the upper layer melts and liquefies (dark blue) and destabilizes the overlying layer (orange). C: Both phases are getting mixed and are emplaced towards the basin of Hellas forming Dao Vallis. As soon as the mixture reaches the plains of Hellas its flows (containing volatiles and sediments) commence to deposit (dark blue flow on the left). D: Under the cold and desiccated atmosphere the volatiles began to sublime (bright blue arrows), leaving just the sediments behind (dark brown lobe). This scenario could have been repeated by the release of deeper volatile-rich layers, causing the deposition of further sheet deposits (not shown in this illustration).*

4.2.2.4 Ice-related Origin

Besides debris flows and/or hyperconcentrated sediment flows which are a mixture of liquid water and solids, a flowing mixture of ice and solids is also a possible scenario. There have been several proposals that Mars had a cold-climate even during the Noachian and Hesperian (e. g., Forget et al., 2013). Hence, the release of water may result in a mixture of slurry ice and sediments, as soon as the flowing body reached the surface and commenced freezing. This ice-debris mixture could explain the high depth values and distinctive flow fronts of currents, as such a mixture would have a higher viscosity. Moreover, this mixture would also have a higher shear strength supporting the transport of large clasts over far distances.

On Earth, there are so-called rock-ice avalanches that are mostly related to steep mountains and glaciers. Their morphologies are very similar to landslides, comprising distinctive lobate flow fronts, (extending up to several kilometers), a hummocky surface, as well as parallel, longitudinal pressure ridges on top of the flow. These mass movements usually consist of a mixture of ice, water, and solids; but the content of each component may vary considerably (Schneider et al., 2011).

Applying these morphologies and geologic settings to the sheet deposits on Mars, there are both differences and similarities. Rock-ice avalanches on Earth are much smaller (<10 km; Schneider et al., 2010) than the extent of the sheet deposits on Mars. Another difference is the physiographic setting. While terrestrial rock-ice avalanches are mainly found in terrain with very steep relief, the Martian sheet flows occurred in a low relief-energy environment. Moreover, the surface of the Martian deposits is generally smoother. A geomorphic similarity of rock-ice avalanche deposits, are parallel ridges on top of the flow. However, they appear much closer to those found on dry landslides than those found in Hellas (compare *Fig. 30* and *Fig. 41*).

Schneider et al. (2011) also evaluated the effect of ice (instead of water) in mass movements. They found that water decreases the friction of the flow much stronger than ice does. As a result, mass movements containing water reach much further than those containing ice.

Synthesizing these observations, the differences between rock-ice avalanche deposits and the sheet deposits of Hellas overweigh the similarities. Hence, it is suggested that the sheet deposits were likely not formed by rock-ice avalanches as those found on Earth. But this does not exclude that an ice-related mechanism still may be possible; there is just no adequate terrestrial analogue for this scenario.

4.3 Synthesis

By synthesizing all observations into a wider context it is possible to derive further information about Hellas Planitia. The applied grid-mapping method has revealed several geographic and geomorphologic characteristics of landforms, providing information about its current climate and climatic past. While ice-related landforms likely represent Amazonian conditions, most of the water–related features may describe an older Hesperian and/or Noachian environment.

The latitude-dependent mantle (LDM) is the most extensive ice-related landform in the study area. It covers most of Hellas Planitia, except for an elongated area in northeast Hellas that seems to be uncovered by this mantling unit. Together with existing atmospheric circulation models, it is most likely that this LDM gap has been formed by a rotating wind system within the basin; a wind that was likely active during the late Amazonian (or even until today?). It is assumed that this warm wind (*Fig. 2*) caused either a sublimation of the volatiles within the LDM or even prevented the deposition of LDM in general, as it requires a sufficient amount of ice/water in the atmosphere to deposit.

A further observation that can be at least partially explained by the same wind system too, is the orientation of the so-called scalloped terrain (erosional features of LDM; *Fig. 11* and *Fig. 13*). The winds are assumed to enter the basin at its southwestern margins were the rim is an even inclined plain without any mountains. This geographic setting causes an unobstructed drainage of cold winds originating from south polar highlands. Such strong atmospheric currents may be able to damage the protective desiccated surface lag of the LDM (Conway and Balme, 2014), and enhance the sublimation of underlying volatiles, causing the scallops.

In contrast, in the lower elevated and central part of Hellas, where no strong winds are assumed, scalloped terrain does not occur at low elevations (most of the scallops occur between -3,000 and 5,000 m). It is possible that the enhanced sublimation at the bottom of Hellas (mainly by solar insolation and -not- by winds), causes a thicker surface lag of the LDM there. As a result, scalloped terrain cannot develop because it requires deep cracks through the lag in order to sublime the covered and subterrestrial volatiles.

Another important observation is the lack of other Amazonian and volatile-rich landforms in the lower elevated parts of Hellas Planitia; especially viscous-flow features (VFF) and gullies. Apparently, the volatiles vanished and/or did not develop at these elevations independently of their phase. A possible scenario for this observation is the dense atmosphere at low elevations that is able to absorb more water than at higher elevations.

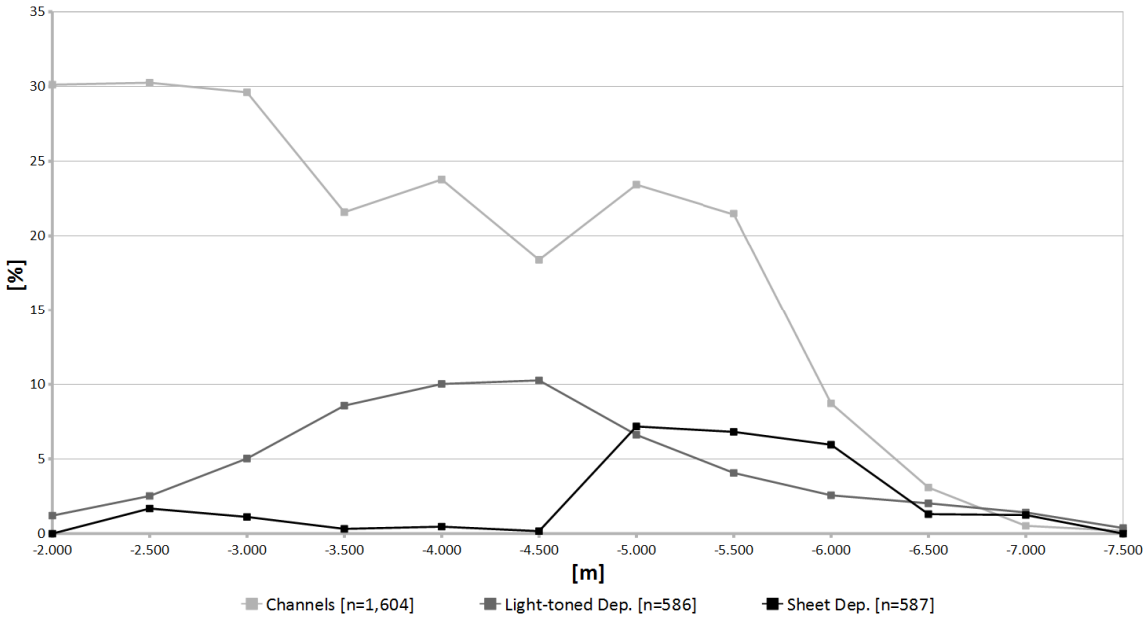

Fig. 44. *Relative distribution of channels, light-toned deposits, and sheet deposits regarding their elevation.*

The most prominent water-related observation of this work is the lack of clear coastal morphologies; except for some small depressions on the floor of the impact basin (*Fig. 28*). Hence, theories of a suggested lake within Hellas (Moore and Wilhelms, 2001) cannot be confirmed. Instead, several other surface features have been detected which are likely of fluvial origin and might help to reconstruct the Hesperian and Noachian environment of Hellas Planitia; i. a., light-toned deposits (LTD), outflow channels, and sheet deposits.

The most significant source for an influx of water, are the large outflow channels in eastern Hellas (Dao, Niger, and Harmakhis Vallis). Their released water originates from subsurficial aquifers that were released by volcanic/hydrothermal activities of the adjacent volcanoes Hadriacus Mons (Kostama et al., 2010 and 2017). Thus, their formation was widely independent of atmospheric conditions. None of these channels reach the bottom of Hellas. All of them terminate at elevations of around -6,000 m. Considering both the lack of shorelines in Hellas and too small amounts of water transported by these channels (Musiol et al., 2011), this observation does not support the existence of an extensive lake either.

Eastern Hellas is also the most prominent area for so-called sheet deposits. Their geography suggests a close relation to the adjacent outflow channels, assuming that they are genetically linked to eachother. There are several other locations where sheet deposits appear (*Fig. 23*). They are commonly found at the base of the inner rim, where several channels drain into Hellas. But they are nowhere as distinctive as at the lower terminus of Dao Vallis (*Fig. 24* and *Fig. 27*).

By classifying sheet deposits as fluvial deposits, as suggested in this work (see chapter 4.2.2), it is possible to test how well they fit into the geologic frame of water-related features as described in the grid-mapping part (*Fig. 23*). Synthesizing these results can also support to test the resilience of the findings, presented in this work.

Sheet deposits show a multi-layered sequence of at least five fluvial outflow events. So it is possible that the other locations of sheet deposits in Hellas were also formed by multiple flood events. Apparently, the sheet flows were not extensive enough to reach the lowest parts of Hellas (*Fig. 39*). Most of them occur between -5,000 and -6,000 m, although more than 50% of the interior plains are located well below -6,000 m (extreme low of Hellas ~-8,500 m).

While channels mainly occur on steeper slopes, sheet deposits are found on low inclined plains. This strongly supports relations between the channels and sheet deposits. The steep channels can be considered as the erosional part of the system, while the flat sheet deposits are their depositional counterpart (source-to-sink).

Despite volcanic activities of the adjacent volcano Hadriacus Mons very likely triggered the melting and release of subsurficial water/ice, the observed sheet deposits are no volcanic flows. Compared to other flows on Mars of unambiguously volcanic origin, the shape of the sheet deposits in Hellas differ significantly. The observed volcanic flows of Amazonian (Arsia Mons, Elysium Mons) and Hesperian age (Hadriacus Mons) are characterized by higher thicknesses and dimensions (note the scale bars at *Fig. 36*), and are widely dissected, likely by aeolian erosion (*Fig. 36a* and *b*). The sheet deposits are also lacking rugged morphologies indicative for (young and pristine) lava flows like plates/floes, grooves, and inflated margins similar to terrestrial pahoehoe lava. Moreover, this work also evaluated a glacial scenario for the formation of these deposits (similar to rock-ice avalanches on Earth). Although the cold Martian environment would like have supported such a transport mechanism, it is, however, assumed to be an unlikely scenario. On Earth such avalanches do not reach further than a very few kilometers, as the ice within the moving flow increases the friction. As result, these flows stop after a short distance. In contrast the sheet deposits observed extend several hundreds of kilometers from their source at the upper reaches of Dao Vallis near Hadriacus Mons.

Considering the geographic and geomorphologic observations, the fluvial scenario for the development of sheet deposits requires fewer assumptions than a purely volcanic or icy origin. However, volcanic and/or hydrothermal activities respectively, of the adjacent Hadriacus Mons still play a role in their development. It is assumed that this edifice caused the melting, and hence, liquefaction of subsurficial deposits containing ice (Kostama et al., 2010; *Fig. 38*), which, in turn, translocated the water and sediments into Hellas. But it remains an open question for

future research which environmental changes terminated the emplacement of sheet deposits. Has the ceasing of volcanic activities stopped further melting, or were the subsurficial ice layers depleted?

A further important landform of very likely water-related origin, are so-called light-toned and layered deposits (*Fig. 6* and *Fig. 26*). They do not show any obvious relation to large channels. Instead, they are apparently linked to the old Noachian highlands north of Hellas, and their small dendritic channel network. Interestingly, LTDs occur on much higher elevations than sheet deposits which are likely the result of fluvial deposition too (*Fig. 13* and *Fig. 39*). LTDs are mainly found between -3,500 and -5,000 m while sheet deposits range from -5,000 to -6,000 m. Despite both landforms are supposed to be of fluvial origin they must have developed within a different sedimentary environment. Ansan et al. (2011) suggested that LTDs might be the remnants of a former subaqueous deltaic environment. But based on the results of grid-mapping of this manuscript, no clear shoreline morphologies were detected in Hellas that might support a former lake (required for the development of sub-aqueous fans). Moreover, grid-mapping did not reveal extensive deltaic morphologies too. Assuming that LTDs were deposited in a subaqueous environment, the water level of the suggested "Sea of Hellas" must have retained at a steady level for certain amount of time, in order to deposit such extensive and deep sediments. Transferring this observation to the formation of shorelines, coastal morphologies should have had enough time to form. However, no distinctive shorelines have been detected in this work. But it has to be emphasized that LTDs are of Noachian age; hence, it is also possible that such morphologies could have been significantly eroded beyond recognition.

Summarizing all water-related landforms, LTDs occur along the northern and northeastern, while sheet deposits are more or less confined to the east. Channels are found all around the rim of Hellas, however, in varying densities. This strongly contrasts to the interior of Hellas, as all of these features almost completely lack there. Hence, three different fluvial environments can be distinguished: (1) The northern LTDs (and channels along the rim) might be deposits of a warmer Noachian environment, possibly caused by surface runoff through the small dendritic channel networks. (2) The sheet deposits at the eastern rim are fluvial deposits triggered by hydrothermal activities of the adjacent Hesperian highland volcanoes. (3) As the interior of Hellas does not show significant evidences of fluvial erosion/deposition, except for a very few Amazonian gullies, it can be assumed, that this part of the basin has never undergone any large-scale fluvial activities.

Combining the results of both the distribution of LTD, sheet deposits, and channels and the geomorphology of sheet deposits, the findings complete each other well. Putting all of these ob-

servations into one piece, Hellas was indeed never filled by a large lake, but the sheet deposits indicate that outflow channels (and maybe the smaller dendritic networks) translocated water into the basin, but the quantity was too low to fill it.

The combination of large-scale research (grid-mapping of Hellas Planitia) and small-scale research (analyses of sheet deposits) resulted in a consistent big picture of the evolution of the impact basin. This consistency, in turn, proved the high resilience of the findings too.

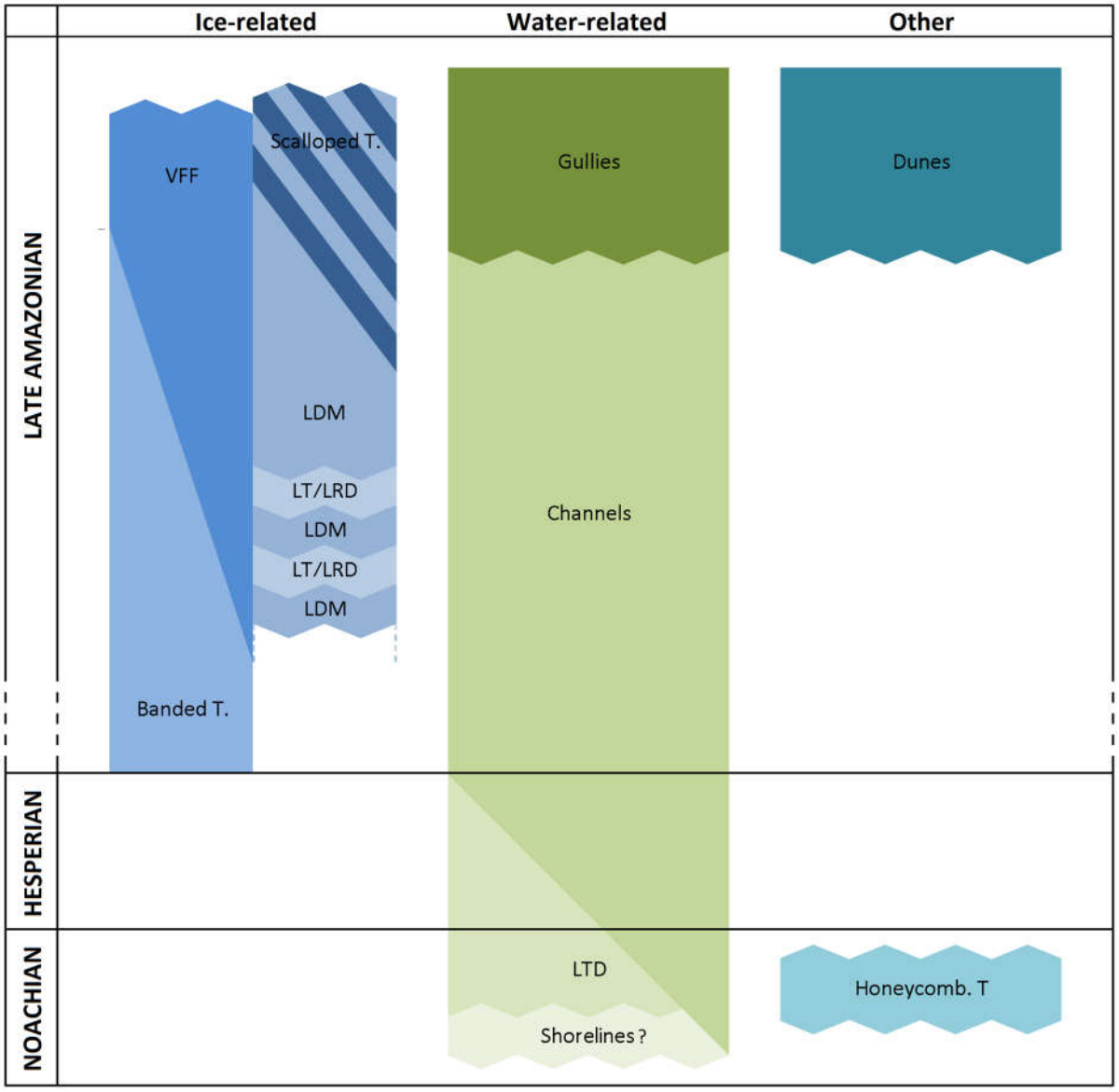

Fig. 45. *Stratigraphy and correlation of ice-related, water-related, and other landforms based on grid-mapping results. Classification of each landform into absolute ages is derived from Bernhardt et al., 2016a (honeycomb terrain), Diot et al., 2016 (banded terrain), and Leonard and Tanaka, 2001 (channels and LTD).*

5. Conclusions

The study of Hellas Planitia at different scales has shown that the Hellas basin is a complex geological system, whose processes are often related to each other. By analyzing the most important surface features by their geography, this work was able to establish an overall view of the historic and present-day evolution of Hellas. The focus of this study was to analyze landforms involving water and/or ice in the deepest basin on Mars. Hellas Planitia is among the places with the highest likelihood for the transient existence of liquid water and ice. The results demonstrated that Hellas contains a substantial diversity of landforms. By applying the newly developed grid-mapping method, it was possible to derive quantitative information about the distribution of these landforms on a large-scale. In order to complete the geomorphologic picture, the characteristics of sheet deposits have been studied at a small-scale in eastern Hellas.

Grid-mapping has been proven to be a successful method to quantify the distribution of multiple small-scale landforms over wide areas. Applying this approach to Hellas, it was possible to map the distribution of water- and ice-related landforms over the entire basin at CTX scale, using a 20×20 km grid. Although 24 different landforms were considered, only 15 of them are significantly abundant in Hellas. Grid mapping improved the understanding of Hellas Planitia and was able to discover characteristics of several landforms that can only be recognizable by a synoptic view. This method is also useful for geoscientific research on other celestial bodies for identifying large-scale coherences or connections between landforms.

One of the major results was found in the distribution of the latitude-dependent mantle (LDM); it covers the study area almost entirely, except for a distinctive region in NE Hellas where an elliptical lack of the LDM cover has been detected. It was found that the LDM distribution in the basin not only depends on latitude, but also on the pattern of wind circulation. Existing global circulation models have revealed clockwise-rotating winds in Hellas, entering in the SW and get successively warmer and drier as they move north (increasing the water absorption capacity). When they reach the northern rim, they turn eastwards causing the sublimation of LDM in the northeastern part of Hellas. As an alternative, the winds may even have prevented the deposition of the LDM at these locations in general. Hence, an LDM cover has never developed in this region.

Similarly, the distribution and orientation of scalloped depressions appears to be controlled by wind. As revealed in this work, scalloped terrain predominantly occurs in the study area where winds are stronger; especially within a gap of the rim in southwestern Hellas where cold south polar air masses drain into the basin. This observation supports hypotheses that the formation of

scalloped terrain not only depends on solar inclination, but on aeolian processes, too. Hence, their distribution fits very well into existing wind circulation models.

Viscous-flow features (VFF) and gullies are further important ice- and water-related landforms. Both require are significant amount of volatile to form and both show a similar distribution regarding their elevation. They are almost completely lacking at low elevations despite of the relatively high relief energy on the floor of Hellas. This may also be the result of the high atmospheric pressure within the basin. The dense atmosphere has a much higher ability to absorb atmospheric water. This atmospheric condition causes an exsiccation of soils. Thus, there are no sufficient volatiles at low elevations, preventing the formation of VFF and gullies (landforms that require large amounts of volatile to develop).

Grid-mapping has also revealed three different types of fluvial landforms in Hellas: (1) large outflow channels, (2) dendritic valley networks, and (3) apparently young Amazonian channels (not older than a very few hundreds or even tens of millions years). The density of the dendritic valley networks varies along the rim, causing an asymmetric distribution. The lowest density is found at the southern rim, suggesting latitude-dependent climatic conditions. A further landform assumed to be caused by fluvial activities, are the so-called sheet deposits which seem to be related to the large outflow channels in the eastern part of Hellas.

Altogether, these water sources were likely too small to host an extensive standing body of water in Hellas. However, there is morphological evidence for an extensive sedimentary bank along the northern and northeastern inner rim of Hellas (consisting of light-toned deposits); but no clear evidence for ancient shorelines was found. However, the floor of Hellas Planitia contains several small depressions with landforms such as possible arcuate shorelines, light-toned deposits, or tombolos that could have been formed by lacustrine processes (*Fig. 26*).

Putting all of these observations into a stratigraphic context, it is possible to give a rough overview of the geomorphological evolution of Hellas Planitia (*Fig. 45*). The oldest, Noachian-aged, landforms of the study area are supposed to be shorelines (assuming the morphologies shown in *Fig. 28* are coastal landforms!), LTD, and the honeycomb terrain. So it is possible that these three landforms are genetically related to each other. During the Hesperian, Hellas Planitia has likely been modified by volcanic and possibly related hydrothermal/fluvial activities (outflow channels, sheet deposits). Fluvial erosion and deposition may have continued until the late Amazonian, however, at much smaller intensities (short gullies). Moreover, most of the ice-related morphologies (e. g., LDM, LRD, LT, scalloped terrain) were likely formed during this epoch too. Observations indicate that periods of deposition of LDM alternated with periods of erosion; whose remnants are LRD and LT. The most recent (and maybe still active) process in this cycle is

the formation of the scalloped terrain. Assuming that VFF consist of the same volatile-rich material, they still may be active too. However, no clear evidence for activities, like deformed craters on top of the VFF, was detected. As sublimation features have been found on top of VFF, they are likely related to LDM, or a similar volatile-rich deposit. Hence, they are assumed to be younger than the banded terrain, were no sublimation features have been found. The origin and evolution of the banded terrain remains an enigmatic question. Like VFF no deformed craters were found, indicating there is no ongoing motion of the lobes.

In order to complete the results of grid-mapping, sheet deposits were identified as a key feature in the fluvial evolution of eastern Hellas. This approach was helpful to test the resilience of the findings gained by grid-mapping. This work described the characteristics of sheet deposits and assessed possible formation scenarios. Volcanic, glacial, and fluvial scenarios were tested, as they are the most likely formation mechanisms. The evaluations are based on geomorphologic and geographic properties, mineralogical observations based on CRISM and OMEGA datasets, thermophysical characteristics, and age determinations.

Geologic mapping identified five distinctive layers of sheet deposits in eastern Hellas Planitia. They are characterized by relatively thick sheets (see *Table 5*) with a volume of several cubic kilometers but tend to be less thick than comparable flows of volcanic origin. Their surface is generally smooth only undulating by a very few meters but it displays some morphologies suggesting fluvial activities and dewatering of sediments. Despite extensive spectroscopic observations have been made (CRISM and OMEGA), no hydrated minerals were detected in the study area of the sheet deposits, most likely due to a layer of surficial dust. Crater counts determined an Amazonian age for the three latest sheet layers (Asd3-5) and a Hesperian to Amazonian age for the two older ones (AHsd1-2), indicating that they are younger than the majority of volcanic processes at Hadriacus Mons to the east. The analyses also revealed a lack of volcanic morphologies like pressure ridges, platy-ridged flows, or inflated flow fronts. A glacial/icy origin is also deemed less likely, as the sheet deposits are to extensive for classic ice-rock avalanches. Hence, all observations suggest that a fluvial origin of the sheet deposits seems more likely than a volcanic or glacial/icy evolution. However, due to possible errors in age determination or unknown lava morphologies and composition, an effusive volcanic emplacement cannot be entirely excluded.

Assuming a fluvial formation, the possible amount of water that might have been involved in the deposition of the sheet flows was also assessed. Our calculations show a high variation of water content, depending on the flow mechanism, which range between 64 and 2,042 km³ for all directly visible sheet deposits in the study area. Even the lower limit shows a significant amount of water leading to transport and deposition of sheet deposits. Despite this substantial

volume of water seems to be large enough to create lakes, it is negligible in contrast to the volume of Hellas measuring ~1,200,000 km^3 (applying the -6,000 m isohypse, being the approximate elevation of the sheet deposits). Moreover, the age determinations as well as the layering and volumes of the sheet deposits in the study area fit well into existing hypotheses of a fluvial multi-phase development of the eastern Hellas outflow channels during the Hesperian and Amazonian.

If sheet flows are of liquid or icy origin, they might be a new agent in the evolution of outflow channels that did not get much attention yet. As these channels did not fill Hellas Planitia (unlike the outflow channels of the northern lowlands), their sheet flow deposits might be considered as one of the earliest stages in the evolution of outflow channels.

Summary

The goal of this study was to quantify and interpret the geography and morphology of fluvial, lacustrine, and glacial landforms in Hellas Planitia, Mars, which is a suitable counterpart to the well-studied northern lowlands of Vastitas Borealis.

This work has applied the so-called grid-mapping method in order to quantify and understand the geography of pre-selected landforms. Complementary, the analyses of sheet deposits, assumed to be a key in the fluvial evolution of out channels, has been carried out by classic geologic and geomorphologic mapping.

Hellas Planitia turned out to be a complex system consisting of many different geological compounds. Compounds that are linked to each other, causing dynamic erosional and depositional imbalances that have formed the face of Hellas. The origin of most of these imbalances is found in the basin's deep and steep topography.

The work revealed evidences that a clockwise-rotating wind regime in the basin's interior eroded or prevented the deposition of LDM in northeastern Hellas. The results support theories that LDM, and hence scalloped terrain too, are landforms containing ice/volatiles as the elongated axial orientation and distribution of the scallops seems to be closely related solar insolation and wind directions.

Moreover, the lack of volatile-rich landforms and features indicating running water and ice, at low elevations indicate that the high air pressure does not favor the existence of water or ice. This is likely caused by a more intense atmospheric absorption of water and ice.

The high-resolution grid-mapping has not detected any clear and widespread coastal morphologies. Only at a very few local depressions possible coastal morphologies were identified. Based on this observation, it appears to be unlikely that Hellas Planitia was ever filled by a large standing body of water; instead this work suggests that merely very small lakes exited at the bottom of the basin at the most. However, it cannot be entirely excluded that a lake once existed within the basin; if it did not exist for a sufficient amount of time (or was mainly in a frozen state), it was maybe not able to form distinctive coastal morphologies, or they are already completely eroded over the last billion years.

Along the northern rim an extensive sedimentary bank has been found. They have been previously described as deltaic deposits in a sub-aqueous environment. But as they are found on very high elevations, they would have required a lake in Hellas, being several kilometers deep. This assumption is opposed by the results of this work that do not support such an extensive lake, as no shorelines have been detected. So it is more likely that these deposits were subaerially deposited by extensive channel networks, detected along the northern and northeastern rim. Their today's dissected facies has very likely been modified by aeolian erosion.

Detailed work on so-called sheet deposits in eastern Hellas Planitia revealed a fluvial emplacement caused by hydrothermal activities around Hadriacus Mons. Hence, volcanic heating of frozen subsurficial layers liquefied and translocated the sediments and volatiles in sheet flows (similar to terrestrial hyperconcentrated sediment flows or debris flows). When volcanic activities ceased, the movement of the sheet flows was stopped too.

Acknowledgements

First of all, I would like to thank E. Hauber for his incredible and extremely helpful support and R. Jaumann for making this work possible.

Furthermore, I want to acknowledge the aid and advice of my colleagues at DLR; I. von der Gathen, F. Schulzeck, S. Adeli, K. Krohn, K. Stephan, and E. Kersten.

I would like to acknowledge the helpful discussions with A. Johnsson (University of Gothenburg), as well as D. Tirsch and B. Heldt (both German Aerospace Center). Moreover, this work would not have been possible without the efforts of the CTX, MOLA, and HRSC team producing and archiving their excellent datasets. Thoughtful comments from three anonymous reviewers helped to improve the manuscript and are highly appreciated (one reviewer for Voelker et al., 2017, and two reviewers for Voelker et al., 2018)

The technical support of K. D. Matz, M. Wählisch, T. Roatsch, and T. Weigelt was a vital part of this work.

Special thanks go to T. Platz, S. van Gasselt, and K. L. Tanaka. I would not have advanced in planetary sciences that far, without their support.

This work has been funded by the HRSC project through the German Aerospace Center (Deutsches Zentrum für Luft- und Raumfahrt). Additionally, this work has been supported by the HRSC project and the COST-STSM (TD1308-090116-070470) program funded by the E.U.

References

Ansan, V., Loizeau, D., Mangold, N., Le Mouélic, S., Carter, J., Poulet, F., Dromart, G., Lucas, A., Bibring, J.-P., Gendrin, A., Gondet, B., Langevin, Y., Masson, Ph., Murchie, S., Mustard, J. F., Neukum, G., 2011. Stratigraphy, mineralogy, and origin of layered deposits inside Terby crater, Mars, Icarus 211, 273–304, doi:10.1016/j.icarus.2010.09.011.

Arkani-Hamed, J., 2005. Giant impact basins trace the ancient equator of Mars, J. Geophys. Res. 110, E04012, doi:10.1029/2004JE002343.

Arkani-Hamed, J., 2010. Hellas: A double-impact basin, American Geophysical Union, Fall Meeting 2010, Abstract #P51A-1409.

Bahrenberg, G., Giese, E., Nipper, J., 1999. Statistische Methoden in der Geographie. Band 1: Univariate und bivariate Statistik, 234p.

Bandfield, J. L., Amador, E. S., Thomas, N. H., 2015. Extensive hydrated silica materials in western Hellas Basin, Mars, Icarus 226 (2013) 1489–1498, http://dx.doi.org/10.1016/j.icarus.2013.08.005.

Basilevskaya, E. A., Neukum, G., and the HRSC Co-Investigator Team, 2006. The Olympus Volcano on Mars: Geometry and Characteristics of Lava Flows, Solar System Research 40 (5), p. 375–383, doi:10.1134/S0038094606050029.

Bernhardt, H., Hiesinger, H., Ivanov, M. A., Ruesch, O., Erkeling, G., Reiss, D., 2015. Photogeologic mapping and the geologic history of the Hellas basin floor, Mars, Icarus 264 (2016) 407–442, http://dx.doi.org/10.1016/j.icarus.2015.09.031

Bernhardt, H., Reiss, D., Hiesinger, H., Ivanov, M. A., 2016. The honeycomb terrain on the Hellas basin floor, Mars: A case for salt or ice diapirism, J. Geophys. Res. Planets, 121, doi:10.1002/2016JE005007.

Bibring, J.-P., Langevin, Y., Mustard, J. F., Poulet, F., Arvidson, R., Gendrin, A., Gondet, B., Mangold, N., Pinet, P., Forget, F., 2006. Global mineralogical and aqueous Mars history derived from OMEGA/Mars express data, Science 312, p. 400–404, doi:10.1126/science.1122659.

Bibring, J.-P., Arvidson, R. E., Gendrin, A., Gondet, B., Langevin, Y., Le Mouelic, S., Poulet, F., Quantin, C., Sotin, C., 2007. Coupled Ferric Oxides and Sulfates on the Martian Surface, Science 317 (5842), p. 1206–1210, doi:10.1126/science.1144174.

Brooker, L., Balme, M. R., Conway, S. J., Hagermann, A., Collins, G. S., 2015. Preliminary grid mapping of fluvial, glacial and periglacial landforms in and around Lyot crater, EPSC Abstracts, Vol. 10, EPSC2015-810.

Burr, D. M. and Parker, A. H., 2006. Grjotá Valles and implications for flood sediment deposition on Mars. Geophys. Res. Lett. 33, L22201, doi:10.1029/2006GL028011.

Cantor, B. A., James, P. B., Caplinger, M., Wolff, M. J,, 2001. Martian Dust Storms: 1999 MOC Observations, J. Geophys. Res. 106, Issue E10, p. 23653-23687, doi:10.1029/2000JE001310.

Cantor, B. A., 2007. MOC observations of the 2001 Mars planet-encircling dust storm, Icarus 186 (2007) 60–96, doi:10.1016/j.icarus.2006.08.019.

Carr, M. H., 2006. The Surface of Mars, 322p.

Carter, J., Poulet, F., Bibring, J.-P., Mangold, N., Murchie, S., 2013. Hydrous minerals on Mars as seen by the CRISM and OMEGA imaging spectrometers: Updated global view, J. Geophys. Res. 118, p. 831–858, doi:10.1029/2012JE004145.

Carter, J., Loizeau, D., Quantin, C., Balme, M., Poulet, F., Gupta, S., Vago, J. L., Bibring, J.-P., 2015. Mineralogic Context of the Circum-Chryse Planitia Candidate Landing Sites for the ExoMars Rover Mission, 46th LPSC, #1988.

Cedillo-Flores, Y., Treiman, A. H., Lasue, J., Clifford, S. M., 2011. CO2 gas fluidization in the initiation and formation of martian polar gullies, Geophys. Res. Lett. 38, L21202, http://dx.doi.org/10.1029/2011GL049403.

Christensen, P. R., 2003. Formation of recent martian gullies through melting of extensive water-rich snow deposits. Nature 422 (6927), 45–48, http://dx.doi.org/10.1038/nature01436.

Christensen, P. R., Jakosky, B. M., Kieffer, H. H., Malin, M. C., McSween Jr, H. Y., Nealson, K., Mehall, G. L., Silverman, S. H., Ferry, S., Caplinger, M., Ravine, M., 2004. The Thermal Emission Imaging System (THEMIS) for the Mars 2001 Odyssey mission, Space Sci. Rev., 110, 85-130.

Chuang, F. C., Noe Dobrea, E. Z., Mest, S. C., Crown, D. A., 2015. Geomorphologic Mapping and Mineralogy of Pits in Intercrater Plains, Northwest Circum Hellas Region, Mars, 46th LPSC, #2542.

Conway S. J., Balme, M. R., 2014. Decameter thick remnant glacial ice deposits on Mars, Geophys. Res. Lett., 41, doi:10.1002/2014GL060314.

Costa, J. E., 1984. Physical Geomorphology of Debris Flows, in Developments and Applications of Geomorphology, edited by J. E. Costa, and P. J. Fleisher, p. 268–317, Berlin Heidelberg, doi:10.1007/978-3-642-69759-3.

Costa, J. E., 1988. Rheologic, geomorphic, and sedimentologic differentiation of water floods, hyperconcentrated flows, and debris flows, In: Flood Geomorphology, edited by V. R. Baker, R. C. Kochel, and P. C. Patton, John Wiley & Sons New York. P. 113-122.

Costard, F. M., Kargel, J. S., 1995. Outwash plains and thermokarst on Mars, Icarus, 114, 93–112, doi:10.1006/icar.1995.1046.

Crown, D. A. and Greeley, R., 1993. Volcanic geology of Hadriaca Patera and the eastern Hellas region of Mars, J. Geophys. Res. 98 (E2), p. 3431–3451, doi:10.1029/92JE02804.

Crown, D. A., Bleamaster, L. F., Mest, S. C., 2005. Styles and timing of volatile-driven activity in the eastern Hellas region of Mars, J. Geophys. Res. 110 (E12), E12S22, 10.1029/2005JE002496.

Crown, D. A., Greeley, R., 2007. Geologic Map of MTM –30262 and –30267 Quadrangles, Hadriaca Patera Region of Mars, Scientific Investigations Map 2936, Atlas of Mars: MTM –30262 and –30267 Quadrangles.

De Blasio, F. V., 2011. Landslides in Valles Marineris (Mars): A possible role of basal lubrication by sub-surface ice, Planet. Space Sci. 59, p. 1384–1392, doi:10.1016/j.pss.2011.04.015.

Dickson, J. L., Head, J. W., Goudge, T. A., Barbieri, L., 2015. Recent climate cycles on Mars: Stratigraphic relationships between multiple generations of gullies and the latitude dependent mantle, Icarus 252,p. 83–94, http://dx.doi.org/10.1016/j.icarus.2014.12.035.

Diniega, S., Hansen, C.J., McElwaine, J.N., Hugenholtz, C.H., Dundas, C.M., McEwen, A.S., Bourke, M.C., 2013. A new dry hypothesis for the formation of martian linear gullies, Icarus 225, 526–537, http://dx.doi.org/10.1016/j.icarus.2013.04.006.

Diot, X., El-Maarry, M. R., Schlunegger, F., Norton, K. P., Thomas, N., Grindrod, P. M., 2014. The geomorphology and morphometry of the banded terrain in Hellas basin, Mars, Planet. Space Sci. 101, p. 118–134, http://dx.doi.org/10.1016/j.pss.2014.06.013.

Diot, X., El-Maarry, M. R., Schlunegger, F., Norton, K. P., Thomas, N., Grindrod, P. M., Chojnacki, M., 2016. Complex geomorphologic assemblage of terrains in association with the banded terrain in Hellas basin, Mars, Planet. Space Sci. 121, p. 36–52, http://dx.doi.org/10.1016/j.pss.2015.12.003.

Dundas, C. M., Byrne, S., McEwen, A. S., 2015a. Modeling the development of martian sublimation thermokarst landforms, Icarus 262, p. 154–169, http://dx.doi.org/10.1016/j.icarus.2015.07.033.

Dundas, C. M., Dieniega, S., McEwen, A. S., 2015b. Long-term monitoring of martian gully formation and evolution with MRO/HiRISE. Icarus 251, p. 244–263, doi:10.1016/j.icarus.2014.05.013.

Ehlmann, B. L., Mustard, J. F., Murchie, S. L., Bibring, J.-P., Meunier, A., Fraeman, A. A., Langevin, Y., 2011. Subsurface water and clay mineral formation during the early history of Mars, Nature 479, p. 53–60, doi:10.1038/nature10582.

Fastook, J. L., Head, J. W., Marchant, D. R., Forget, F., 2008. Tropical mountain glaciers on Mars: Altitude-dependence of ice accumulation, accumulation conditions, formation times, glacier dynamics, and implications for planetary spin-axis/orbital history, Icarus 198, p. 305–317, doi:10.1016/j.icarus.2008.08.008.

Feldman, W. C., Prettyman, T.H., Maurice, S., Plaut, J. J., Bish, D. L., Vaniman D. T., Mellon, M. T., Metzger, A. E., Squyres, S. W., Karunatillake, S., Boynton, W. V., Elphic, R. C., Funsten, H. O., Lawrence, D. J., Tokar, R. L., 2004. Global distribution of near-surface hydrogen on Mars, J. Geophys. Res. 109, E09006, doi:10.1029/2003JE002160.

Fergason, R. L., Christensen, P. R., Kieffer, H. H., 2006. High-resolution thermal inertia derived from the Thermal Emission Imaging System (THEMIS): Thermal model and applications, J. Geophys. Res. 111(E12004), doi:10.1029/2006JE002735.

Forget, F., Hourdin, F., Fournier, R., Hourdin, C., Talagrand, O., Collins, M., Lewis, S. R., Read, P. L., Huot, J.-P., 1999. Improved general circulation models of the Martian atmosphere from the surface to above 80 km, J. Geophys. Res. 104, E10, p. 24155–24176, doi:10.1029/1999JE001025.

Forget, F., Haberle, R. :, Montmessin, F., Levrard, B., Head, J. W., 2006. Formation of glaciers on Mars by atmospheric precipitation at high obliquity, Science 311, 368–371, doi:10.1126/science.1120335.

Forget, F., Wordsworth, R., Millour, E., Madeleine, J.-B., Kerber, L., Leconte, J., Marcq, E., Haberle, R. M., 2013. 3D modelling of the early martian climate under a denser CO2 atmosphere: Temperatures and CO2 ice clouds, Icarus 222 (1), p. 81–99, doi:10.1016/j.icarus.2012.10.019.

Freundt, A., Wilson, C. N. J., Carey, S. N., 2000. Ignimbrites and block-and-ash flow deposits, in: Encyclopedia of Volcanoes, edited by Sigurdsson, H., Houghton, B., McNutt, S.R., Rymer, H., Stix, J., p. 581–599, Academic Press, New York.

Fuller, E. R., and Head III, J. W., 2002. Amazonis Planitia: The role of geologically recent volcanism and sedimentation in the formation of the smoothest plains on Mars. J. Geophys. Res. 107(E10), 5081, doi:10.1029/2002JE001842.

Gaffey, S. J., McFadden, L. A., Nash, D., Pieters, C. M., 1993. Ultraviolet, visible, and near-infrared reflectance spectroscopy: Laboratory spectra of geologic materials, in Remote Geochemical Analysis: Elemental and Mineralogical Composition, edited by C. M. Pieters and P. A. J. Englert, p. 43–77, Cambridge University Press, New York.

Ghatan, G. J. and Zimbelman, J. R., 2006. Paucity of candidate coastal constructional landforms along proposed shorelines on Mars: Implications for a northern lowlands-filling ocean, Icarus 185, p. 171–196, doi:10.1016/j.icarus.2006.06.007.

Giacomini, L., Massironi, M., Martellato, E., Pasquare, G., Frigeri, A., Cremonese, G., 2009. Inflated flows on Daedalia Planum (Mars)? Clues from a comparative analysis with the Payen volcanic complex (Argentina), Planet. Space Sci. 57, p. 556–570, doi:10.1016/j.pss.2008.12.001.

Golombek, M.P., Bridges, N.T., 2000. Erosion rates on Mars and implications for climate change: Constraints from the Pathfinder landing site, J. Geophys. Res. Earth Surf. 105, p. 1,841–1,853, doi:10.1029/1999JE001043.

Greeley, R., Leach, R., White, B., Iverson, J., Pollacl, J. B., 1980. Threshold wind speeds for sand on Mars: Wind tunnel simulations, Geophys. Res. Lett. 7 (2), p. 121–124.

Gregg, T. K. P., 2016. Patterns and processes: Subaerial lava flow morphologies: A review, Journal of Volcanology and Geothermal Research, doi:10.1016/j.jvolgeores.2017.04.022.

Gwinner, K., Scholten, F., Preusker, F., Elgner, S., Roatsch, T., Spiegel, M., Schmidt, R., Oberst, J., Jaumann, R., Heipke, C., 2010. Topography of Mars from global mapping by HRSC high-resolution digital terrain models and ortho images: characteristics and performance, Earth Planet. Sci. Lett. 294, p. 506–519, doi:10.1016/j.epsl.2009.11.007.

Haberle, R. M., McKay, C. P., Schaeffer, J., Cabrol, N. A., Grin, E. A., Zent, A. P., Quinn, R., 2001. On the possibility of liquid water on present-day Mars, J. Geophys. Res., 106(E10), 23317–23326, doi:10.1029/2000JE001360.

Haberle, R. M., Murphy, J. R., Schaeffer, J., 2003. Orbital change experiments with a Mars general circulation model, Icarus 161, 66–89, doi:10.1016/S0019-1035(02)00017-9.

Haltigin, T. W., Pollard, W. H., Dutilleul, P., Osinski, G. R., Koponen, L., 2014. Co-evolution of polygonal and scalloped terrains, southwestern Utopia Planitia, Mars, Earth Planet. Sci. Let. 387, p. 44–54, http://dx.doi.org/10.1016/j.epsl.2013.11.005.

Hansen, C. J., Thomas, N., Portyankina, A., McEwen, T., Becker, S., Herkenhoff, K., Kieffer, H., Mellon, M., 2010. HiRISE observations of gas sublimation-driven activity in Mars' southern polar regions: I. Erosion of the surface, Icarus 205, p. 283–295, doi:10.1016/j.icarus.2009.07.021

Hargitai, H. I. , Gulick, V. C., Glines, N. H., 2017. Discontinuous drainage systems formed by highland precipitation and ground-water outflow in the Navua Valles and southwest Hadriacus Mons regions, Mars, Icarus 294, p. 172–200, http://dx.doi.org/10.1016/j.icarus.2017.03.005.

Harrison, T. N., Osinski, G. R., Tornabene, L. L., Jones, E., 2015. Global documentation of gullies with the Mars Reconnaissance Orbiter Context Camera and implications for their formation, Icarus 252, p. 236–254, http://dx.doi.org/10.1016/j.icarus.2015.01.022.

Hartmann, W. K. and Neukum, G., 2001. Cratering chronology and the evolution of Mars. Space Sci. Rev. 96, p. 165–194, doi:10.1007/978-94-017-1035-0_6.

Hauber, E., Orgel, C., van Gasselt, S., Reiss, D., Johnsson, A., Ramsdale, J. D., Balme, M. R., Conway, S. J., Costard, F., Gallagher, C., Kereszturi, Á., Platz, T., Séjourné, A., Skinner, J. A., Swirad, Z., Losiak, A., 2015. Mapping Mars' northern plains: Origins, evolution and response to climate change–A new overview of recent ice-related landforms in Acidalia Planitia, 46th LPSC, #1359.

Hayward R. K., Fenton, L. K., Titus, T. N., 2014. Mars Global Digital Dune Database (MGD3): Global dune distribution and wind pattern observations, Icarus 230, p. 38–46, http://dx.doi.org/10.1016/j.icarus.2013.04.011.

Head, J. W., Mustard, J. F., Kreslavsky, M. A., Milliken, R. E., Marchant, D. R., 2003. Recent ice ages on Mars, Nature 426, p. 797–802, doi:10.1038/nature02114.

Head, J. W., Marchant, D. R., Ghatan, G. J., 2004. Glacial deposits on the rim of a Hesperian-Amazonian outflow channel source trough: Mangala Valles, Mars, Geophys. Res. Lett. 31, L10701, doi:10.1029/2004GL020294.

Hoffman, N. and Tanaka, K. L., 2002. Co-existing "Flood" and "Volcanic" Morphologies in Elysium as Evidence for Cold CO2 or Warm H2O Outbursts. 33rd LPSC, #1505.

Howard, A. D., 2000. The Role of Eolian Processes in Forming Surface Features of the Martian Polar Layered Deposits, Icarus 144, p. 267–288, doi:10.1006/icar.1999.6305.

Howard, A. D., Spiga, A., Moore, J. M., 2012. The Deepest Basin on Mars is Formed by Aeolian Erosion: Western Hellas Planitia, 43rd LPSC, #1105.

Hubbard, B., Souness, C., Brough, S., 2014. Glacier-like forms on Mars, The Cryosphere 8, p. 2047–2061, doi:10.5194/tc-8-2047-2014.

Hungr, O., Evans, S. G., Bovis, M. J., Hutchinson, J. N., 2001. A Review of the Classification of Landslides of the Flow Type, Environmental and Engineering Geoscience, Vol. 7 (3), p. 221–238, doi:10.2113/gseegeosci.7.3.221.

Hutchinson, J. N., 1988. General Report: Morphological and Geotechnical Parameters of Landslides in Relation to Geology and Hydrogeology. In Bonnard, C. (Editor), Proceedings, 5th International Symposium on Landslides, A. A. Balkema, Rotterdam, Vol. 1, p. 3–36, doi:10.1016/0148-9062(89)90310-0.

Ivanov, B. A., 2001. Mars/Moon cratering ratio estimates. Space Sci. Rev. 96, p. 87–104, doi:10.1007/978-94-017-1035-0_4.

Jaumann, R., Neukum, G., Behnke, T., Duxbury, T. C., Eichentopf, K., Flohrer, J., van Gasselt, S., Giese, B., Gwinner, K., Hauber, E., Hoffmann, H., Hoffmeister, A., Köhler, U., Matz, K.-D., McCord, T. B., Mertens, V., Oberst, J., Pischel, R., Reiss, D., Ress, E., Roatsch, T., Saiger, P., Scholten, F., Schwarz, G., Stephan, K., Wählisch, M., and the HRSC Co-Investigator Team, 2007. The high-resolution stereo camera (HRSC) experiment on Mars Express: Instrument aspects and experiment conduct from interplanetary cruise through the nominal mission, Planet. Space Sci. 55 (7-8), p. 928–952, doi:10.1016/j.pss.2006.12.003.

Jenness, J., 2012. Repeating shapes for ArcGIS. Jenness Enterprises. Available at: http://www.jennessent.com/arcgis/repeat_shapes.htm.

Kahre, M. A., Hollingsworth, J. L., Haberle, R. M., Wolff, M. J., 2014. Understanding the formation and evolution of water ice clouds in the Hellas basin during NH summer on Mars, 8th International Conference on Mars, #1308.

Keszthelyi, L., Thordarson, T., McEwen, A., Haack, H., Guilbaud, M.-N., Self, S., Rossi, M. J., 2004. Icelandic analogs to Martian flood lavas, Geochem. Geophys. Geosyst. 5, Q11014, doi:10.1029/2004GC000758.

Keszthelyi, L. P., Denlinger, R. P., O'Connell, D. R. H., Burr, D. M. 2007. Initial insights from 2.5D hydraulic modeling of floods in Athabasca Valles, Mars. Geophys. Res. Lett. 34, L21206, doi:10.1029/2007GL031776.

Kieffer, H. H., Jakosky, B. M., Snyder, C. W., 1992. The planet Mars: From antiquity to the present, in Mars, edited by H. H. Kieffer et al., University Arizona Press, Tucson, London.

Kneissl, T., van Gasselt, S., Neukum, G., 2011. Map-projection-independent crater size–frequency determination in GIS environments – New software tool for ArcGIS. Planet. Space Sci. 59, p. 1243–1254, doi:10.1016/j.pss.2010.03.015.

Kostama, V.-P.,Kreslavsky, M. A., Head, J. W., 2006. Recent high-latitude icy mantle in the northern plains of Mars: Characteristics and ages of emplacement, Geophys. Res. Lett. 33, L11201, doi:10.1029/2006GL025946.

Kostama, V.-P., Ivanov, M. A., Raitala, J., Törmänen, T., Korteniemi, J., Neukum, G., 2010. Evidence for multiple ice deposits on the northeastern rim of Hellas basin, Mars, Earth Planet. Sci. Lett. 294, p. 321–331, doi:10.1016/j.epsl.2009.11.021.

Kostama, V.-P., Kukkonen, S., Raitala, J., 2017. Resurfacing event observed in Morpheos basin (Eridania Planitia) and the implications to the formation and timing of Waikato and Reull Valles, Mars. Planet. Space Sci. 140, p. 35–48, doi: 10.1016/j.pss.2017.04.001.

Kraal, E.R., Asphaug, E., Moore, J.M., Lorenz, R.D., 2006. Quantitative geomorphic modeling of martian bedrock shorelines. J. Geophys. Res. 111, E03001, doi:10.1029/2005JE002567.

Kreslavsky, M. A., Head, J. W., 2002a. Fate of outflow channel effluents in the northern lowlands of Mars: The Vastitas Borealis Formation as a sublimation residue from frozen ponded bodies of water, J. Geophys. Res. 107, E12 (5121), doi:10.1029/2001JE001831.

Kreslavsky, M. A., Head, J. W., 2002b. Mars: Nature and evolution of young latitude-dependent water-ice-rich mantle, Geophys. Res. Lett. 29(15), 1719, doi:10.1029/2002GL015392.

Kukkonen, S., Kostama, V.-P., 2018. Modification history of the Harmakhis Vallis outflow channel, Mars, based on CTX-scale photogeologic mapping and crater count dating, Icarus 299, p. 46–67, doi:10.1016/j.icarus.2017.07.014.

Laskar, J., Correia, A. C. M., Gastineau, M., Joutel, F., Levrard, B., Robutel, P., 2004. Long term evolution and chaotic diffusion of the insolation quantities of Mars. Icarus 170, 343–364. http://dx.doi.org/10.1016/j.icarus.2004.04.005

Lefort, A., Russell, P.S., Thomas, N., McEwen, A.S., Dundas, C.M., Kirk, R.L., 2009. Observations of periglacial landforms in Utopia Planitia with the High Resolution Imaging Science Experiment (HiRISE), J. Geophys. Res., 114, E04005, doi:10.1029/2008JE003264.

Leonard, G.J., Tanaka,K.L., 2001. Geologic map of the Hellas region of Mars. US Geol. Surv. Misc. Invest. Ser. Map I-2694.

Leverington, D. W., 2011.Volcanic origin for the outflow channels of Mars: Key evidence and major implications, Geomorphology 132, p. 51–75, doi:10.1016/j.geomorph.2011.05.022.

Levrard, B., Forget, F., Montmessin, F., Laskar, J., 2004. Recent ice-rich deposits formed at high latitudes on Mars by sublimation of unstable equatorial ice during low obliquity, Nature 431, 1072–1075, doi:10.1038/nature03055.

Levy, J. S., Head, J. W., Marchant, D., 2009. Thermal contraction crack polygons on Mars: Classification, distribution, and climate implications from HiRISE observations, J. Geophys. Res. 114, E01007, doi:10.1029/2008JE003273.

Levy, J. S., Fassett, C. I., Head, J. W., 2016. Enhanced erosion rates on Mars during Amazonian glaciation, Icarus 264, p. 213–219, doi:10.1016/j.icarus.2015.09.037.

Lucchitta, B. K., 1979. Landslides in Valles Marineris, Mars, J. Geophys. Res. 84, p. 8097–8113, doi:10.1029/JB084iB14p08097.

Madeleine, J.B., Head, J. W., Forget, F., Navarro, T., Millour, E., 2014. Recent Ice Ages on Mars: The Role of Radiatively Active Clouds and Cloud Microphysics, Geophys. Res. Lett. 41, 4873-4879, doi:10.1002/2014GL059861.

Malin, M. C., Bell III, J. F., Cantor, B. A., Caplinger, M. A., Calvin, W. M., Clancy, R. T., Edgett, K. S., Edwards, L., Haberle, R. M., James, P. B., Lee, S., W., Ravine, M. A., Thomas, P. C., Wolff, M. J., 2007. Context camera investigation on board the Mars Reconnaissance Orbiter, J. Geophys. Res. 112, E05S04, doi:10.1029/2006JE002808.

Mangold, N., Allemand, P., 2003. Ductile deformation in Hellas floor: Salt diapirs or crustal domes? 6th International Conference on Mars, #3047.

Mangold, N., 2005. High latitude patterned grounds on Mars: Classification, distribution and climatic control, Icarus 174, (2), p. 336–359, doi:10.1016/j.icarus.2004.07.030.

Mangold, N., 2011a. Water ice sublimation-related landforms on Mars, Geological Society, London, Special Publications 2011, v. 356, p. 133-149, doi: 10.1144/SP356.8.

Mangold, N. 2011b. Ice sublimation as a geomorphic process: A planetary perspective, Geomorphology 126, p. 1–17, doi:10.1016/j.geomorph.2010.11.009.

Marra, W. A., Hauber, E., de Jong, S. M., Kleinhans, M. G., 2015. Pressurized groundwater systems in Lunae and Ophir Plana (Mars): Insights from small-scale morphology and experiments. GeoResJ 8, p. 1–13, doi:10.1016/j.grj.2015.08.001.

McEwen, A. S., Eliason, E. M., Bergstrom, J. W., Bridges, N. T., Hansen, C. J., Delamere, W. A., Grant, J. A., Gulick, V. C., Herkenhoff, K. E., Keszthelyi, L., Kirk, R. L., Mellon, M. T., Squyres, S. W., Thomas, N., Weitz, C. M., 2007. Mars Reconnaissance Orbiters high resolution imaging science experiment (HiRISE). J. Geophys. Res. 112(E5), doi:10.1029/2005JE002605.

Mellon, M. T., Arvidson, R. E., Sizemore, H. G., Searls, M. L., Blaney, D. L., Cull, S., Hecht, M. H., Heet, T. L., Keller, H. U., Lemmon, M. T., Markiewicz, W. J., Ming, D. W., Morris, R. V., Pike, W. T., Zent, A. P., 2009. Ground ice at the Phoenix Landing Site: Stability state and origin, J. Geosphys. Res. 114, E00E07, doi:10.1029/2009JE003417.

Mest S. C., Crown, D. A. 2001. Geology of the Reull Vallis Region, Mars, Icarus 153, p. 89–110, doi:10.1006/icar.2001.6655.

Michael, G. G. and Neukum, G., 2010. Planetary surface dating from crater size–frequency distribution measurements: Partial resurfacing events and statistical age uncertainty. Earth Planet. Sci. Lett. 294, 223–229, doi:10.1016/j.epsl.2009.12.041.

Michael, G. G., Platz, T., Kneissl, T., Schmedemann, N., 2012. Planetary surface dating from crater size–frequency distribution measurements: A quantitative test of spatial randomness. Icarus 218, p. 169–177, doi:10.1016/j.icarus.2011.11.033.

Milazzo, M. P., Keszthelyi, L. P., Jaeger, W. L., Rosiek, M., Mattson, S., Verba, C., Beyer, R. A., Geissler, P. E., McEwen, A. S., and the HiRISE Team, 2009. Discovery of columnar jointing on Mars, Geology 37 (2), p. 171–174, doi:10.1130/G25187A.1.

Milkovich, S. M., Head, J. W., Marchant, D. R., 2006. Debris-covered piedmont glaciers along the northwest flank of the Olympus Mons scarp: Evidence for low-latitude ice accumulation during the Late Amazonian of Mars. Icarus 181, p. 388–407, doi:10.1016/j.icarus.2005.12.006.

Milliken, R. E., Mustard, J. F., Goldsby, D. L., 2003. Viscous flow features on the surface of Mars: Observations from high-resolution Mars Orbiter Camera (MOC) images, J. Geophys. Res 108(E6), 5057, doi:10.1029/2002JE002005.

Millour, E., Forget, F., Spiga, A., Navarro, T., Madeleine, J.-B., Montabone, L., Pottier, A., Lefevre, F., Montmessin, F., Chaufray, J.-Y., Lopez-Valverde, M. A., Gonzalez-Galindo, F., Lewis, S. R., Read, P. L., Huot, J.-P., Desjean, M.-C., and the MCD/GCM development team, 2015. The Mars Climate Database (MCD version 5.2), EPSC Abstracts, Vol. 10, EPSC2015-438.

Mischna, M. A., Richardson, M. I., Wilson, R. J., McCleese, D. J., 2003. On the orbital forcing of Martian water and CO2 cycles: A general circulation model study with simplified volatile schemes, J. Geophys. Res. 108(E6), 5062, doi:10.1029/2003JE002051.

Moore, J. M., Wilhelms, D. E., 2001. Hellas as a Possible Site of Ancient Ice-Covered Lakes on Mars, Icarus 154, p. 258–276, doi:10.1006/icar.2001.6736.

Moore, J. M., Wilhelms, D. E., 2007. Geologic Map of Part of Western Hellas Planitia, Mars. U.S. Geological Survey Geologic Investigations, 2953, 80225.

Morgenstern, A., Hauber, E., Reiss, D., van Gasselt, S., Grosse, G., Schirrmeister, L., 2007. Deposition and degradation of a volatile-rich layer in Utopia Planitia and implication for climate history on Mars, J. Geophys. Res. 112, E06010, doi:10.1029/2006JE002869.

Mouginis-Mark, P. J., Christensen, P. R., 2005. New observations of volcanic features on Mars from the THEMIS instrument. J. Geophys. Res. 110, E08007, doi:10.1029/2005JE002421.

Musiol, S., Cailleau, B., Platz, T., Kneissl, T., Dumke, A., Neukum, G., 2011. Outflow activity near Hadriaca Patera, Mars: Fluid-tectonic interaction investigated with High Resolution Stereo Camera stereo data and finite element modeling, J. Geophys. Res. 116 (E08001), doi:10.1029/2010JE003791.

Mustard, J. F., Cooper, C. D., Rifkin, M. K., 2001. Evidence for recent climate change on Mars from the identification of youthful near-surface ground ice, Nature 412, p. 411–414, doi:10.1038/35086515.

Mustard, J. F., Poulet, F., Head, J. W., Mangold, N., Bibring, J.-P., Pelkey, S. M., Fassett, C. I., Langevin, Y., Neukum, G., 2007. Mineralogy of the Nili Fossae region with OMEGA/Mars Express data: 1. Ancient impact melt in the Isidis Basin and implications for the transition from the Noachian to Hesperian, J. Geophys. Res. 112 (E8), E08S03, doi:10.1029/2006JE002834.

Neukum, G., Jaumann, R., Hoffmann, H., Hauber, E., Head, J. W., Basilevsky, A. T., Ivanov, B. A., Werner, S. C., van Gasselt, S., Murray, J. B., McCord, T., and the HRSC Co-Investigator and Experiment Team, 2004a. Recent and episodic volcanic and glacial activity on Mars revealed by the High Resolution Stereo Camera, Nature 432, p. 971–979, doi:10.1038/nature03231.

Neukum, G., Jaumann, R., and the HRSC Co-Investigator and Experiment Team, 2004b. HRSC: the High Resolution Stereo Camera on Mars Express. In: Mars Express : The Scientific Payload ESA-SP, 1240. ESA. ISBN 92-9092-556-6.

Neumann, G. A., Zuber, M. T., Wieczorek, M. A., McGovern, P. J., Lemoine, F. G., Smith, D. E., 2004. Crustal structure of Mars from gravity and topography, J. Geophys. Res., 109, E08002, doi:10.1029/2004JE002262.

Orgel, C., Hauber, E., ., Skinner, J. A., van Gasselt, S., Ramsdale, J. D., Balme, M. R., Séjourné, Kereszturi, Á., 2015. Distribution, origin and evolution of hypothesized mud volcanoes, thumbprint terrain and giant polygons in Acidalia, Utopia and Arcadia Planitiae: Implications for sedimentary processes in the northern lowlands of Mars, 46th LPSC, #1862.

Panizza, M., 1996. Environmental geomorphology – Developments in earth surface processes, Vol. 4, p. 267.

Parsons, J. D., Whipple, K. X., Simoni, A., 2001. Experimental study of the grainflow, fluid-mud transition in debris flows, J. Geol. 109, p. 427–447, doi:10.1086/320798.

Pasckert, J. H., Hiesinger, H., Reiss, D., 2012. Rheologies and ages of lava flows on Elysium Mons, Mars, Icaurs 219, p. 443–457, doi:10.1016/j.icarus.2012.03.014.

Platz, T., Michael, G. G., Tanaka, K. L., Skinner Jr., J. A., Fortezzo, J. M., 2013. Crater-based dating of geological units on Mars: Methods and application for the new global geological map. Icarus 225, p. 806–827, doi:10.1016/j.icarus.2013.04.021.

Plescia, J. B., 2003. Cerberus Fossae, Elysium, Mars: a source for lava and water. Icarus 164, p. 79–95, doi:10.1016/S0019-1035(03)00139-8.

Poulet, F., J.-P. Bibring, J. F. Mustard, A. Gendrin, N. Mangold, Y. Langevin, R. E. Arvidson, B. Gondet, and C. Gomez, 2005. Phyllosilicates on Mars and implications for early Martian climate, Nature 438, p. 623–627, doi:10.1038/nature04274.

Poulet, F., Gomez, C., Bibring, J.-P., Langevin, Y., Gondet, B., Pinet, P., Belluci, G., Mustard, J., 2007. Martian surface mineralogy from Observatoire pour la Mineralogie, l'Eau, les Glaces et l'Activite on board the Mars Express spacecraft (OMEGA/MEx): Global mineral maps, J. Geophys. Res. 112, E08S02, doi:10.1029/2006JE002840.

Ramsdale, J., Balme, M., Conway, S., Gallagher, C., van Gasselt, S., Hauber, E., Orgel, C., Séjourné, A., Skinner, J., Costard, F., Johnsson, A., Losiak, A., Reiss, D., Swirad, Z., Kereszturi, A., Smith, I., Platz, T., 2017. Grid-based mapping: a method for rapidly determining the spatial

distributions of small features over very large areas, Planet. Space Sci. 140, p. 49–61, https://doi.org/10.1016/j.pss.2017.04.002.

Richardson, M. I., Wilson, R. J., 2002. Investigation of the nature and stability of the Martian seasonal water cycle with a general circulation model, J. Geophys. Res., 107(E5), 5031, doi:10.1029/2001JE001536.

Rodine, J. D., Johnson, A. M., 1976. The ability of debris, heavily freighted with coarse clastic materials, to flow on gentle slopes, Sedimentology 23, p. 213–234.

Ruff, S.W., Christensen, P. R., 2002. Bright and dark regions on Mars: Particle size and mineralogical characteristics based on Thermal Emission Spectrometer data, J. Geophys. Res. 107, doi10.1029/2001JE001580

Saar, M. O. and Manga, M, 1999. Permeability-porosity relationship in vesicular basalts, Geophys. Res. Lett. 26 (1), p. 111–114, doi:10.1029/1998GL900256.

Salese, F., Ansan, V., Mangold, N., Carter, J., Ody, A., Poulet, F., Ori G. G., 2016. A sedimentary origin for intercrater plains north of the Hellas basin: Implications for climate conditions and erosion rates on early Mars, J. Geophys. Res. Planets 121, doi:10.1002/2016JE005039.

Schneider, D., Huggel, C., Haeberli, W., Kaitna, R., 2011. Unraveling driving factors for large rock–ice avalanche mobility, Earth Surf. Process. Landforms 36, p. 1948–1966, doi:10.1002/esp.2218.

Schon, S. C., Head, J. W., Milliken, R. E., 2009. A recent ice age on Mars: Evidence for climate oscillations from regional layering in mid-latitude mantling deposits, Geophys. Res. Lett. 36, L15202, doi:10.1029/2009GL038554

Schon, S. C., Head, J. W., Fassett, C. I., 2012. Recent high-latitude resurfacing by a climate-related latitude-dependent mantle: Constraining age of emplacement from counts of small craters, Planet. Space Sci.69, p. 49–61, http://dx.doi.org/10.1016/j.pss.2012.03.015

Schorghofer, N., 2008. The Lifetime of Ice on Main Belt Asteroids, The Astrophysical Journal 682, p. 697–705, doi:10.1086/588633.

Seibert, N. M., Kargel, J. S., 2001. Small-scale Martian polygonal terrain: Implications for liquid surface water, Geophys. Res. Lett. 28 (5), p. 899–902, doi:10.1029/2000GL012093.

Séjourné, A., Costard, F., Gargani, J., Soare, R. J., Fedorov, A., Marmo, C., 2011. Scalloped depressions and small-sized polygons in western Utopia Planitia, Mars: a new formation hypothesis, Planet. Space Sci. 59, Issues 5–6, p. 412–422, http://dx.doi.org/10.1016/j.pss.2011.01.007.

Séjourné, A., Costard, F., Losiak, A., Swirad, Z. M., Balme, M. R., Conway, S. J., Gallagher, C., Hauber, E., Johnsson, A. E., Kereszturi, A., Orgel, C., Platz, T., Ramsdale, J. D., Reiss, D., Skinner Jr., J. A., van Gasselt, S., 2015. Mapping the Northern Plains of Mars: Origins, Evolution and Response to Climate Change – A New Overview of Recent Ice-Related Landforms in Utopia Planitia, 46th LPSC, #1328.

Self, S. and Sparks, R. S. J., 1978. Characteristics of widespread pyroclastic deposits formed by the interaction of silicic magma and water, Bulletin of Volcanology 41:196, doi:10.1007/BF02597223.

Shinbrot, T., Duong, N.-H., Kwan, L., Alvarez, M. M., 2003. Dry granular flows can generate surface features resembling those seen in Martian gullies, Proceedings of the National Academy of Sciences 101 (23), p. 8542–8546, doi: 10.1073/pnas.0308251101.

Siili, T., Haberle, R. M., Murphy, J. R., Savijärvi, H, 1999. Modelling of the combined late-winter ice cap edge and slope winds in Mars Hellas and Argyre regions, Planet. Space Sci. 47, p. 951–970, http://dx.doi.org/10.1016/S0032-0633(99)00016-1.

Smith, D. E., Zuber, M. T., Solomon, S. C., Phillips, R. J., Head, J. W., Garvin, J. B., Banerdt, W. B., Muhleman, D. O., Pettengill, G. H., Neumann, G. A., Lemoine, F. G., Abshire, J. B., Aharonson, O., Brown, C. D., Hauck, S. A., Ivanov, A. B., McGovern, P. J., Zwally, H. J., Duxbury, T. C., 1999. The global topography of Mars and implications for surface evolution. Science 284, p. 1421–1576. doi:10.1126/science.284.5419.1495

Smith, D.E., Zuber, M. T., Frey, H. V., Garvin, J. B., Head, J. W., Muhleman, D. O., Pettengill, G. H., Phillips, R. J., Solomon, S. C., Zwally, H. J., Banerdt, W. B., Duxbury, T. C., Golombek, M. P., Lemoine, F. G., Neumann, G. A., Rowlands, D. D., Aharonson, O., Ford, P. G., Ivanov, A. B., Johnson, C. L., McGovern, P. J., Abshire, J. B., Afzal, R. S., Sun, X., 2001. Mars Orbiter Laser Altimeter: Experiment summary after the first year of global mapping of Mars. J. Geophys. Res. 106, 23689–23722. http://dx.doi.org/10.1029/2000JE001364.

Soare, R.J., Burr, D.M., Wan Bun Tseung, J.M., 2005. Possible pingos and a periglacial landscape in northwest Utopia Planitia, Icarus 174, p. 373–382, doi:10.1016/j.icarus.2004.11.013.

Soare, R.J., Kargel, J.S., Osinski, G.R., Costard, F., 2007. Thermokarst processes and the origin of crater-rim gullies in Utopia and western Elysium Planitia. Icarus 191, 95–112, http://dx.doi.org/10.1016/j.epsl.2008.05.010

Soare, R. J., Osinski, G. R., Roehm, C. L., 2008. Thermokarst lakes and ponds on Mars in the very recent (late Amazonian) past, Earth Planet. Sci. Lett. 272, p. 382–393, http://dx.doi.org/10.1016/j.epsl.2008.05.010

Soare, R. J., Séjourné, A., Pearce, G., Costard, F., Osinski, G. R., 2011, The Tuktoyaktuk Coastlands of northern Canada: A possible "wet" periglacial analog of Utopia Planitia, Mars, Geol. Soc. Amer. Spec. Pap. 483, p. 203–218, doi: 10.1130/2011.2483(13).

Sturges, H. A., 1926. The choice of class interval. Journal of the American Statistical Association 21, p. 65–66.

Tanaka, K. L., Chapman, M. G., Scott, D. H., 1992. Geologic map of the Elysium region of Mars: U.S. Geological Survey Miscellaneous Investigations Series Map I–2147, scale 1:5,000,000.

Tanaka, K. L., Leonard, G. J., 1995. Geology and landscape evolution of the Hellas region of Mars. J. Geophys. Res. 100, p. 5407–5432, doi:10.1029/94JE02804.

Tanaka, K. L., Skinner Jr., J. A., Dohm, J. M., Irwin III, R. P., Kolb, E. J., Fortezzo, C. M., Platz, T., Michael, G. G., Hare, T. M., 2014. Geologic Map of Mars: U.S. Geological Survey, Scientific Investigations Map, 3292, scale 1:20,000,000.

Thomson, B. J., Bridges, N. T., Milliken, R., Baldridge, A., Hook, S. J., Crowley, J. K., Marion, G. M., de Souza Filho, C. R., Brown, A. J., Weitz, C. M., 2011. Constraints on the origin and evolution of the layered mound in Gale Crater, Mars using Mars Reconnaissance Orbiter data, Icarus 214, Issue 2, p. 413–432, http://dx.doi.org/10.1016/j.icarus.2011.05.002

Thordarson, T., and Self, S., 1998. The Roza Member, Columbia River Basalt Group: A gigantic pahoehoe lava flow field formed by endogenous processes?, J. Geophys. Res. 103 (B11), p. 27,411–27,445, doi:10.1029/98JB01355.

Tirsch, D., Jaumann, R., Pacifici, A., Poulet, F., 2011. Dark aeolian sediments in martian craters: Composition and sources. J. Geophys. Res. 116, E03002. http://dx.doi.org/10.1029/2009JE003562.

Treiman, A.H., 2003. Geologic settings of martian gullies: Implications for their origins. J. Geophys. Res. 108 (E4), 8031. http://dx.doi.org/10.1029/2002JE001900.

Ulrich, M., Morgenstern, A., Günther, F., Bauch, K. E., Hauber, E., Rössler, S., Schirrmeister, L., 2010. Thermokarst in Siberian ice-rich permafrost: comparison to asymmetric scalloped depressions on Mars, J. Geophys. Res. 115, E10009, doi:10.1029/2010JE003640.

Ulrich, M., Hauber, E., Herzschuh, U., Härtel, S., Schirrmeister, L., 2011. Polygon pattern geomorphometry on Svalbard (Norway) and western Utopia Planitia (Mars) using high-resolution stereo remote-sensing data, Geomorphology 134, p. 197–216, doi:10.1016/j.geomorph.2011.07.002.

Van Gasselt, S., Hauber, E., Neukum, G., 2007a. Cold-climate modification of Martian landscapes: A case study of a spatulate debris landform in the Hellas Montes region, Mars, J. Geophys. Res. 112, E09006, doi:10.1029/2006JE002842.

Van Gasselt, S., 2007b. Cold-climate landforms on Mars, Berichte aus der Geowissenschaft, D 188, Freie Universität Berlin.

Van Gasselt, S., Hauber, E., Neukum, G., 2010. Lineated valley fill at the Martian dichotomy boundary: Nature and history of degradation, J. Geophys. Res. 115, E08003, doi:10.1029/2009JE003336.

Varnes, D. J., 1978. Slope Movement Types and Processes. In Schuster, R. L., and Krizek, R. J., (Editors), Landslides, Analysis and Control, Special Report 176: Transportation Research Board, National Academy of Sciences, Washington, DC, p. 11–33.

Voelker, M., Platz, T., Tanaka, K. L., Fortezzo, C. M., R. Fergason, Hare, T. M., 2013. Hyperconcentrated flow deposits and valley formation of Havel Vallis, Xanthe Terra, Mars, 44th LPSC, #2886.

Voelker, M., Hauber, E., Schulzeck, F., Jaumann, R., 2017a. Grid-mapping Hellas Planitia, Mars – Insights into distribution, evolution and geomorphology of (Peri)-glacial, fluvial and lacustrine landforms in Mars' deepest basin, Planet. Space Sci. 145, p. 49–70, doi:10.1016/j.pss.2017.07.012.

Voelker, M., Hauber, E., Jaumann, R., 2017b. Extensive Sheet Deposits in Eastern Hellas Planitia - Volcanic Flows or Cryofluvial Deposits - A Comparison, 48th LPSC, #1426.

Voelker, M., Hauber, E., Stephan, K., Jaumann, R., 2018. Volcanic flows versus water- and ice-related outburst deposits in eastern Hellas: A comparison, Icarus 307, p. 1–16, https://doi.org/10.1016/j.icarus.2018.02.023.

Weischet, W., 2002. Einführung in die Allgemeine Klimatologie – Physikalische und meteorologische Grundlagen, 6th edition, Gebrüder Bornträger, p. 276, Berlin, Stuttgart.

Weiss, D. K., Head, J. W., 2017 Salt or ice diapirism origin for the honeycomb terrain in Hellas basin, Mars?: Implications for the early martian climate, Icarus 284, p. 249–263, https://doi.org/10.1016/j.icarus.2016.11.016.

Werner S. C. 2008. The early martian evolution---Constraints from basin formation ages, Icarus 195, Issue 1, p. 45–60, http://dx.doi.org/10.1016/j.icarus.2007.12.008.

Williams, D. A., Greeley, R., Zuschneid, W., Werner, S. C., Neukum, G., Crown, D. A., Gregg, T. K. P., Gwinner, K., Raitala, J., 2007. Hadriaca Patera: Insights into its volcanic history from Mars Express High Resolution Stereo Camera, J. Geophys. Res. 112, E10004, doi:10.1029/2007JE002924.

Williams, D. A., Greeley, R., Fergason, R. L., Kuzmin, R., McCord, T. B., Combe, J.-P., Head, J. W., Xiao, L., Manfredi, L., Poulet, F., Pinet, P., Baratoux, D., Plaut, J. J., Raitala, J., Neukum, G., the HRSC Co-Investigator Team, 2010. The Circum-Hellas Volcanic Province, Mars: Overview. Planet. Space Sci. 57, p. 895–916. doi:10.1016/j.pss.2008.08.010.

Willmes, M., Reiss, D., Hiesinger, H., Zanetti, M., 2012. Surface age of the ice-dust mantle deposit in Malea Planum, Mars, Planet. Space Sci. 60, p. 199–206, doi:10.1016/j.pss.2011.08.006.

Wilson, L. and Head, J. W., 1994. Mars: review and analysis of volcanic eruption theory and relationships to observed landforms. Rev. Geophys. 32, p. 221–263, doi:10.1029/94RG01113.

Wilson, S., Howard, A. D., Moore, J. M., Grant, J. A., 2007. Geomorphic and stratigraphic analysis of Crater Terby and layered deposits north of Hellas basin, Mars, J. Geophys. Res. 112, E08009, doi:10.1029/2006JE002830.

Wiseman, S. M., Arvidson R. E., Wolff M. J., Smith M. D., Seelos F. P., Morgan F., Murchie S. L., Mustard J. F., Morris R. V., Humm D., McGuire P. C., 2016. Characterization of artifacts introduced by the empirical volcano-scan atmospheric correction commonly applied to CRISM and OMEGA near-infrared spectra, Icarus 269, p. 111–121. doi:10.1016/j.icarus.2014.10.012.

Xiao, Z., and Strom, R. G., 2012. Problems determining relative and absolute ages using the small crater population, Icarus 220, p. 254–267, doi:10.1016/j.icarus.2012.05.012.

Zalewska (Andrzejewska), N. E., 2013. Hellas Planitia as a potential site of sedimentary minerals, Planet. Space Sci. 78, p. 25–32,. doi:10.1016/j.pss.2012.12.006.

Zanetti, M., Hiesinger, H., Reiss, D., Hauber, E., Neukum, G., 2010. Distribution and evolution of scalloped terrain in the southern hemisphere, Mars, Icarus 206, p. 691–706, doi:10.1016/j.icarus.2009.09.010.

Zimbelman, J. R., Garry, W. B., Bleacher, J. E., Crumpler, L. S.,2011. Inflation Features on the Distal Pahoehoe Portion of the 1859 Mauna Loa Flow, Hawaii: Implications for Evaluating Planetary Lava Flows, 42nd LPSC, #2443.

Zuschneid and van Gasselt (2014) Evidence for Volcanism on the Western Hellas Basin Floor, 46th LPSC, #1858.

Der Lebenslauf ist in der Online-Version aus Gründen des Datenschutzes nicht enthalten.

List of Publications and Conference Contributions

Voelker, M., Hauber, E., Stephan, K., Jaumann, R., 2018. Volcanic flows versus water- and ice-related outburst deposits in eastern Hellas: A comparison, Icarus 307, p. 1–16, https://doi.org/10.1016/j.icarus.2018.02.023.

Voelker, M., Hauber, E., Schulzeck, F., Jaumann, R., 2017. Grid-mapping Hellas Planitia, Mars – Insights into distribution, evolution and geomorphology of (Peri)-glacial, fluvial and lacustrine landforms in Mars' deepest basin, Planet. Space Sci. 145, p. 49–70, doi:10.1016/j.pss.2017.07.012.

Voelker, M., Hauber, E., Jaumann, R., Grid-Mapping of Hellas Planitia, Mars - Geostatistical Analyses of Cold-Climate Landforms, DPS meeting #48, Pasadena, California, USA, Oct. 2016 (talk).

Voelker, M., Hauber, E., Jaumann, R., Distribution and Evolution of Cold-Climate Landforms in a Subpolar and Hyperarid Environment, Hellas Planitia, Mars, 11th International Conference on Permafrost, Potsdam, DE, Jun. 2016 (talk).

Voelker, M., Hauber, E., Jaumann, R., Distribution and Geomorphology of the Latitude-Dependent Mantling Deposit in Hellas Planitia, Mars, 47th Lunar and Planetary Science Conference, The Woodlands, Texas, USA, Mar. 2016 (talk).

Voelker, M., Hauber, E., Jaumann, R., Distribution and Evolution of Lacustrine and Fluvial Features in Hellas Planitia, Mars, Based on Preliminary Results of Grid-Mapping, 47th Lunar and Planetary Science Conference, The Woodlands, Texas, USA, Mar. 2016 (poster).

Voelker, M., Hauber, E., van Gasselt, S., Jaumann, R., Grid Mapping of Hellas Planitia - Preliminary Results from the Northern Impact Rim, European Planetary Science Congress 2015, Nantes, France, Sep./Oct. 2015 (talk).

Voelker, M., Platz, T., Tanaka, K. L., Fortezzo, C. M., Fergason, R., Hare, T. M., Hyperconcentrated Flow Deposits and Valley Formation of Havel Vallis, Xanthe Terra, Mars, 44th Lunar and Planetary Science Conference, The Woodlands, Texas, USA, Mar. 2013 (poster).

Voelker, M., Platz, T., Tanaka, K. L., Fortezzo, C. M., Fergason, R., Hare, T. M., Geological Mapping of Havel Vallis, Xanthe Terra, Mars: Stratigraphy and Reconstruction of Valley Formation, 43rd Lunar and Planetary Science Conference, The Woodlands, Texas, USA, Mar. 2012 (poster).

As a co-author:

Hauber, E., Jonas, T., *Voelker, M.*, Knapmeyer, M., Grott, M., Matz, K.-D., 2014. Fault Scaling On Mars: Slip Distribution and Displacement-Length Relationship Derived from HRSC Data, 45th Lunar and Planetary Science Conference, The Woodlands, Texas, USA, Mar. 2014.

Hauber, E., *Voelker, M.*, Gwinner, K., Knapmeyer, M., Grott, M., Matz, K.-D., 2013. Fault scaling on Mars: Slip distribution and displacement-length relationship derived from HRSC data, European Planetary Science Congress 2013, London, UK, Sep. 2013.